Analysis of the Indented Cylinder by the use of Computer Vision

Buus, Ole Thomsen; Jørgensen, Johannes Ravn; Carstensen, Jens Michael

Publication date:
2013

Document Version
Publisher's PDF, also known as Version of record

Analysis of the Indented Cylinder by the use of Computer Vision

Ole Thomsen Buus
PhD Thesis

Published version: 23rd of April 2013
(with minor corrections and style changes)

Principal Supervisor	Johannes Ravn Jørgensen, Associate Professor, Department of Agroecology, Science and Technology, Aarhus University, Denmark.
Project Supervisor	Jens Michael Carstensen, Associate Professor, Department of Informatics and Mathematical Modelling, Technical University of Denmark, Denmark.
Assessment committee	Bernd Wollenweber, Associate Professor, Department of Agroecology, Science and Technology, Aarhus University, Denmark.
	Rasmus Jørgensen, Associate Professor, Institute of Chemical Engineering, Biotechnology and Environmental Technology, University of Southern Denmark, Denmark.
	Gunilla Borgefors, Professor in Image Analysis and Remote Sensing, Swedish University of Agricultural Sciences, Uppsala, Sweden.

Thesis submitted to Aarhus University, Science and Technology
in fullfillment of the requirements for the degree Doctor of Philosophy

Aarhus, Denmark
April 2013

Signature: _____
Ole Thomsen Buus

Preface

This thesis has been submitted to the Graduate School of Science and Technology (GSST) at the faculty of Science and Technology, Aarhus University, Aarhus to meet the requirements for obtaining the PhD degree. The original research presented here was carried out from May 2009 to April 2013. The work was mainly conducted at AU Flakkebjerg, Slagelse in collaboration with Technical University of Denmark, Lyngby, Copenhagen and Westrup A/S, Slagelse.

Summary

The research summarised in this PhD thesis took advantage of methods from computer vision to experimentally analyse the sorting/separation ability of a specific type of seed sorting device – known as an "*indented cylinder*". The indented cylinder basically separates incoming seeds into two sub-groups: (1) "long" seeds and (2) "short" seeds (known as length-separation). The motion of seeds being physically manipulated inside an active indented cylinder was analysed using various computer vision methods. The data from such analyses were used to create an overview of the machine's ability to separate certain species of seed from each other.

Seeds are processed in order to achieve a high-quality end product: a batch of a single species of crop seed. Naturally, farmers need processed clean crop seeds that are free from non-seed impurities, weed seeds, and non-viable or dead crop seeds. Since the processing is based on physical manipulation of the seeds themselves, their individual shape and size becomes very relevant. The problem of modelling such physical parameters for various species of seed, grown under various environmental circumstances, is a very complex one. The general problem of modelling and controlling seed processing equipment can be expected to be complex. Due to the involvement of seeds, the problem will naturally inherit all their biological complexities. In addition to this, because of the very large number of individual seeds, the problem also involves a granular media and thus inherits all the complexities related to that as well.

The project arrived at a number of results of high scientific and practical value to the area of applied computer vision and seed processing and agricultural technology in general. The results and methodologies were summarised in one conference paper and two journal papers. These three papers, referred to as Paper I, Paper II, and Paper III can be found in Appendix A, B, and C, respectively. These three papers represent the very first examples of published/submitted work that thoroughly analyse and verify the separation ability of the indented cylinder by the use of computer vision (or image analysis). Moreover, the imagery data sets, generated as a result of actual recordings of sorting experiments using the indented cylinder, are novel by their high dimensionality and size. Paper II in Appendix B makes one of these data sets available online as a cite-aware imagery data set.

The work summarised in this thesis is very much related to the task of constructing models from observed data. This field is known as empirical model development or more specifically as "system identification". System

identification deals specifically with estimating mathematical models from observed dynamic states (time series) of inputs and outputs to and from some physical system under investigation. The contribution of the work is to be found primarily within the problem domain of experimentation for system identification. Computer vision techniques were used to acquire observations of a measure of separation efficiency of the indented cylinder. Such techniques for observation are likely to be very relevant for experimentation in a laboratory for system identification purposes.

This work should therefore be seen as an important step towards future research in system identification of the indented cylinder. The technical solutions developed are currently novel and represent an ideal platform for future applied research into empirical model development. Finally, this work should also be considered as an early step toward a paradigm shift where the best parameters for the indented cylinder are not mainly determined by "rule of thumb" and other forms of heuristics, but are instead optimized parameters tied to an actual theory of seed separation in the indented cylinder.

Sammendrag (Danish Summary)

Forskningen opsummeret i denne ph.d.-afhandling benyttede sig af metoder fra computer vision til eksperimentelt at analysere sorteringsevnen i en specifik type af frøsorteringsmaskine - kendt som en "triøre" (på engelsk: "indented cylinder"). En triøre adskiller hovedsageligt indkommende frø i to undergrupper: (1) "lange" frø og (2) "korte" frø (kendt som længdeseparation). Den måde frø bevæger sig på under fysisk manipulation inden i en aktiv triøre, blev analyseret ved hjælp af forskellige computer vision metoder. Data fra disse analyser blev herefter anvendt til at skabe et overblik over maskinens evne til at separere visse arter af frø fra hinanden.

Frø renses og sorteres for at opnå en høj kvalitet i slutproduktet: en batch som udelukkende indeholder kerner fra en enkelt afgrødeart. Landmænd har naturligvis brug for forarbejdede afgrødefrø, der er fri for urenheder såsom ukrudtsfrø og ikke-levedygtige eller døde afgrødefrø. Da sortering er baseret på en fysisk manipulation af frøene, er deres individuelle form og størrelse meget relevant. Modellering af sådanne fysiske parametre for forskellige arter af frø, dyrket under forskellige dyrkningsforhold, er et meget komplekst problem. Det mere generelle problem med at modellere og styre frøsorteringsudstyr kan således også forventes at være meget komplekst. Dette er til dels på grund af problemets involvering af frø, hvor det jo så naturligvis arver deres biologiske kompleksitet. På grund af det meget store antal af individuelle frø, vil problemet samtidigt også involvere et granulært materiale og arver derved også alle kompleksiteterne beslægtet med dette.

Projektet nåede frem til en række resultater af stor videnskabelig og praktisk værdi for anvendt computer vision, frøforarbejdning og landbrugsteknologi generelt. Resultaterne og metoderne blev samlet i en konferenceartikel og to tidsskriftsartikler. Disse tre artikler, der omtales som Paper I, Paper II, og Papir III kan findes i hhv. Appendix A, B, og C. Disse tre artikler repræsenterer de første eksempler på publiceret/indsendt arbejde som grundigt analyserer triørens sorteringsevne ved anvendelse af computer vision (eller billedanalyse). Udover dette, er der også de billeddatasæt, der blev skabt som et resultat af optagelser af egentlige sorteringsforsøg med triøren. Disse datasæt er af hidtil uset dimensionalitet og omfang, og i Paper II i bilag B er et af disse datasæt gjort tilgængelige online som et citérbart billeddatasæt.

Den forskning der opsummeres i denne ph.d.-afhandling er stærkt re-

lateret til problemet med at konstruere modeller ud fra observerede data. Dette felt er kendt som empirisk modeludvikling (på engelsk: “empirical model development”) eller mere specifikt som "systemidentifikation"(på engelsk: “system identification”). I systemidentifikation er målet at estimere matematiske modeller ud fra observerede dynamiske tilstande (tidsserier) af input og output til og fra det fysiske system, som undersøges. Bidraget skal findes primært inden for udarbejdelse af eksperimenter til system identifikation. Computer vision teknikker blev anvendt til at erhverve observationer af separations-effektiviteten i triøren. Sådanne teknikker til observation vil sandsynligvis være meget relevante i forbindelse med eksperimenter til system identifikation i et laboratorium.

Dette arbejde bør derfor ses som et vigtigt skridt i retning mod fremtidig forskning inden for system identifikation af triøren. De udviklede tekniske løsninger er i øjeblikket nye og repræsenterer en ideel platform for fremtidig anvendt forskning inden for empirisk modeludvikling. Endelig bør dette arbejde også betragtes som et tidligt skridt mod et teknologisk paradigmeskifte, hvor de bedste parametre for triøren ikke bestemmes alene ud fra diverse “tommelfingerregler” og andre former for heuristiske huskeregler, men er i stedet optimerede parametre bundet til en egentlig teori om længde-separation af frø i triøren.

List of Publications

Papers

Paper I: Buus O.T., Carstensen J.M., Jørgensen, J.R., 2011. **Analysis of Seed Sorting Process by Estimation of Seed Motion Trajectories**, in: Heyden, A., Kahl, F. (Eds.), Image Analysis. Springer Berlin / Heidelberg. volume 6688 of Lecture Notes in Computer Science, pp. 273–284 (*published*). The version printed in the proceedings is available in Appendix A.

Paper II: Buus O.T., Jørgensen, J.R., Carstensen J.M., 20xx. **Analysis of the Indented Cylinder Part 1: Preliminary Image Analysis Experiments**. Second revision to be resubmitted in 2013 to Computers and Electronics in Agriculture. The working draft is available in Appendix B.

Paper III: Buus O.T., Jørgensen, J.R., Carstensen J.M., 20xx. **Analysis of the Indented Cylinder Part 2: Length Separation Ability**. Second revision to be resubmitted in 2013 to Computers and Electronics in Agriculture. The working draft is available in Appendix C.

Posters

Poster I: Buus O.T., Carstensen J.M., Jørgensen, J.R., 2010. **Towards Tracking of Seeds in an Indented Cylinder**. Industrial Visionday 2010 in May 2010 at Technical University of Denmark, Lyngby, Denmark. The poster is available in Appendix D.

Poster II: Buus O.T., Carstensen J.M., Jørgensen, J.R., 2011. **Analysis of Seed Sorting Process by Estimation of Seed Motion Trajectories**. Scandinavian Conference in Image Analysis 2011 in May 2011, Ystad, Sweden. The poster is available in Appendix E.

Table of Contents

Chapter 1

Introduction

1.1 Background

According to the latest UN projections, the world population could reach 9.15 billion by the year 2050 (Alexandratos and Bruinsma, 2012). To meet the increased demand, global agricultural production in 2050 will need to increase by 60-70 percent relative to its 2005/2007 level. While this is only a smaller increase in the production achieved by the agricultural sector over the last 50 years, these projections still raise great concern on how the increased demand can be met in a sustainable way (The Economist, 2011).

A major part of this increased production will be derived from improved yields of cereals and other seed crops. The average global cereal yield growth has been almost linear for the past half century and future projections toward year 2050 follow this linear trend as well (Alexandratos and Bruinsma, 2012). Maintaining such production trends in a sustainable way is a complicated problem that involves several different agricultural concerns. Some of these concerns are in regard to future resources such as water and land with potential for rainfed cereal production, as well as post-harvest management which involve all processes of seed-handling, storage, drying and cleaning after the crop has been harvested.

1.1.1 Seed Health and Quality

A general post-harvest concern is that of achieving seeds of good *seed health*. Sustainable production of cereal crops requires that the embryonic plant (i.e. the seed) is in good health so that germination in the soil can initiate. Seed health is one of the several aspects of *seed quality* – a complicated concept involving physical, physiological, and genetic aspects (Bishaw et al., 2007; Hampton, 2002). Earlier work (summarised in Delouche et al., 1995) has shown that a positive correlation exists between physical aspects of seeds and seed quality; e.g. between seed size and seed quality parameters such as germination ability and seed vigour. Bishaw et al. (2007) broadly defines high quality seed as "... seed of an adapted variety with high genetic varietal, species, and physical purity; high germination and vigor; free from seed-

borne pests (fungi, bacteria, viruses, insects, nematodes, parasitic weeds); and properly cleaned, treated, tested and labeled".

1.1.2 Physical Purity

The concept of "physical purity" is at the crux of the applied research summarised in this PhD dissertation: After harvest, crop seeds still contain a number of contaminants (weed seeds, insects, etc.) and possibly larger impurities (stones, stems, leaves, etc.) that must be removed in later-stage post-harvest seed cleaning or sorting processes in order to achieve a physical pure seed lot. Naturally, farmers need processed clean crop seeds that are free from non-seed impurities and non-viable or dead crop seeds (Schmidt, 2007). This problem lies as the heart of the seed industry itself: "The seed industry exists only to provide high-quality seed to farmers so they can produce more on the same land, and produce it more efficiently and cost-effectively. This means providing improved seed which offers the greatest potential at a reasonable cost" (from Gregg and Billups, 2010b, first paragraph in foreword).

An optimal seed cleaning/sorting process is one that results in seeds of as high a seed quality as possible (Gregg and Billups, 2010b, chp. 1). The choice on whether or not farmers use good seeds or bad seeds, can influence whole national economies and affect the general standard of living of people (Gregg and Billups, 2010a). Achieving an optimal seed cleaning/sorting process is for such reasons very important and it is therefore also a both interesting and necessary applied research focus. A more detailed introduction to the problem of seed sorting is given in Section 1.2.

1.1.3 High Complexity

Primitive seed cleaning/sorting is linked to the domestication of seed crops ever since man took up cultivation in the Fertile Crescent 10 000 years ago (Vavilov, 1926). These methods can still be seen today when farmers in rural areas use natural wind to separate light materials such as dust, chaff and leaves from the seeds. This ancient method is known as "winnowing". See Figure 1 for an example.

However, achieving an optimal cleaning/sorting outcome depends on an understanding of the cleaning processes and on the ability to control them properly given different input (Pearson, 2003). Herein lies the issue of potentially high complexity: Seed cleaning/sorting processes are generally complicated. First of all, due to the involvement of seeds themselves, cleaning processes will naturally involve all the inherent biological complexities and physical appearance of the seeds. And seeds can be considered complicated in themselves: The individual seeds involved are nothing less than "... neatly packaged forms of embryonic life complete with a built-in food supply" (Harmond et al., 1965).

Figure 1: An example on how traditional winnowing can be used for rice cleaning/sorting. The grain is thrown up in the air or slowly poured into a pile. Natural wind is used (from Schmidt, 2007).

The importance of shape and size

Since the processing is based on actual physical manipulation of the seeds themselves, their individual shape and size of different species become very relevant. This is exemplified by, for instance, the differences in the desired crop seeds and the weed seeds in a harvested seed lot. For instances, machines for post-harvest seed sorting (also known as upgrading) usually take direct advantage of distinguishable physical characteristics of the individual seeds (Grochowicz, 1980, chp. 1). Obtaining a complete overview of all physical differences for various species of seed, grown under various environmental conditions, would easily become complicated or even intractable (Harper et al., 1970; Robert et al., 2008; Martre et al., 2011).

Moisture content

Shape and size are not the only complicating factors to take into consideration. Moisture content, i.e. the content of water in a seed, is one example of an important physical factor of a seed's physical condition. Under Danish conditions, wheat and barley are ideally harvested at a moisture content of 14 % (Olsen and Hansen, 1980). However, in years with problematic harvest conditions as in 2011, cereals may be harvested with a water content above 20 % (Pedersen, 2011).

Previous work reports on the coefficient of friction of seeds against surfaces of, e.g. compressed plastic, galvanized iron, and plywood (Karimi et al., 2009) and also glass, stainless steel (Tabatabaeefar, 2003). Besides these materials, Kalkan and Kara (2011) also reported estimates of the friction coefficient with fiberglass and steel. These and other works are in unanimous agreement: The friction coefficient generally increases with increased moisture content. Kalkan and Kara (2011) mentions that this might be due to the larger contact area of a moist and therefore softer seed.

A granular material

Because of the very large number of individual seeds involved in seed cleaning, the seeds acts as a granular media and the problem of seed cleaning therefore inherits all the complexities related to that as well. The dynamics of granular media is generally considered complex (Jaeger et al., 1996; Rajchenbach, 2000; Campbell, 2006; Forterre and Pouliquen, 2008). The measurement of various physical characteristics of these biological granular media can be very useful – especially for cereals and other crop species. For instance, knowledge of the mass of wheat pr. m^3 (test weight) and the weight of a 1000 seeds (thousand kernel weight; TKW) can be used in estimating the number of individual wheat kernels involved in each m^3 of material processed. Given the experimentally verified particle density of $\sim$1300 kg/m^3 (Jayas and Cenkowski, 2006, sec. 24.2.2, p. 577) and likewise for a $\sim$30 g thousand kernel weight, both measured at a $\sim$10 % moisture content (Tabatabaeefar, 2003; Kalkan and Kara, 2011), such an estimate will be in the range of 40 to 43 million kernels pr. m^3.

1.1.4 A Brief on the Purpose of the Work

Though Chapter 2 will specify exactly the overall aims and objectives of this work, it seems fitting to give a brief account on the motivation and overall purpose here.

Motivation

Due to the already mentioned issues with system complexity, an optimal use of seed sorting machinery easily becomes difficult. It would be of high relevance for the seed cleaning industry if this difficulty could somehow be

minimised. For instance, much hands-on experience is required by technicians before they are able to successfully initialise and adjust sorting machines for an optimal outcome (personal communication: Westrup A/S). An insight into how the input affects the output of the process in seed sorting machinery represents a possible minimisation of the complexity involved in achieving an optimal use or configuration of these kinds of machines. Achieving such an insight could arguably bring more certainty into the expected outcome of seed sorting and it could also lessen the requirements for training technicians.

Overall purpose

The purpose of this work was therefore to achieve an insight into the relationship between the input and the output of the process in the "indented cylinder" – a central machine in post-harvest seed cleaning processes. The indented cylinder is said/assumed to use the individual seed kernel length as the single physical distinguishing characteristic to achieve a physical separation. The result is thus binary division of the input material into "long" and "short" material (see Gregg and Billups, 2010b, chp. 24 and Grochowicz, 1980, chp. 7). An optimal configuration of the indented cylinder can be loosely defined as a configuration that most likely will result in the most optimal separation between the seeds in the input material. Section 1.3 gives an introduction to the general operating principle of the indented cylinder and presents an overview of the related literature.

Approach

Achieving an insight into the input-output relationship of any system is essentially a problem of empirical model development, i.e. the field of methods used for estimating mathematical models of systems by observing their output given a known input. In control theory this problem is also known as "system identification" (Ljung, 2010). Section 1.4 gives a brief introduction to the problem of empirical model development. Solving the problem of achieving the aforementioned insight for the indented cylinder, depends on finding the solution to a number of non-trivial technical and scientific challenges. These challenges belonged primarily to the areas of digital imaging, computer vision and image analysis.

Digital imaging was used to experimentally observe/record the movement of different species of seeds while they were being physically manipulated inside the indented cylinder. The resulting digital recordings were processed using methods from computer vision. The intent was to extract data from the recordings that could be used to probabilistically quantify the ability of the indented cylinder to separate seeds of different kernel lengths. The specific objectives involved the development of digital imaging experiments and computer vision methods that would make it possible to extract such data.

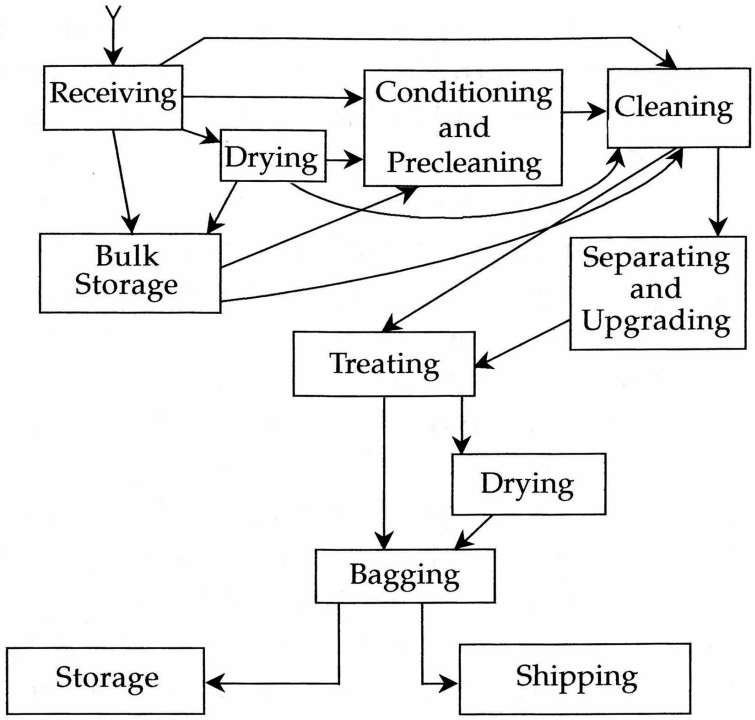

Figure 2: Overview of processing steps in seed conditioning. Source: Gregg and Billups (2010b).

1.2 Seed Sorting

The sorting of seeds is a sub-task within the broader scope of *seed conditioning*. Combine harvested seeds from the fields will contain foreign material such as stems, leaves, stones, dead insects, etc., in addition to the crop seeds themselves. Moreover, the material will suffer from other problems such as non-optimal crop seeds of low quality, dead or broken crop seeds, and weed seeds (Desai, 2004; Schmidt, 2007; Bishaw et al., 2007). Seed conditioning is a segment of the seed industry that deals with improving the quality of seed by removing such foreign material and any excess moisture that may exist in the raw material. The aim of the seed industry is to supply the farmers and end-users with a better quality of seed and it is therefore simultaneously quality and business oriented (Gregg and Billups, 2010b, chp. 1).

Seed conditioning deals specifically with the entire chain of processing steps necessary to produce a healthy seed product, free from impurities, and which is both highly functional and saleable. Figure 2 gives an overview of the processing steps involved in conditioning the incoming raw material. After being received, the first four steps are (Gregg and Billups, 2010b):

Drying: The material is usually dried down rapidly in a drying facility removing any excess moisture. This can be important for some seed species but also crucial in years and locations of humid harvest conditions (Pedersen, 2011). The drying process is naturally dependent on the introduction of heat to the system. Most commercial dryers

are automatically controlled such that energy is used most optimally. The control problem is usually solved as a multi-objective optimisation problem (Farkas, 2003b).

Conditioning and Precleaning: After drying, the conditioning and precleaning steps ensure that the material can flow more easily through subsequent operations. These precleaning steps involve special machines suitable for this purpose. One example is a *scalper* used for the removal of very large or very small impurities from the raw material. This machine it is similar to the basic *air-screen cleaner* used in the next step. Another example is a *thresher* used for "debearding", i.e. the removal of awns, husks, and hairs from the seeds. This is particulary relevant for oats, barley, and some vegetable and flower seeds, and for many grass seeds.

Cleaning: This step is also known as basic cleaning and the aim is to remove inert material, weed seeds, crop seeds of other species, and broken crop seeds. The basic air-screen cleaner is usually used for this purpose.

Separating and Upgrading: Sometimes weed or other crop seeds, or low-quality seeds of the pure crop can still be present in the material. Machines for separating and upgrading take advantage of the physical distinguishing characteristics that might exist between crop seeds and other unwanted particles. Seed sorting can be considered as yet another sub-task of seed separation and upgrading.

1.2.1 Mechanical Separation Of Seeds

The separation outcome is considered as being mainly dependent on the various individual physical characteristics of the seeds (Brandenburg, 1977). Examples of such physical characteristics are: the size, length, weight, shape, and colour, etc. (Gregg and Billups, 2010b; Harper et al., 1970). A correlation has been shown to exist for certain seed species between general seed size and seed quality (Delouche et al., 1995; Guberac et al., 1998) and to the germination process in general.

Figure 3 show the main three dimensions of a seed: (1) length, (2) thickness, and (3) width. Attaining an overview of the physical properties of various species of seed is crucial for further adjustment of the existing machines and for the development of new kinds of sorting machines (Harmond et al., 1965; Jayas and Cenkowski, 2006; Riahi and Ramaswamy, 2003; Sablani and Ramaswamy, 2003). Several such overviews have been published, for instance for barley (Öztürk and Esen, 2008; Tavakoli et al., 2009; Sologubik et al., 2013). New methods to determine these characteristics keep developing as well (Karaj and Müller, 2010).

This work has looked into the technological aspect of seed sorting, i.e. the mechanical separation of seeds – and the optimization of those aspects. Some previous studies on this areas exist. For instance, El-Awady et al.

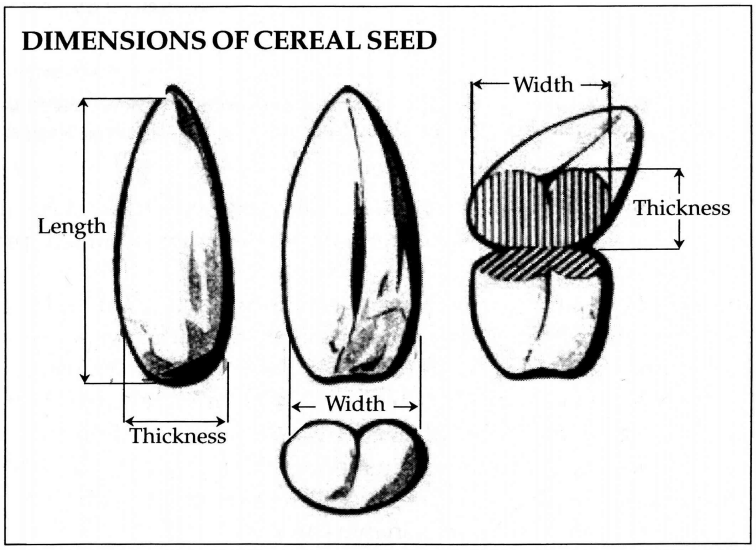

Figure 3: Example of the three dimensions of a seed. A wheat seed is used as an example. Source: Gregg and Billups (2010b).

(2009) investigated the improvement of a winnowing and cleaning machine for rice with the goal of reducing impurities and loss of good seeds. They developed a winnowing prototype and interesting regression models. Moreover, they concluded on choices of governing parameters such as air speed, moisture content, and feeding rate. Moreover, Simonyan et al. (2010) developed a mathematical model of the cleaning efficiency of a stationary grain thresher. The model applied the principles from dimensional analysis as the theoretical foundation. Dimensional analysis was also used by Căsăndroiu et al. (2009) to mathematically model the cleaning process on plane sieves. Yuan et al. (2006) investigated how to control an air-screen cleaner to get the most optimal result. They applied a hybrid intelligent approach involving the use of an artificial neural network and genetic algorithms. A pneumatic separator was designed by Panasiewicz et al. (2012) and analysed using crushed mixtures of three lupine varieties. They determined correlations between separation process parameters and separation process efficiency. The automated modelling and control aspects of post-harvest technologies have also been investigated quite intensely for seed drying systems and sorting of fruits (see reviews, e.g. Farkas, 2003b; Studman, 2001). Recently, interest has been shown in applying artificial intelligence techniques to control such processes (e.g. Farkas, 2005, 2003a).

The indented cylinder

The indented cylinder is used for seed sorting or upgrading and uses mainly the length of the seeds as the physical distinguishing characteristic. The indented cylinder basically separates incoming seeds into two sub-groups: (1) “long” seeds and (2) “short” seeds (Brandenburg, 1977; Gregg and Billups, 2010a, chp. 24). The indented cylinder was chosen as the seed

sorting/separation device of primary scientific focus throughout the entire project. Because of this, Section 1.3 will introduce the general functionality of the indented cylinder in more detail.

The gravity separator

Other machines for seed sorting exist. A machine that is usually used after the indented cylinder is the gravity separator (Gregg and Billups, 2010b, chp. 24 and 25). This machine separates seeds based on their individual weight. It requires that the seeds are relatively homogeneous in terms of their individual physical size or length – something that the indented cylinder takes care of. Balascio et al. (1988) modelled the granular flow on a gravity separator table. The particle movement was modelled as a stochastic process (see also Balascio et al., 1987a,b).

Other technologies

As Chapter 2 will specify in more details, the project took use of digital imaging and methods from computer vision (or image analysis) as the mechanism for empirical sampling of some relevant output variables of the indented cylinder. Computer vision is the scientific endeavour of attempting to give intelligent eyes to computers. Work in related areas, such as artificial intelligence and object recognition, has been going on for at least 60 years – ever since the invention of the first digital computers (McCarthy et al., 1955; Dinneen, 1955; Selfridge and Neisser, 1960; Besl and Jain, 1985). These fields have since matured and grown into vast subject areas and very active fields of research. Over time they gave birth to the field of computer vision – a field of research that aims to develop robust methods for extracting visual information coded in the pixels of digital images. The aim is usually to produce numerical or symbolic information useful for making decisions (Shapiro and Stockman, 2001; Sonka et al., 2008). As both a basic and applied computer scientific research discipline, the field relies heavily on methods from geometry, statistics, physics, and learning theory, etc. to extract visual information from the data stored in the pixels (Forsyth and Ponce, 2011; Szeliski, 2010).

The work by Berlage et al. (1984b) and Cooper and Berlage (1985) are examples of earlier work on the application of image analysis to improve the accuracy of seed sorting and conditioning in general. The methods applied are simple but effective. Cooper and Berlage (1986) devised an early vision system making it possible to create a database of physical properties of seeds. Here Cooper and Berlage interestingly concluded that "data can be gathered on about three seeds per minute". Berlage et al. (1989) investigated the general problem and need for applying new technologies to seed sorting and cleaning – computer vision was of primary focus.

The automation and optimisation of the inspection and classification of seeds by the use of computer vision/image analysis continues to be important – especially for non-invasive seed germination testing (Dell'Aquila,

2007, 2009). A more recent addition to the line of seed sorters that apply a simple form of image analysis is the colour sorter. This machine classifies individual seeds based on their colour using a variety of different sensors. Seed sorters are usually used at the very end of the conditioning after all applicable mechanical processing have been applied (Gregg and Billups, 2010b; Schmidt, 2007; Desai, 2004).

The classification of seeds that are not moving is usually addressed as a straightforward object recognition problem. Douik and Abdellaoui (2010) addressed the problem of classifying cereal grains by focusing on a set of different features and classifiers. A trained *artificial neural network* (ANN) was one of the classifiers applied. Guevara-Hernandez and Gomez-Gil (2011) did similar work with supervised classification of wheat and barley grains. *Discriminant analysis* (DA) and *k-nearest neighbour* (k-NN) were used for supervised classification. The quite popular and also generally very successful supervised ANN approach was again used by Chhabra and Reel (2011) for wheat quality evaluation. Szczypiński and Zapotoczny (2012) carried out a very detailed approach for quality evaluation and classification of barley kernels. The work employed orientation estimation and surface structure assessment of individual barley kernels.

The studies mentioned so far have in common that they are not dealing with the actual physical sorting of seeds. The research has instead focused primarily on the image analysis task of classifying seeds which have been statically placed in front of a camera. The focus has instead been on developing entirely new machines for sorting – usually based on the colour sorter as a frame of reference. Xun et al. (2006) developed an automatic seed sorting system based on machine vision for the automated classification of red and white wheat seeds. The system was capable of processing 15 seeds per second with a classification rate of more than 92 %. Pearson et al. (2008) developed a similar system for the inspection of wheat and other grains. The system was capable of processing 30 seeds per second with an accuracy from 95 % to 99 %. The experiment was done using hard red and hard white wheat kernels. Pearson (2009) developed yet another high-speed, low-cost, image based sorting device capable of processing 75 seeds per second. Slight colour differences and small defects in the surface of the seeds were the basis for the classification. A new interesting innovation in seed sorting was recently patented by Keil (2010). The ideas behind this invention – a new machine for the sorting of granules – seem to have been inspired by the operational characteristics of the indented cylinder. Finally, the separation of seeds using high-intensity electric fields has been investigated for some time as well (Abdel-Salam et al., 2004; Butunoi et al., 2011).

1.3 The Indented Cylinder

The indented cylinder mainly uses the length of the individual seeds as the distinguishing physical characteristic. It is generally used to separate an incoming seed material into two sub-divisions: (1) “long” seeds and (2)

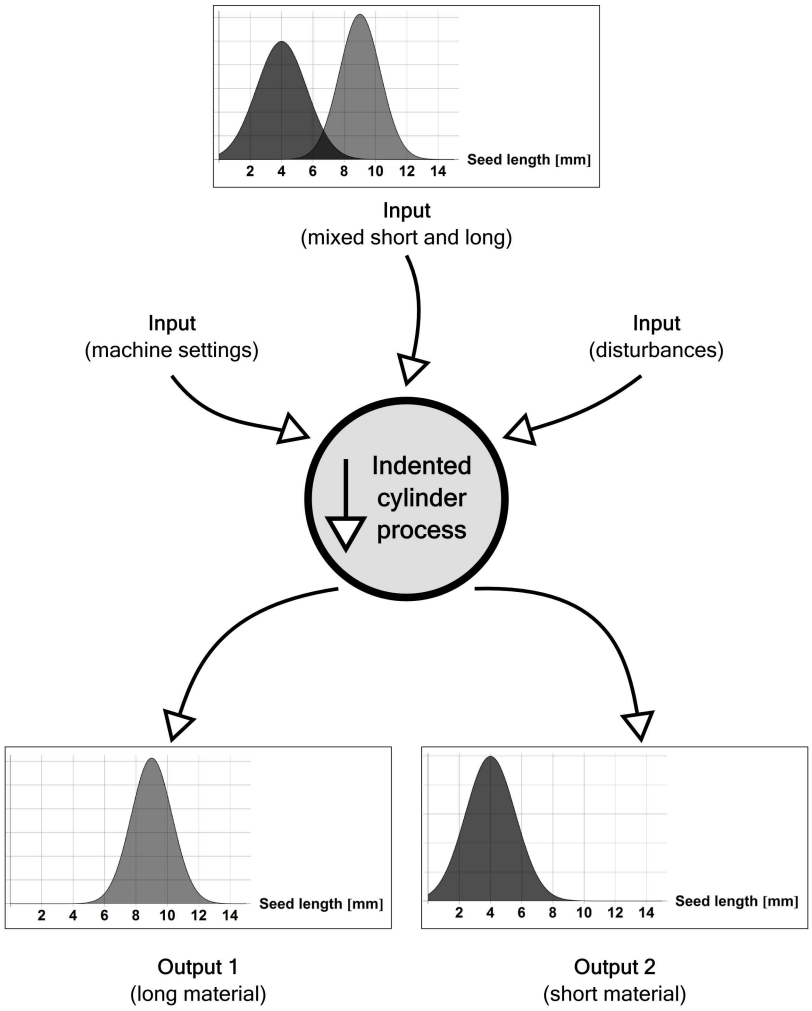

Figure 4: Conceptual model of the indented cylinder process.

"short" seeds. This is also the reason why the indented cylinder is usually known as a "length separator" (Brandenburg, 1977; Gregg and Billups, 2010a, chp. 24). The process that it carries out is likewise known as "length sorting".

Figure 4 is a graphical representation of the ideal length separation process in the indented cylinder. In the top we see a plot of two normal distributions with different means and standard deviations. These are examples on the possible length distributions of the seeds in the input material. The circle in the middle is the indented cylinder process. This process receives several inputs: (1) the mixed seeds, (2) machine settings, and also (3) measured and unmeasured disturbances. The output is binary as explained earlier: (1) "long" seeds and (2) "short" seeds. The final two distribution plots show the two individual normal distributions from "long" and "short" seeds – now separated from each other.

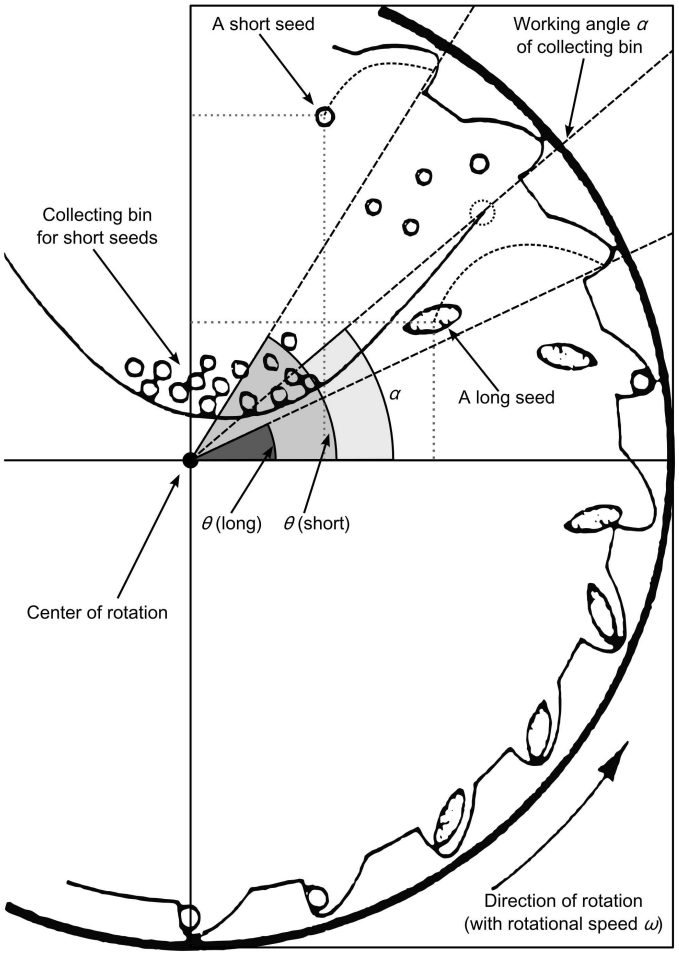

Figure 5: The indented cylinder seen from the front. The overlay graphics show the angles θ^{long} and θ^{short} for two seeds having left the cylinder wall in a parabolic-like trajectory. Modified from Lampeter (1965).

Reality

The scenario depicted in Figure 4 is highly simplified and should be considered unrealistic. The length distribution of the input material can in most circumstances not be statistically modelled as ideally consisting of two already fully known fractions of "long" and "short" seeds. A more realistic way of statistically modelling the length distribution of the input material, would be by using a mixture distribution of normal random variables with a related Gaussian mixture density. The number of underlying normal random variables of such a mixture distribution would ideally be two, although that might not always be the case.

1.3.1 General Functionality

The most basic component of the indented cylinder is a sloped steel cylinder indented with similarly sized and shaped tightly located indents on its inner surface. Such a cylinder is usually produced from a steel plate which has

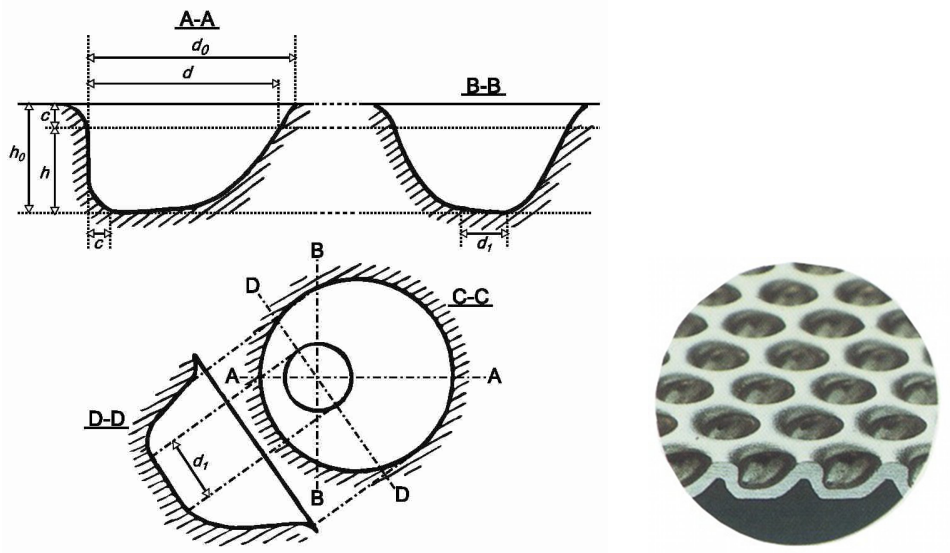

(a) (b)

Figure 6: Geometry and photo of stamped drop shaped indents in the indented cylinder: (a) geometry of stamped drop shaped indents in the indented cylinder (also defines the working indent parameter d), modified from Grochowicz (1980, chp. 6); (b) photo of drop shaped indents. Source: Online Westrup A/S product brochure (reprinted through the courtesy of Westrup A/S, Denmark).

had the indents stamped into its surface. The plate is hereafter shaped into a cylinder and welded at the seam (personal communication, Westrup A/S).

The cylinders used in the experiments had indents with a geometry identical or at least closely similar to what is depicted in Figure 6. The indents have a working diameter d – seen in Figure 6a.

The geometry

Figure 5 gives an overview of the geometry and parameters. While the cylinder is rotating with a constant rotational speed ω, seeds are fed continuously into the cylinder from the elevated end (e.g. by using a vibrational feeder) (Gregg and Billups, 2010b). The seeds land in the bottom of the cylinder where a layer of seeds will eventually form. Due to the rotation of the cylinder, the bottom of this layer is continuously disturbed by the inner surface of the cylinder. The particles of this bottom layer will be caught by the inner surface and carried up along the cylinder circumference. The seeds will be thrown off the the inner surface at an individual "angle of escape" θ. This angle of escape varies from particle to particle and depends on the amount of "resting support" the individual particles have on the inner surface of the cylinder.

The operating principle

A fraction of the input material will consist of seeds or other large particles that will generally not fit into the indents. It such a case they will usually be influenced solely by the friction with the cylinder surface between the indents. Alternatively they might fit, but because of their longer lengths their centre of gravity will not rest inside the indents. These two scenarios will generally result in low resting support during the rotation.

Other seeds or other small particles (i.e. dust and broken seeds) will be small enough to fit into the indents and rest in them for a short while, before being thrown out again. This is especially true for seeds/particles with a length similar to or shorter than the depth of the indents. The centre of gravity of such seeds will generally be inside the indents – resulting in a high resting support during rotation.

The following two fractions of the material are continuously formed by the inner cylinder surface:

The unlifted fraction: The fraction of the material with low resting support in the indents during rotation. The seeds/particles in this fraction will be carried up to a certain angle of escape θ^{long} at which point they will be thrown off the inner surface of the cylinder. This fraction of the input is referred to as the "unlifted" fraction.

The lifted fraction: The fraction of the material with high resting support in the indents during rotation. The seeds/particles in this fraction will be carried up to a certain angle of escape θ^{short} at which point they will be thrown off the inner surface of the cylinder. This fraction of the input is referred to as the "lifted" fraction.

Generally, due to the difference in resting support, θ^{long} is smaller than θ^{short}; hence the names "unlifted" and "lifted". This expected physical phenomenon is referred to here as the "lifting phenomenon".

The collecting bin

The indented cylinder is also equipped with a collecting bin mounted on the cylinder's axial support. This collecting bin is adjustable and has a working angle α with the horizontal (Gregg and Billups, 2010b; Grochowicz, 1980). See Figure 5.

When the particles in the lifted fraction are thrown off the inner surface of the cylinder they are caught by this collecting bin – given of course that its working angle α has been correctly adjusted for this to be possible. These caught particles – now specifically classified as "short" seeds/particles – are transferred away and out from the system. The particles in the unlifted fraction are not caught by the collecting bin. These particles – now specifically classified as "long" seeds – – will instead fall down into the bottom of the cylinder again and fall out of the lower end of the sloped cylinder and exit the system from there.

Separation and sorting

A important distinction between separation and sorting in the indented cylinder can be made:

Separation: The length-based separation carried out by the rotating inner surface of the cylinder and its indents.

Sorting: The final outcome as a result of the collecting bin catching the lifted fraction and not catching the unlifted fraction.

The inner surface of the cylinder and the indents make up the parts of the machine that are solely responsible for the actual separation of the lifted and unlifted fractions. The ability to separate is thus completely independent of the existence of the collecting bin that mainly functions as a form of adjustable "memory" for the cylinder inner surface. The ability to sort, on the other hand, is dependent on the collecting bin because without it the separation is quickly "forgotten".

A measure of performance

To say anything about the whether the resulting length distributions of the long or short seeds are correct in any way, one must naturally have had to introduce some kind of predetermined knowledge on the actual contents of the input material. In other words, a cleaning technician will usually know what kind of sorting outcome to accept and what kind to reject. For example, if the input material consisted of a mix of whole and broken barley kernels, the technician will naturally expect broken kernels in the short fraction and whole kernels in the long fraction.

Defining a formal measure of performance for the indented cylinder is not trivial. Can a definition of an optimal sorting outcome somehow be formalised using the language of mathematics? This is one of the basic questions behind the research in this thesis. To provide an answer to this question, the concept of "optimal" will first have to be further defined. An optimal sorting outcome could, for example, be one with a minimum "overlap" between two original sub-populations in the input material. This can be seen as a form of "criterion of optimality" for the indented cylinder. Overlap could here be defined as the amount of "short" seeds that ended up in the division that ideally should contain only "long" seeds, plus the amount of "long" seeds that ended up in the division that ideally should contain only "short" seeds. Then then following question arises: Is this ideal situation achievable in any realistic way? These kinds of questions are related to the problem of empirical model development – a challenging problem that Section 1.4 takes a closer look at.

1.3.2 Previous Work

The indented cylinder is, in a historic context, a relatively new invention (Nobbe, 1876; Kurth, 1877; Johnson, 1938; Mjolsness, 1939). Grochowicz

(1980, chp. 2) mentions that:

> "The [1840s] brought the archetypes of the currently used cylindrical screens, that is, cylindrical and polygonal sieves, as well as the archetypes of the trier built by the Frenchman Vachon."

The word "trier" is often used in older English literature. This is just another word for "indented cylinder" which was (likely) borrowed from French where that same word means to sort or select. In Danish the name for the machine is a "triøre" – a transliteration inspired by the original French word.

The most early engineering literature in which actual in-depth analyses of the indented cylinder took place, is represented primarily by Polish and Russian works from the 1940s and onwards. Various kinds of seed cleaning machinery were investigated in this important older body of work which was later summarised by Grochowicz (1980). Another example is the work by Brandenburg and Harmond (1966) whom made an attempt to improve the indented cylinder by developing a new prototype of it.

Grochowicz (1980, chp. 7) presented relatively simple models for the behaviour of the seeds in an indented cylinder. In these models, a seed is modelled as a dimensionless body. Furthermore, the modelling is carried out in two dimensions only – assuming that the motion of a seed is constrained to a plane perpendicular to the cylinder's axis of rotation. Usually two primary variations are used: Free-body diagrams of forces acting on a seed (1) between the indents and (2) inside the indents. The active element of the indents is simplified to a small piece of an increasingly inclined surface. The event for when a seed leaves the surface or an indent is expressed through trivial force equivalences involving friction forces and forces of normal pressure (dependent on the cylinder's rotational velocity ω and gravity acceleration g).

Grochowicz (1980, chap. 7) also presented a more elaborate model for both a long and a short seed inside an indent. This model takes into account the points of support in the indent that would differ for both kinds of seeds. These models give expressions for θ^{long} and θ^{short}. Moreover, given the fact that they depend on local biological parameters (seed length, friction coefficient, moisture content, etc.), the ranges of θ^{long} and θ^{short} are likely to overlap, making a complete separation difficult.

Modern work – after 1980

The observation, system identification, and/or modelling of existing seed sorting devices, such as the indented cylinder, by the use of a modern technology such as computer vision and of other computer derived technologies, has received some attention in later years – albeit to a limited degree.

The modern body of literature specific to the analysis of the indented cylinder is represented by the following seven works:

Fouad (1980): Fouad contributed with an early and important analysis of, perhaps, the most complex and still least understood parameter of the

indented cylinder: an analysis of cylindrically shape indents (referred to as "cells" in the work). Fouad concluded with recommendations on the most optimal range of shape parameters.

Berlage et al. (1984a): Berlage et al. continued the effort to improve the indented cylinder once again. A new special (laboratory-scaled) indented cylinder equipped with round-role perforated metal was developed. The new model was reported to have self-cleaning capability in the form of a brush that rotates with the cylinder and removed seeds lodged in the holes of the perforated metal. The concluding remarks mention that the separation was influenced mainly by cylinder rotational speed ω, cylinder slope (with current model fixed at 0.7°; see Figure 11 on page 34), and the working angle α of the collecting bin.

Churchill et al. (1989): Churchill et al. made some interesting and early attempts at achieving a reproducible set of rules (a "decision-support system") for length separation using the indented cylinder (laboratory-scaled). They used three different rotational speeds ω, three different indent working diameters d (here called "pockets" instead of "cells"), and three different collecting-bin working angles α – resulting in a total of 27 experiments. An early computer vision system was used to measure the lengths of precleaned Stevens wheat. The authors concluded that all three parameters had significant impact on the length distribution of seeds in the lifted fraction ("short" seeds) and no significant impact in the length distribution of seeds in the unlifted ("long" seeds) fraction.

Choon-Ki et al. (2009): Choon-Ki et al. looked at the indented cylinder (laboratory-scaled) for finding the optimum operation conditions for removing broken rice. They used 41 different varieties of rice, three different indent working diameters r, and three different settings of the collecting-bin working angle α (rotational speed ω was apparently not varied). The work was summarised by giving recommendations on the indent working diameter for different rice varieties.

Huimin et al. (2011): Huimin et al. presented an overview of the important mechanical laws governing the motion of the long and short seeds in the indented cylinder. The equations that they arrived at, are mostly similar to those previously given by Grochowicz (see Grochowicz, 1980, chp. 7).

Buus et al. (2011): This work represents the first published paper (Paper I) from this PhD Project and the printed version from the SCIA[1] 2011 proceedings is available in Appendix A (page 75). This and other work written as a result of the scientific work carried out in this PhD project is addressed more directly in Section 3.1 (page 33). Buus et al. installed a high-speed machine camera in front of a laboratory-scaled

[1]Scandinavian Conference in Image Analysis.

(a) Indented cylinder shown with doors. (b) Same model shown without doors.

Figure 7: Industry-scale indented cylinder (Westrup A/S, TR series) shown with and without doors. This particular series supports cylinders with a diameter of 600 mm and a length from 1910 mm to 2910 mm. Source: Product brochure with specifications (reprinted through the courtesy of Westrup A/S, Denmark).

indented cylinder. The image sequences were post-processed and time-series of angle of escape θ were extracted. The materials and methods and the results are further described in Chapter 3 (page 33) and Section 4.1 (page 47), respectively.

Sorica et al. (2012): The work by Sorica et al. is highly relevant and presents some important conclusions. A high-speed camera was installed in front of a laboratory-scaled indented cylinder in much the same way as it was done in the experiments of this PhD project (Buus et al., 2011). Sorica et al. applied the use of variables from the indents themselves to construct a physical model used to simulate angle of escape θ and the parabolic trajectories of short seeds (impurities). A good correlation is shown between model and reality and this despite simplifying assumptions in the mathematical model such as the use of point-masses and the neglection of any drag forces on the seeds.

The works by Choon-Ki et al. (2009) and Sorica et al. (2012) represent the only literature published by others, that is directly comparable to the work of this PhD project – especially when it comes to the experimental methods applied (Buus et al., 2011). These works, among others, will be revisited in Chapter 4 where their importance and relevance will be discussed.

1.3.3 Two Different Scales

The indented cylinder is available in two different scales: (1) industry scale and (2) laboratory scale. Figure 7 shows an example of an industry scale indented cylinder model – with and without doors. Several of such cylinders are usually combined in series such that the output from one cylinder is further separated in a second cylinder. It is not unusual to see four or more cylinders combined in a series. Such configurations make it possible to increase capacity and carry out complicated separations with multiple outputs and process raw material containing particles of several different

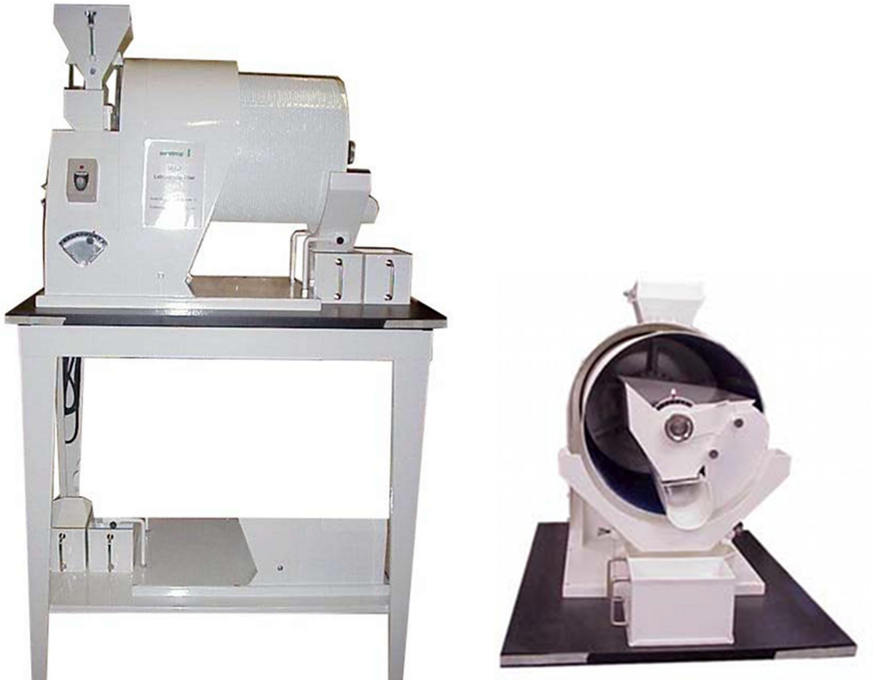

(a) Laboratory scaled indented cylinder seen from the side.

(b) Same model seen from the front.

Figure 8: The laboratory scaled indented cylinder (Westrup LA-T model). Source: Product brochure with specifications (reprinted through the courtesy of Westrup A/S, Denmark).

lengths. The experiments carried out in the PhD project were all done using a single laboratory scaled indented cylinder (Westrup LA-T model). Such a device is depicted from two different angles in Figure 8. This models supports cylinder with a radius of $r = 200\,\text{mm}$ and a depth of $500\,\text{mm}$.

It was generally *not* assumed that the conclusions drawn from experiments, using the laboratory scaled indented cylinder, were directly applicable to industry scaled indented cylinders. The differences in both cylinder diameter and length should not be ignored. This issue of scale is important in other industries where the rotating cylinder is used as well (Ding et al., 2001; Demagh et al., 2012).

Figure 9 shows two schematics of the laboratory scaled indented cylinder. The schematic in Figure 9a gives an overview of the various components of the indented cylinder. These are:

1. The cylinder itself (also sometimes referred to directly as the mantle of the indented cylinder machine).

2. A knob used to loosen the collecting bin and adjusts its angle. This collecting bin is mounted on an axial support as seen in Figure 8b.

3. Vibrating feeder for introducing a continuous flow of material into the cylinder. The schematic in Figure 9b shows how the seeds fall from the vibrating feeder and enters the volume of the cylinder.

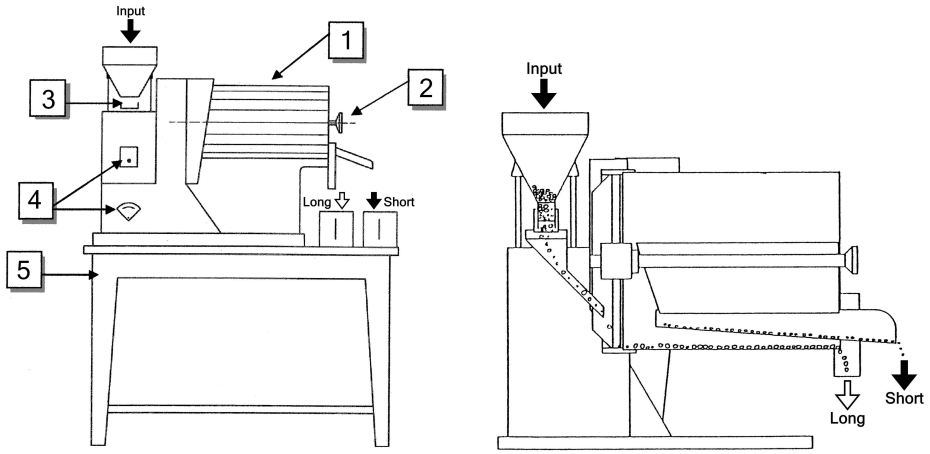

(a) (b)

Figure 9: Technical representations of the laboratory scaled indented cylinder. Source: Langkilde and Nydam (1973).

4. Switches for controlling the vibrating feeder (top) and the rotational speed (bottom). The rotational speed was controlled by adjusting the tension in the gear-belt driving the cylinder. This was physically done by changing the position of the electric motor by the use of this knob. The rotational speed was an important independent variable in the experiments and was thus changed a great number of times.

5. The main on/off switches.

1.3.4 Granular Materials in Rotating Cylinders

Rotating cylinders are used in many industrial processes for separation as well as for mixing. Understanding the behaviour of granular material in rotating cylinders (and kilns as well) is important for modelling segregation and mixing of industrial particles (Ristow, 2000; Seiden and Thomas, 2011). Hajra and Khakhar (2011) investigated the radial segregation of ternary mixtures in a rotating cylinder and Ward and Hourigan (2012) looked at the general segregation of binary mixtures in a tilted rotating cylinder.

One interesting fact about granular media, is that it has an ability to segregate when shaken (Ottino and Khakhar, 2000). The larger particles of the disturbed media will tend to rise to the surface – an effect usually referred to as the "Brazil-nut effect" (Mobius et al., 2001). This can be a problem for certain industries that rely on the optimal mixing of powders and other types of granular media (Obregón et al., 2010a,b; Bridgwater, 2012).

The interesting technology known as positron emission particle tracking (PEPT) is of high relevance here. Introduced by Parker et al. (1993), PEPT is used for achieving an in-depth understanding of the flow of granular material in engineering equipment (Leadbeater and Parker, 2011; Leadbeater et al., 2012). The basic idea is to introduce one or more radioactive particles

into a granular material. The particle's emission of γ-rays is hereafter used to infer their three-dimensional position in a finite volume of space. Parker et al. (1997) reported on the use of PEPT for the tracking of spherical particle motion in rotating drums.

In other works (e.g. Pöschel and Buchholtz, 1995; Pereira et al., 2011; Third et al., 2011) the movement of granular material in rotating cylinders has been simulated by computer – usually by applying the popular *discrete element method* (DEM) proposed by Cundall and Strack (1979). The relatively recent reviews by Zhu et al. (2007) and Zhu et al. (2008) gives a broad overview of the literature dealing with simulations of granular material (or "particulate systems"). Of these two reviews, Zhu et al. (2007) also gives a very useful introduction to the theory of DEM simulations.

1.4 Empirical Model Development

The field known as empirical model development, or more specifically as "system identification", deals with estimating mathematical models from observed dynamic states (time series) of inputs and outputs to and from some physical system under investigation (Ljung, 1999, 2010). Ogunnaike and Ray (1994, p. 645) and Pearson (2003) specify three important problems involving a set U of inputs, a set Y of outputs, and a model M:

- Simulation: Given M and U, determine Y.
- Control: Given Y and M, determine U.
- Identification: Given U and Y, determine M.

1.4.1 Experimentation

A mathematical model M estimated through system identification would represent a general relationship between the inputs and the outputs of the physical system S – in this case the indented cylinder (laboratory scaled). Estimating such a model from observations require that experimentation with the indented cylinder is somehow technically possible. The above set of three problems is therefore extended with experimentation as a fourth problem. They can now all alternatively be defined as follows:

- Simulation: Given M and U, determine Y (system S is not involved).
- Control: Given S, Y, and M, determine U.
- Identification: Given S, U, and Y, determine M.
- Experimentation: Given S and U, determine Y (model M is not involved).

The problem of experimentation now involves a real physical system S with which you can experiment, i.e. manipulate input U and observe the corresponding output Y. Model M represents a mathematical approximation of physical system S.

Questions

Experimentation is the task of sampling output Y of the indented cylinder – given a known input U. This task represents a technical and scientific non-trivial problem. To even begin to address it, one must find answers to the following two questions:

- What set of variables should be considered as input and output?
- What kind of mechanism or sensor could be used for observation of the chosen output variables?

1.4.2 Input-Output Variables of the Indented Cylinder

The two identifiers U and Y are both without any kind of mathematical structure. A set of measurable input variables and set of measurable output variables will need to defined for experimentation to be possible.

Variables for input U

Input U of the indented cylinder could consist of the following:

1. Statistical properties of the length of the seeds in the input material, length being the longest dimension of a seed – as exemplified in Figure 3 (8). As mentioned briefly in Section 1.3.1, these will likely be properties of a univariate mixture density consisting of a number of normal components/sub-populations (see, for instance, Frühwirth-Schnatter, 2006, chp. 1, for a thorough introduction to the theory and notation of mixture distributions).
2. The three input parameters as defined in Section 1.3.1:
   a) the cylinder rotational speed ω,
   b) the indent working diameter d,
   c) and the working angle α of the collecting bin.

Variables for output Y

The exact choice of output variables will depend on at least the following two concepts: (1) measurability and (2) relevance. Measurability again depends on the choice of sampling mechanism or sensor and relevance depends on the purpose of the system under investigation.

The project took use of digital imaging and methods from computer vision as the mechanism for empirical sampling of output variables of the indented cylinder. The variables therefore had to be observable to a digital camera. Alternatively, if this was not the case, it had to be possible to derive the variables from the raw pixels using methods from computer vision.

In regards to relevance, the chosen set of output variables had to carry information about the performance of the indented cylinder, i.e. how efficient it was at separating the input material. In other words, digital imaging and methods from computer vision were used to derive a measure of "separation efficiency".

1.4.3 A Measure of Separation Efficiency

Section 1.3.1 introduced the concept of the unlifted and lifted fractions of the input material. This was referred to as the lifting phenomenon. This is a continuous phenomenon with measure of separation efficiency – or **SE** measure.

A definition

This work implemented the following definition of an **SE** measure of the indented cylinder:

- any statistical difference between two univariate probability density functions that pairwise model the estimated probabilities of angle of escape θ for seeds in the lifted and unlifted fraction.

The above definition, intentionally kept mathematically unspecific, requires that estimations of probabilities of angle of escape θ are available. Such probabilities will have been estimated from the data available in two time series holding values of angle of escape θ (in its full range from $-\pi/2\,\text{rad}$ to $\pi/2\,\text{rad}$) sampled from the indented cylinder process using digital imaging and methods from computer vision over a finite period of time.

The magnitude of the **SE** measure will depend, at least, on the two parameters ω and d. A parameter which it will be entirely independent of, is the working angle α of the collecting bin. This parameter governs only the final sorting result and ω and d can be adjusted fully independently of α.

The basic idea

Although Chapter 2 will define a more specific set of technical hypotheses, the basic idea is as follows: Consider the experimental scenario in where a high-speed machine vision camera is installed in front of the opening of a laboratory scaled indented cylinder, such that it observes a scene similar to the one depicted in Figure 5 (page 12). Consider now the content of high speed recordings of such a scene. The resulting image sequences will contain

individual seeds caught in mid-air after having been thrown off the rotating inner cylinder surface at different values of angle of escape θ.

If methods from computer vision, applied to each image (or frame) in a high speed image sequence, are able to (i) detect the presence of individual seeds, (ii) estimate their real-world location, and (ii) individually classify them as either a "short" or a "long" seed (given that the input material consist of two sub-populations), and if a plausible model for a seed's trajectory can be devised, then it should be possible to derive the corresponding angle of escape θ from the estimated location of each detected seed. This becomes particularly simple if a seed's trajectory is assumed to follow a parabolic curve (see Buus et al., 2011, also available in Appendix A).

This technical solution has a few assumptions. First of all, it is assumed that a seed leaves the cylinder inner surface in a plane closely perpendicular to the rotational axes of the cylinder. Secondly, this plane is also assumed to be closely perpendicular to the line-of-sight vector introduced into the geometry because of the machine vision camera. Thirdly and finally, the concept of "closely" is assumed to involve an error small enough so that it can be ignored. Section 3.2 describes the exact details behind the experimental setup used in the work (the "model of observation").

Stochastic processes and random variables

Let the pair of time series of observations of angle θ^{long} and θ^{short} (see Section 1.3.1) be modelled as the realisations of two stochastic processes of K random variables:

$$\text{(i)} \quad \Theta_1^{\text{long}}, \ldots, \Theta_K^{\text{long}} \qquad \text{and} \qquad \text{(ii)} \quad \Theta_1^{\text{short}}, \ldots, \Theta_K^{\text{short}} \,,$$

respectively.

Interestingly, this way of mathematically expressing the data available is not general enough. One cannot be sure about the number of seeds detected at each time step – this will fluctuate. There could even be time steps with no observations. Each observation in each of the two time-series will therefore consist of an individual number of scalar θ values. It will be a vector time series but with a varying vector length for each time step. This had an impact on the way data from these time series was used. One way to deal with this technicality, was to simply aggregate observations from all K time steps into two sets or (very) high-dimensional vectors $\boldsymbol{\theta}^{\text{long}}$ and $\boldsymbol{\theta}^{\text{short}}$. This form of full aggregation became the method of choice in most cases – except when time indices were needed. Chapter 3 will further specify the details of these and other choices made in the actual scientific work carried out.

Estimating the SE measure

The content of vector $\boldsymbol{\theta}^{\text{long}}$ and $\boldsymbol{\theta}^{\text{short}}$ can be used to estimate the parameters for an appropriate choice of univariate parametric distribution (location-scale family). This will result in two probability density functions: (1) a model for the distribution of angle of escape θ^{long} for unlifted seeds (i.e.

"long" seeds) estimated from the contents of $\boldsymbol{\theta}^{\text{long}}$, and (2) a model for the distribution of angle of escape θ^{short} for lifted seeds (i.e. "short" seeds) estimated from the contents of $\boldsymbol{\theta}^{\text{short}}$. The **SE** measure is thus any statistical distance between these two fitted probability density functions.

Statistical distances

Statistical distances are measures of distance between two random variables or two probability distributions. One example of a statistical distance is the Hellinger distance (Hellinger, 1909; Nikulin, 1989). This distance is also known as the Jeffreys-Matusita distance (Matusita, 1956, 1955; Bruzzone et al., 1995) and can be used to quantify the similarity between two probability distributions.

The Hellinger distance $H(f, g)$ between two probability density functions $f(x)$ and $g(x)$ is the square root of the squared Hellinger distance defined as

$$\begin{aligned} H^2(f,g) &= \frac{1}{2}\int\left(\sqrt{f(x)}-\sqrt{g(x)}\right)^2 dx \\ &= 1-\int\sqrt{f(x)g(x)}dx \\ &= 1-BC(f,g) \\ &= \frac{1}{2}\left\|\sqrt{f}-\sqrt{g}\right\|_2^2 \ , \end{aligned}$$

where $BC(f, g)$ is the Bhattacharyya coefficient (Bhattacharyya, 1943). The Hellinger distance goes from 0 (zero) to 1 (one). A distance of 0 corresponds to a complete similarity between f and g and a distance of 1 to no similarity. The use of the L_2-norm also indicates that the Hellinger distance satisfies the axioms of a true metric: nonnegativity, symmetry, and the triangle inequality.

Chapter 2 will extend on the details covered in this section. It will specify the motivation, overall aim(s), and define the technical hypotheses and objectives of the work needed to acquire the θ time series using the proposed technologies of digital imaging and methods from computer vision.

Chapter 2

Aims and Objectives

2.1 Motivation

As mentioned in the beginning of Chapter 1, physical purity is one of several important seed quality parameters. Achieving a high separation efficiency naturally leads to a higher physical purity in the resulting seed material(s). It can therefore also be argued that high separation efficiency leads to a high seed quality of the end-product. This is a very important potential outcome since ensuring that seeds are of high quality is required for alleviating some of the important agricultural challenges mentioned in Section 1.1.

That section also made it clear that the seed sorting mechanisms used to achieve physical purity in seeds involve a high system complexity. This complexity usually makes it difficult to use seed sorting machinery in an optimal way. It would be of high relevance for the seed cleaning industry if this difficulty could somehow be minimised. For instance, much hands-on experience is required by technicians before they are able to successfully initialise and adjust sorting machines for an optimal outcome (personal communication: Westrup A/S).

An insight into how the input affects the output of the process in the indented cylinder could represent a possible minimisation of the complexity involved in achieving an optimal use or configuration of this machine. An optimal configuration of the indented cylinder can be loosely defined as a configuration that most likely will result in the best possible separation between long and short seeds. Achieving such an insight could arguably bring more certainty into the expected outcome of the binary separation between long and short seeds and it could also lessen the requirements for training technicians.

2.1.1 Modernisation of a Technological Paradigm

Agriculture is of course not a new thing and seed sorting was needed in ancient times as well. Investigations into the history of agriculture have helped pinpoint when man started to systematically take advantage of plants and animals – the act of which is known as domestication. Vavilov (1926) was the first to look at the history of domestication of plants and animals. This

cultural phenomenon apparently began many thousands of years ago. Different regions of the world started at different times: Turkey, 10 000 years ago (Braidwood et al., 1969); Thailand, 13 000 years ago (Gorman, 1969); and Mexico, 8000 years ago (MacNeish, 1964).

However, today, thousands of years later, generally not much innovation seems to have taken place for the industry in the applied technologies. Most of the machines used today for seed conditioning are basically improved versions of the ancient original ideas on the employment of individual physical characteristics of seeds for separating them.

Carrying out the most optimal sorting or separation seems to be based a great deal on the principles of rule of thumb. For instance, Langkilde and Nydam (1973) mention that "seeds with a length of less than 2/3 of the [indent] diameter will be carried upwards by the cylinder rotation". Another example is Madsen and Langkilde (1987a) who mention that "a speed of approx. [36 r/min] is suitable for most seeds". Moreover, according to Madsen and Langkilde, other seeds might be better cleaned at a rotational speed ω from 25 r/min to 30 r/min.

Such rules of thumb represent a set of heuristics that can be used for optimal adjustment of cleaning machines. Other examples of heuristics are those by Madsen and Langkilde (1987b). Madsen and Langkilde present numerous flow diagrams with optimal choices for cleaning procedures for a large number of seed species. Such heuristics and diagrams are all examples of simple models of seed cleaning and sorting and to derive them must have required a great deal of early experimentation. The seed industry would benefit greatly from continued experimentation and research into this area.

Technologies for seed conditioning are essential tools for making some staple foods available for mankind on a global scale (Gregg and Billups, 2010b). The industry demands high efficiency on both quantity and quality. Any mathematical model, however complicated, would need to take this contradiction into account. This is difficult and there might be too many heuristics to cover, too many species of seeds, too much seasonal variation, too much dust, too many insects, stones, stems, leaves, dead seeds, ... for any form of paradigm shift to occur over night.

Finally, since granular materials are ubiquitous, the seed industry might not be the only industry that, in the long run, could benefit from a continued effort. Any solutions developed could perhaps be made generally applicable for identification of a greater range of machines with which granular material is manipulated using rotating cylinders.

2.2 Overall Aim

The overall aim of this work was to achieve an insight into the relationship between the input and the output of the process in an indented cylinder – specifically a laboratory scaled version of an indented cylinder. Achieving this insight requires the use of concepts from from the area of empirical model development – especially system identification and experimentation.

For system identification to be possible, the problems of experimentation had to be addressed first.

A more specific overall aim therefore became to solve the technical problem of experimentation as described in Section 1.4.1. With this technical aim in mind, the following following primary and secondary overall aims were specified:

Primary overall aim: Estimate an **SE** measure of a laboratory scaled indented cylinder as defined in Section 1.4.3. Do this for a fixed choice of input material and for a preselected range of input variables ω and d.

Secondary overall aim: Determine the ranges of input variables ω and d that can result in the largest **SE** of a laboratory scaled indented cylinder.

Achieving the secondary aim was naturally contingent on achieving a working solution to the primary aim. Section 5.1 revisits these aims and concludes on them.

2.3 Hypotheses

The definition of the **SE** measure in Section 1.4.3 involves the existence of univariate probability estimates of angle of escape θ for both long and short seeds. Achieving an estimate of the **SE** measure therefore directly depends on the technical feasibility of somehow acquiring probability estimates of angle of escape θ.

This work proposes that digital imaging and methods from computer vision/image analysis can be used for this. This proposal of tool is used directly as the following main hypothesis of this thesis:

- The observation/sampling of an **SE** measure of the indented cylinder can be made possible by the use of digital imaging and methods from computer vision.

Consider the experimental scenario in where a high-speed machine vision camera is installed in front of the opening of a laboratory scaled indented cylinder such that it observes a scene similar to the one depicted in Figure 5 (page 12). That scene shows how individual seeds are being thrown off a rotating inner cylinder surface at different values of angle of escape θ.

With such a scenario the following can be considered plausible:

1. Individual seeds will be visible in each recorded high speed digital image or frame and can be detected and segmented from the background.

2. The two-dimensional location of each seed in each frame can be estimated and used to mathematically derive the corresponding angle

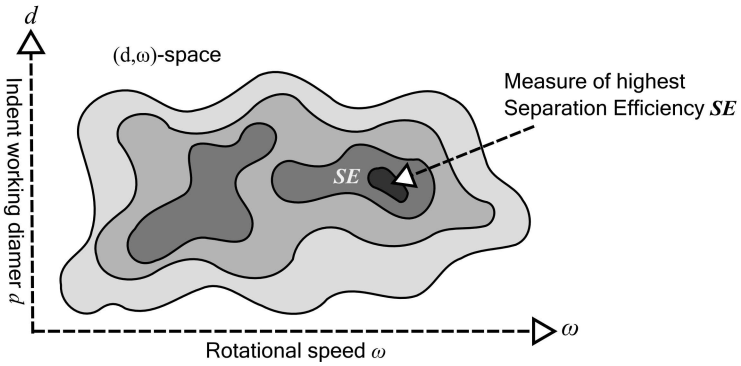

Figure 10: The "separation efficiency" (**SE**) measure in a (ω, d)-space.

of escape θ on the circumference of the cylinder, making possible the sampling of a time-series of angle of escape θ values.

3. If more than one class of seed (e.g. difference in species) is used in the seed mixtures introduced to the laboratory scaled indented cylinder in the experiments, the individual seeds can each be classified as their correct class by the use of supervised or non-supervised learning techniques.

4. The combination of the location estimate and classification of individual seeds, makes possible the sampling of time-series of angle of escape θ for each class/species of seed used.

2.4 Objectives

The following objectives were defined:

1. Design high speed digital imaging experiments with the intent of recording the movement of seeds when they are being physically manipulated inside an operating laboratory-scaled indented cylinder. The contents of the recorded scene should be comparable to the contents of the technical drawing shown in Figure 5 (page 12).

2. Carry out such imaging experiments for:

   a) a number of cylinder rotational speeds ω_i,

   b) for a number of indent working diameters d_i,

   c) and for a number of different mixtures of seeds – of both the "unary" and "binary" kind. The unary mixtures should contain only one sub-population of seeds. There should be two unary mixtures: (i) one corresponding to "long" seeds and (ii) another one corresponding to "short" seeds. The binary mixtures should contain two sub-populations of seeds: (i) one that corresponds to "short" seeds and (ii) another one that corresponds to "long"

seeds. The different mixtures should vary in their mixture ratios of these two sub-populations.

3. Post-process the resulting high-speed sequences of frames by the use of methods from computer vision. Select among existing computer vision methods or develop new computer vision methods to solve the following post-processing problems:
   a) segmentation/detection of individual seeds from the background,
   b) and (if possible, for the binary mixtures) classification of each detected seed as being either a "long" or a "short" seed. This classification step is needed to re-acquire knowledge on which of the two input sub-populations each seed originate from.
4. Develop a mathematical model that describes the two-dimensional trajectory of a seed from the point at which it leaves the inner surface of the cylinder.
5. For each of the previously chosen values of ω_i, d_i, and input mixtures, do the following:
   a) For each seed detected in each high speed frame, estimate its approximate two-dimensional real-world location.
   b) For each seed detected in each high speed frame, estimate its corresponding angle of escape θ at which it left the inner cylinder surface. This requires a combination of the previously estimated two-dimensional location and the previously developed model that described a seed's two-dimensional space-trajectory.
   c) Combine these estimate of θ from all times into a (vector) time series. If classification of "long" and "short" seeds were possible, then create two vector time series: (ii) one with time-indexed vectors containing estimated values of angle of escape θ for 'long" seeds, and (2) another one with time-indexed vectors containing estimated values of angle of escape θ for 'short" seeds.
   d) If two time series are available, estimate an **SE** measure by using the (aggregated) contents of the two time-series for "long" and for "short" seeds.
6. Determine the ranges of values for ω_i and d_i in which the local maximum **SE** measure were estimated.

The last objective above corresponds to determining a maxima in a predetermined discrete (ω, d)-space. Figure 10 exemplifies this by graphically emphasising a subset of (ω, d)-space for which the maximum **SE** measure was estimated.

Details on the applied materials and methods are presented in Chapter 3. Chapter 4 presents an overview of the results and discusses them in relation to recent related work. The work is concluded in Chapter 5 with some perspectives on future work.

Chapter 3

Materials and Methods

3.1 On the Written Work

This thesis also contains Appendix A, B, and C – each respectively holding a copy of the written body of research work: Paper I, II, and III. The work in these three papers address all the objectives of the research at different levels of complexity and by the use of different methods. The three papers show results derived from two distinct sets of imaging experiments.

The results of Paper I were derived from the first set which involved the use of broken and whole barley (*Hordeum vulgare* L.) seeds in the indented cylinder. Paper II and III are companion papers and the results that they present were derived from the second set of imaging experiments. These experiments involved the use of polished rice (*Oryza sativa* L.), wheat (*Triticum aestivum* L.), and cannabis (*Cannabis sativa* L.) seeds. The same laboratory scaled indented cylinder was used in both sets of experiments and the two experimental approaches were similar though with some minor technical differences. The specific model of the laboratory scaled indented cylinder was a Westrup LA-T model. This models supports cylinders with a radius of $r = 200\,\text{mm}$ and a depth of $500\,\text{mm}$.

3.2 A Model of Observation

Computer vision was used for the observation of an indented cylinder actively manipulating and separating seeds. The intent with this observation was to derive empirical data from the physical state of the seeds. The experimental approach was to place a machine vision camera in front of the opening of the cylinder as seen in Figure 11 in such a way that the seeds could be observed while in motion inside the cylinder. This figure is also available in its original context in Paper II as Figure 7. One important detail: The collecting bin was removed before doing any imaging experiments. It was found to be too large an obstacle – the seeds and their fall trajectories were simply not visible with the collecting bin mounted. The removal of the collecting bin obviously disabled the machine's ability to do any actual sorting. This fact was of no particular concern as the primary focus

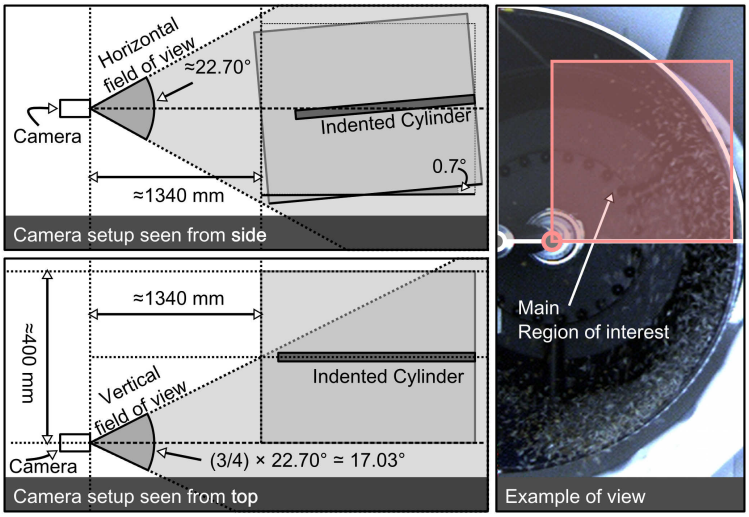

Figure 11: Geometry of camera setup as used in the experiments of Paper II.

was entirely on the inner cylinder surface and its ability to carry out the separation given choices of ω and d.

3.2.1 The scene model

The scene observed by the camera is best described by the "scene model" depicted in Figure 12a. This model is a circle with the four quadrants I, II, III, and IV highlighted in different shades of grey. Only quadrant I and IV were recorded in the experiments and of these two, only the upper quadrant I was analysed. The dynamics of the granular material in the bottom of the cylinder was thus not investigated in this research.

Simplifying assumptions

In previous models of the indented cylinder, the modelling was done in two dimensions (Grochowicz, 1980; Huimin et al., 2011). This work did the same, and a seed's parabolic trajectory was therefore modelled as being confined to a plane in three-dimensional cartesian space. This plane was first and foremost assumed to be parallel with gravity vector $\boldsymbol{g} = [0, -g, 0]^\top = [0, -9.82\,\mathrm{m\,s^{-2}}, 0]^\top$. The camera was levelled using a bull's eye spirit level on the camera tripod. The camera's "line-of-sight" vector could thus be considered perpendicular to gravity vector $\boldsymbol{g}$ as well. The parabolic trajectories observed in the image sequences were therefore considered parallel to the image plane in the local camera coordinate system (perspective distortion was ignored). This image plane was also assumed to be perpendicular to the cylinder's own axis of rotation, although it would not be exactly perpendicular due to the slight horizontal tilt that the experimental scale indented cylinder has with a horizontal baseline (about 0.7° in the actual model used).

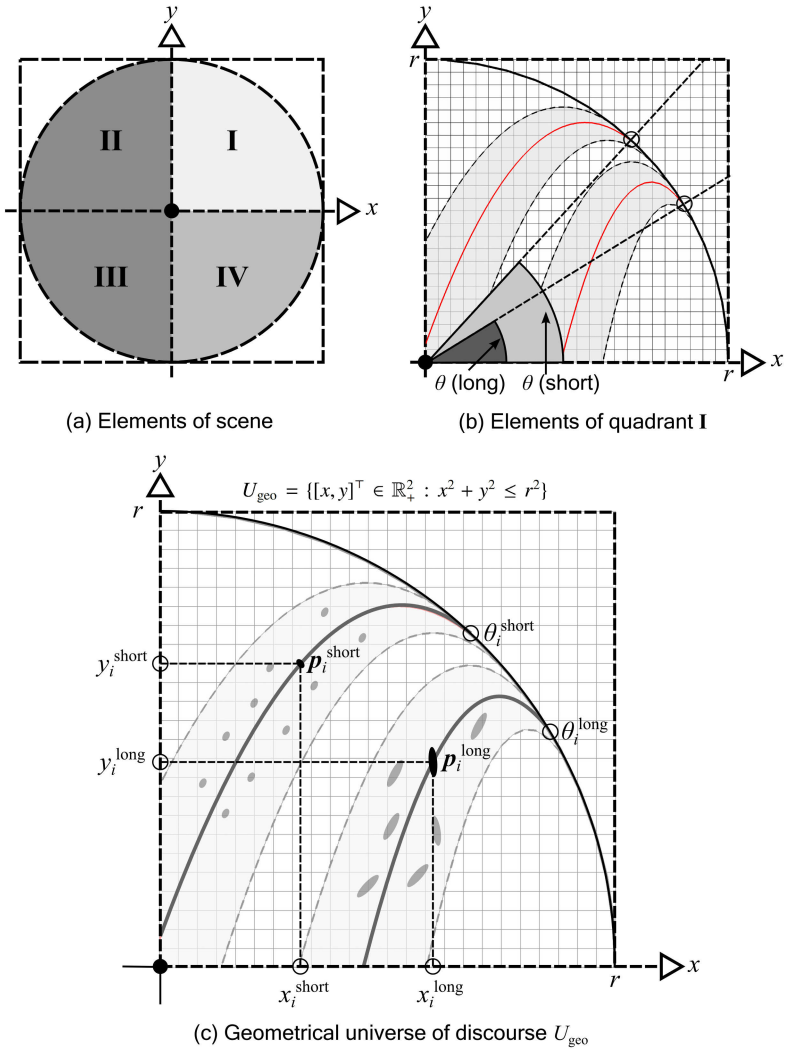

(a) Elements of scene (b) Elements of quadrant **I**

(c) Geometrical universe of discourse U_{geo}

Figure 12: Elements of scene model and geometrical universe of discourse U_{geo}: (a) The "scene model" – a circle that represents the basic geometric foundation of the "model of observation"; (b) Quadrant I of the scene model with the two bundles of parabolas superimposed; (c) The geometrical universe of discourse U_{geo} is the space where the physical modelling takes place. This space is defined as a subset of two-dimensional cartesian space (r is the radius of the indented cylinder).

3.2.2 Bundles of seed trajectories

When a seed leaves an indent, whether short or long, the most obvious and simplest assumption is that it will do so in a parabolic trajectory – influenced now only by gravity $\boldsymbol{g}$. The angle at which a particle leaves the cylinder, is here referred to as the "angle of escape" θ. Angle of escape θ is an absolutely crucial variable and it plays a major role in the definition of the **SE** measure. Figure 12b shows quadrant I of the scene model (r is the radius of the indented cylinder). Two bundles of seed trajectories are superimposed onto this figure as ideal parabolic curves. These curves are tangent to the

cylinder circumference at an angle of escape θ. The upper set of parabolic curves represents trajectories for short particles and the lower set of curves represents trajectories for long particles. The location and spread of these two bundles will be characterised by the stochastic nature of angle θ^{long} and θ^{short}.

A geometrical universe of discourse U_{geo}

Figure 12c shows the region of the (x, y)-plane ($\mathbb{R}^2$) that corresponds to the (projected) volume of space observed in the experiments. This geometrical universe of discourse was defined as $U_{\text{geo}} = \{[x, y]^\top \in \mathbb{R}^2_+ : x^2 + y^2 \leq r^2\}$; i.e. a subset of the two-dimensional set of non-negative real numbers $\mathbb{R}^2_+ = \{[x, y]^\top \in \mathbb{R}^2 : x \geq 0 \wedge y \geq 0\}$. The origin $[0, 0]^\top$ was mapped to the centre of rotation of the cylinder as a point of reference. This area was recorded with a colour machine vision camera catching visible seeds in mid-air at discrete points in time. The basic computer vision tasks were to establish the following two things about each seed visible in each frame: (1) its location $\boldsymbol{p} \in U_{\text{geo}}$ and (2) its class – i.e. whether it is long or short. These two tasks represented some interesting challenges due to the scene's complexity in number of individual objects, unavoidable problems with self-occlusions, noise, etc. The method sections in the three papers all primarily focus on the computer vision techniques used to solve these two tasks. Especially Paper III, which has a substantial focus on both theory and software implementation. The work in Paper I involves only the first task.

3.2.3 Estimation of angle of escape θ

The estimated location of any visible seed detected in quadrant I is modelled as a point $\boldsymbol{p} = [x, y]^\top$ in U_{geo}. The assumption is that this seed will have been caught in mid-air in a free fall parabolic trajectory. Point $\boldsymbol{p}$ will thus be assumed to intersect a parabola that is tangent with the cylinder circumference at angle of escape θ with the x-axis. The problem of estimating angle of escape θ from point $\boldsymbol{p}$ was addressed as a minimisation problem in $\mathbb{R}$. Section 3.2 of Paper I presents a numerical solution to this problem and Section 4.2 of Paper III presents a closed-form solution.

The intermediate results from the image analysis (involving detection and classification) and the post-processing (involving the estimation of θ from point $\boldsymbol{p}$) was two time-series of θ^{long} and θ^{short} sampled over a finite duration of time (5 s in Paper I and 10 s in Paper II+III). Two such time-series were sampled for each chosen setting of ω and d and in Paper II+III also for a number of different mixture ratios of long and short seeds.

Random variables

Section 1.4.3 defined this pair of time series of observations of angle θ^{long} and θ^{short} to be, respectively, the realisations of two stochastic processes of

random variables:

$$\begin{aligned} &\text{(i)} \quad \Theta_1^{\text{long}}, \ldots, \Theta_k^{\text{long}}, \ldots, \Theta_K^{\text{long}} \quad \text{and} \\ &\text{(ii)} \quad \Theta_1^{\text{short}}, \ldots, \Theta_k^{\text{short}}, \ldots, \Theta_K^{\text{short}} \, . \end{aligned}$$

No assumption were made about the exact distribution or interdependency of the individual random variables in each of these two time series. For a time series, it is generally not safe to assume anything other than a form of dependency between each random random variable (Chatfield, 2004, chp. 1).

The number of seeds detected at each time step was not considered deterministic due the dependence on the correctness of the algorithmic choices from the image analysis. It was is therefore assumed that the number of observations would fluctuate over time for both time series. Results from Paper II even show this to be true for rice. This represented a problem for the statistical analysis – especially of time series analysis was needed. The simplest approach became to aggregate all observations from all K time steps from either time series into two individual vectors $\boldsymbol{\theta}^{\text{long}}$ and $\boldsymbol{\theta}^{\text{short}}$.

The data available in these two high-dimensional vectors can be modelled as being the realisation of two new *normally distributed* univariate random variables: (i) $\Theta_{\text{A}}^{\text{long}}$ and (ii) $\Theta_{\text{A}}^{\text{short}}$. The subscript "A" denotes the fact that these are the aggregated data sets from all time steps. These variables have expected values $\mu_{\Theta,A}^{\text{long}}$ and $\mu_{\Theta,A}^{\text{short}}$, and standard deviations $\sigma_{\Theta,A}^{\text{long}}$ and $\sigma_{\Theta,A}^{\text{long}}$.

3.2.4 On the SE measure

The width of the gap between the two trajectory bundles introduced in Figure 12b quantifies how easy it will be to adjust angle α in such a way that a minimum amount of overlap will occur in the final sorting outcome. A larger such width will naturally make this task easier and thereby increase the overall likelihood of a minimum overlap in the final sorting outcome. The width of this gab between the two groups of particles leaving the inner surface is one way of quantifying the "efficiency" of the lift: The larger a gap created by the inner surface and its movement, the higher the efficiency can be said to be. The width and location of this gap is measured on the circumference of the cylinder in U_{geo} and is thus expressed on the same domain as the angle of escape θ.

The **SE** measure was therefore defined as any statistical difference between two normal distributions with expected values (population averages) $\mu_{\Theta,A}^{\text{short}}$ and $\mu_{\Theta,A}^{\text{long}}$, and standard deviations (population spreads) $\sigma_{\Theta,A}^{\text{short}}$ and $\sigma_{\Theta,A}^{\text{long}}$.

Paper I did not involve an actual analysis of the **SE** measure, but focused primarily on extracting individual data sets of θ values for analysis. Paper III, on the other hand, made a substantial contribution to the definition of the **SE** measure. Paper III used two different statistical distances:

(1) numerical difference of population averages $\mu_{\Theta,A}^{\text{short}}$ and $\mu_{\Theta,A}^{\text{long}}$ and (2) the Hellinger distance between the two normal distributions.

The closed-form expression of the squared Hellinger distance $H^2(P,Q)$ between two normal distributions $P \sim \mathcal{N}(\mu_1, \sigma_1^2)$ and $Q \sim \mathcal{N}(\mu_2, \sigma_2^2)$ is as follows:

$$H^2(P,Q) = 1 - \sqrt{\frac{2\sigma_1\sigma_2}{\sigma_1^2+\sigma_2^2}}\,\exp\left(-\frac{1}{4}\frac{(\mu_1-\mu_2)^2}{\sigma_1^2+\sigma_2^2}\right) \quad .$$

In contrast to the numerical difference of population averages, the Hellinger distance also takes into account the population spreads $\sigma_{\Theta,A}^{\text{short}}$ and $\sigma_{\Theta,A}^{\text{long}}$ (Hellinger, 1909; Matusita, 1955, 1956; Bruzzone et al., 1995; Nikulin, 1989).

3.3 Imaging Experiments and Analysis

Papers I, II, and III all share some details in the overall approach. All three papers present results from experiments in which a camera was placed in front of the indented cylinder and the motion of the seeds were recorded for later analysis using various computer vision techniques. The same camera was used for all recordings: a Point Grey Grashopper (GRAS-03K2C-C) colour machine vision CCD camera with VGA resolution (640×480 pixels). The camera was placed at a distance such that the width of the cylinder (400 mm) corresponded as closely as possible, width the width of the projected scene onto the CDD sensor (as per the model of observation described earlier; see Figure 11). Furthermore, all analysis was done in post-processing, i.e. after all recordings had taken place.

3.3.1 Special software for camera control and image acquisition

All recording was done at ∼260 frames/s. This frame rate is faster than normal video (usually at 30 frames/s or less) and the acquisition of images from the camera to secondary computer storage thus required special software. The design and development of such a software utility (internally referred to as "CamClient") became part of the necessary preparations prior to carrying out the first set of imaging experiments. CamClient was built using C++ on 64-bit Linux and the development made use of the Point Grey FlyCapture 2.0 SDK for camera control and image acquisition through the IEEE-1394b interface (Firewire 800). This relatively simple utility allowed the isochronous transfer of images from the camera to the main memory of the computer used. After a recording session was finished, the indented cylinder was stopped and CamClient could be set to copy all images from memory to disk. CamClient was used throughout the project for all high-speed recording.

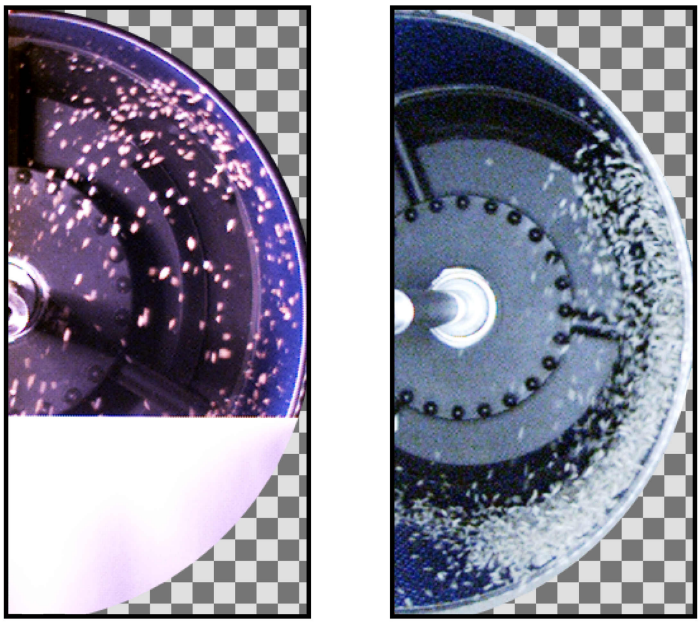

(a) Example of a frame from the first set of experiments

(b) Example of a frame from the second set of experiments

Figure 13: Examples of frames from the two sets of experiments.

3.3.2 Experiments

First set of experiments

These experiments were done using whole and broken barley seeds. The mixture was created using 50 % whole and 50 % broken seeds. These percentages were based on particle count – not weight. Given the assumption that the weight of one broken seed was exactly half of the weight of one whole seed, the final weight ratios w^{whole} and w^{broken} could be calculated by the use of weighted averages (although the weighting cancels out in this particular case):

$$w^{\text{whole}} = \frac{2}{2}\frac{50}{100} \Big/ \left(\frac{1}{2}\frac{50}{100} + \frac{2}{2}\frac{50}{100}\right) = 1 - w^{\text{broken}} = \frac{2}{3},$$
$$w^{\text{broken}} = \frac{1}{2}\frac{50}{100} \Big/ \left(\frac{1}{2}\frac{50}{100} + \frac{2}{2}\frac{50}{100}\right) = 1 - w^{\text{whole}} = \frac{1}{3}.$$

A 2000 g mixture thus contained $\frac{2}{3}2000\,\text{g} = \sim 1333.33\,\text{g}$ of whole barley seeds and $\frac{1}{3}2000\,\text{g} = \sim 666.67\,\text{g}$ of broken barley seeds.

Figure 13a shows an example of a frame from the data set of high-speed image sequences created in these experiments. The camera was configured in such a way that its line-of-sight was vertically parallel with the axis of rotation of the cylinder. Moreover, the focal length of the monofocal lens was 25 mm. The result was an image that, along with projections of the seeds caught in mid-air, also included a highly spatially compressed projection of the inner surface of the cylinder. Illumination for the first set of imaging experiments was provided by a 150 W halogen modelling light (SOLO 1600 B) placed between camera and cylinder.

v	ω_v (r/min)	ω_v (rad s^{-1})
1	26.03	2.73
2	27.19	2.85
3	29.05	3.04
4	31.23	3.27
5	33.96	3.56
6	36.71	3.84
7	39.73	4.16
8	42.60	4.46
9	46.02	4.82
10	49.08	5.14

(a)

s	d_s (mm)
1	5.5
2	6.0
3	6.5
4	7.0

(b)

Table 1: The values for the parameters ω and d: (a) The ten values for the cylinder rotational speed $\omega_1, \ldots, \omega_{10}$ in both r/min (revolutions per minute) and rad s^{-1} (angle frequency); and (b) the four indent working diameter values $d_1, \ldots, d_4$ in mm. The indent diameters were taken directly from product documentation but the rotational speed values were estimated using the recorded imagery and a between-frame time of $1/260\,\text{s} \approx 3.8\,\text{ms}$.

The experiments resulted in 20 image sequences each containing 1300 frames, which at ∼260 frames/s equates to a duration of 5 s per sequence. These 20 sequences were recorded for 10 different rotational speeds of the cylinder and 2 indent working diameters. The 10 settings of ω was in the range from 26 r/min (*revolutions per minute*) to 49 r/min with an average step of 2.56 r/min. These 10 manually estimated rotational speeds can be found in Table 1. Two values of d were used: (1) 6.0 mm and (2) 7.0 mm. Besides these 20 sequences, a single "background-only" sequence was also created. The scene recorded here was the empty cylinder with no seeds in it (recorded with $\omega = \sim 34$ r/min).

It was considered whether to take advantage of the imaged area in which the seeds can be seen to leave the cylinder inner surface. Such considerations led to preliminary attempts at tracking individual seeds from the point at which they leave the inner cylinder surface to the point at which they exit the frame again. The method for tracking was the popular Kalman filter – an algorithm for iteratively estimating a more true signal when prior observations are characterised by additive noise (Kalman, 1960; Ekstrand, 2012). Theory and results of these early tracking experiments are available in Poster I in Appendix D. These results are briefly summarised in Section 4.1.4 (page 51). Tracking the seeds in these images proved difficult due to the high number of self-occluding objects. The tracking of objects in images is a very active research field within computer vision (Yilmaz et al., 2006; Salti et al., 2012; Tang and Peng, 2012; Zhang and Song, 2013). Although tracking is generally considered challenging – and other less complicated

methods eventually prevailed – it was early on deemed highly valuable to be able to track the seeds inside the inner cylinder volume. This would have allowed the creation of a full set of spatiotemporal locations for each individually tracked seed.

Second set of experiments

The second set of experiments was considerably more substantial than the first set. Instead of using whole and broken seeds for simulating long and short sub-divisions of a binary mixture, these experiments involved the use of "model species", i.e. species of seeds that by their length and colour could be used to model the presence of long or short seeds in the indented cylinder. Rice and wheat seeds were used as a model for long seeds and cannabis seeds were used as a model for short seeds. The colour of the seeds was also important for later supervised classification. The same 10 values for ω were used and a total of 4 values for d were used: (1) 5.5 mm, (2) 6.0 mm, (3) 6.5 mm and (4) 7.0 mm (also listed in Table 1). The final data set consisted of 360 image sequences – all recorded at different values of ω, d, and for various mixture ratios of long and short seeds (e.g. 4 different choices of d, 10 different settings of ω, and 9 different mixture ratios). Besides these 360 sequences, 10 "background-only" sequences were also created – one for each rotational speed. Both unary and binary mixtures were used. The mixtures were created using the same weight scaling approach as previously introduced. Each of the 360 sequences contained 2600 frames corresponding to a duration of 10 s per sequence.

Figure 13b shows an example of a frame created in this second set of experiments. This frame originates from a sequence recorded in a session where only rice was used (a unary mixture). The camera line-of-sight was configured in such a way that it was parallel with the right side of the cylinder instead of with its axis of rotation (see Figure 11). The monofocal lens was also changed to one with a focal length of 12 mm instead of the previous 25 mm. When comparing Figure 13b with Figure 13a the difference in imaging geometry is visible. Although this difference was generally ignored in later analyses, the overall perspective distortion was believed to be of less concern in the second set of experiments than it might have been in the first set. Moreover, in the first set of experiments the lower part of the cylinder was blocked by a piece of plastic to prevent spill of material. This was not the case for the second set of experiments, allowing analyses of the dynamics taking place in quadrant IV (as per Figure 12a).

The use of different forms of illumination in the two sets of experiments is also quite apparent when comparing Figure 13a and Figure 13b. Choosing the correct form of illumination is very important in imaging experiments such as these. Some sources of light have certain properties that may be either beneficial, if used correctly, or fully destructive if used incorrectly (for an overview of the theory of scene illumination, see Sinha, 2012). In the second set of experiments illumination was provided by a prototype LED-plate: A metal plate with 189 light emitting diodes (LEDs) mounted in a grid

(the colour temperature of the LEDs was 10 000 K). See Figure 6 in Paper II for photographs of this illumination prototype developed and manufactured by Videometer A/S, Denmark. This LED-based illumination resulted in a more even distribution of light in the scene. Shadows and other unwanted artifacts are for instance visible in Figure 13a but not in Figure 13b. The overall light intensity was lower for the LED-based illumination, which let to the use of more gain on the CCD, which in turn resulted in slightly more image noise.

3.3.3 Methods Applied in the Papers

Paper I

Paper I was the result of the first attempts at analysing the recorded frames as per the model of observation described in Section 3.2. The basic tasks carried out for each frame in all 20 sequences were: (1) find the locations $\boldsymbol{p}_i \in U_{\text{geo}}$ of all seeds visible in quadrant I (see Figure 12a), (2) estimate θ_i for all seed locations $\boldsymbol{p}_i$, and (3) store all θ_i in a data structure holding all θ values from all frames in the current sequence. This resulted in 20 data structures (or vectors) each containing observations of angle of escape θ over a duration of 5 s. The population mean and standard deviations of these 20 vectors were estimated individually. Figure 5 in Paper I shows, for a selected number of these vectors, the resulting θ-histograms including a superimposed normal-fit. Furthermore, these samplings of θ over time were also used to show that the "lifting phenomenon" of the indented cylinder seems to be quite stationary (see Figure 6 in Paper I).

Paper I did not involve the classification task, i.e. the task of determining whether or not a seed is a whole (long) seed or a broken (short) seed. It was found technically difficult for two main reasons. Taking advantage of any difference in individual physical geometry of each seed (broken or half versus whole) by the use of the pixel geometry proved to be unfeasible due to the low pixel resolution of the machine vision camera and the camera-to-cylinder distance dictated by the model of observation. The use of clustering or supervised segmentation techniques, such as K-means (Siddiqui and Mat Isa, 2012; Christ and Parvathi, 2012), support vector machines (Ke and Zhang, 2011; Yang et al., 2012; Guerrero et al., 2012) or artificial neural networks (Egmont-Petersen et al., 2002; Karasulu and Balli, 2010; Bharathi and Subashini, 2011; De et al., 2012), was also not applicable, since no natural discriminating difference in pixel value could be defined between whole and broken barley seeds (i.e. they would have the same colour).

Paper II

Paper II+III represent an extension on the methodology published in Paper I. Given the fact that we are talking about two companion papers, this extension is of course of considerable complexity – in both methodology and theory. Paper II (Part one of two) establishes all details on the second

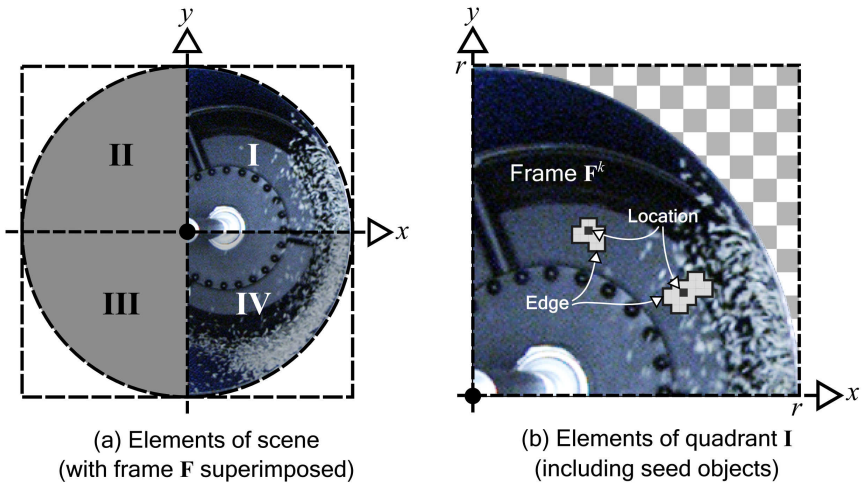

Figure 14: Elements of scene and Quadrant I with a frame from the second set of imaging experiments superimposed.

set of experiments, such as the arguments for choosing the three species of seeds, information on setting up the camera in front of the cylinder, the sequence of operations in the experiments, details on the creation of the unary and binary mixtures of seeds, etc. Paper II also presents some results on some relatively simple image processing techniques for image segmentation applied on the sequences recorded using only the unary mixtures. These segmentation trials resulted in some interesting plots of signals carrying information about the amount of seeds visible in quadrant I over time (Figure 11 in Paper II). These signals indicate a strong oscillatory behaviour of rice seeds when manipulated by the inner cylinder surface. A one-sided frequency power spectrum of two of such signals are shown in Figure 12 in Paper II.

Paper III

Paper III (Part 2 of 2) begins with a detailed set of arguments for what is referred to in this chapter as the model of observation described in Section 3.2 (see Section 2 in Paper III). The paper hereafter gives a detailed account of the methodology behind the two tasks of (1) detecting the visible seeds in any frame and (2) classifying or labelling these detected seeds as being either a cannabis, wheat, or a rice seed.

Figure 14a shows the scene model again where the frame from Figure 13b has been superimposed onto quadrant I and IV. Figure 14b shows quadrant I and the upper part of this frame with some added details. This frame is the k-th frame $\mathbf{F}^k$ (superscript, not exponentiation), where $k = 1, \ldots, K = 2600$. The gray regions shown are "seed-regions": connected components that indicate an area in the image plane that contains a seed. The goal of the image analysis in Paper III was to arrive at such semantically well-defined regions (i.e. correctly labelled) for all frames in all binary

sequences. Moreover, each seed-region in the current frame should have a single one of its pixels marked as the approximate location estimate of that seed-region in the image plane. This approximate location is used in the post-processing to estimate a value of angle of escape θ for each available seed-region. Finding the seed-regions was primarily a problem of image segmentation – segmentation being the task of dividing an image into coherent regions. Such regions are usually simpler representations of the original raw pixel data. The task of segmentation is a highly active sub-field of computer vision and it is considered a crucial first step (see reviews e.g. Pal and Pal, 1993; Zhang et al., 2008; Heimann and Meinzer, 2009; Jayadevappa et al., 2011).

The overall goal was two sample time-series containing estimates of θ^{long} and θ^{short} from all frames $\mathbf{F}^k$ from the image sequences recorded using only binary mixtures of long and short seeds. Figure 15 shows this general classification and θ-value sampling process (downwards from top) carried out on a single sequence of all frames $\mathbf{F}^k$ over time (from left to right). The top part of the graphics shows the "image" universe of discourse U_{img} – a square subset of the two-dimensional integer plane $\mathbb{N}_0^2$. The current frame $\mathbf{F}^k$ will at some point have been simplified to two sets: (1) one with approximate locations $\boldsymbol{p}_i^{\text{long}} \in U_{\text{img}}$ and (2) one with approximate locations $\boldsymbol{p}_i^{\text{short}} \in U_{\text{img}}$. The pixel coordinates in these two sets are hereafter converted into coordinates in U_{geo} using a conversion function (a linear interpolation). Staying in the parlance of coordinate space conversion, the U_{geo} coordinates in both sets are now again converted into a one-dimensional real angle of escape space $\Theta = \{\theta \in \mathbb{R} : 0 \leq \theta \leq \frac{\pi}{2}\}$. The sampling process in Figure 15 concludes with these two sets containing (labelled) θ values for all detected long and short seeds in all frames $\mathbf{F}^k$. Finally, a statistical distance between two estimated univariate normal θ-distributions is calculated. This distance represents an estimate of the **SE** measure in the current (ω, d)-coordinate.

The task of classifying the detected seed-regions as either "long" or "short" was posed as a general two-level hierarchical segmentation problem. Conceptually, in the first level, all pixels were segmented into regions of "background" and "non-background" and in the second level, pixels in "non-background" regions were further segmented into either "short" or "long". Arriving at such a two-level segmentation for each frame in any binary sequence was done by using a combination of one-class and general multi-class supervised classification techniques.

As previously mentioned, the second set of experiments involved the use of unary and binary mixtures of model species mimicking the presence of long and short seeds in the recorded frames. The indented cylinder was also recorded with no seeds in it. This resulted in the availability of three kinds of sequences, i.e. (1) "background-only", (2) "unary" and (3) "binary " sequences. Consider the k-th "background-frame" $\mathbf{B}^k$ from any background-only sequence. It would only be natural to assume that all pixels in such a frame, are solely part of the background of the cylinder and nothing else. Frame $\mathbf{B}^k$ can therefore be considered as a source of training examples of background pixels. Such examples may be sampled, pre-labelled as "back-

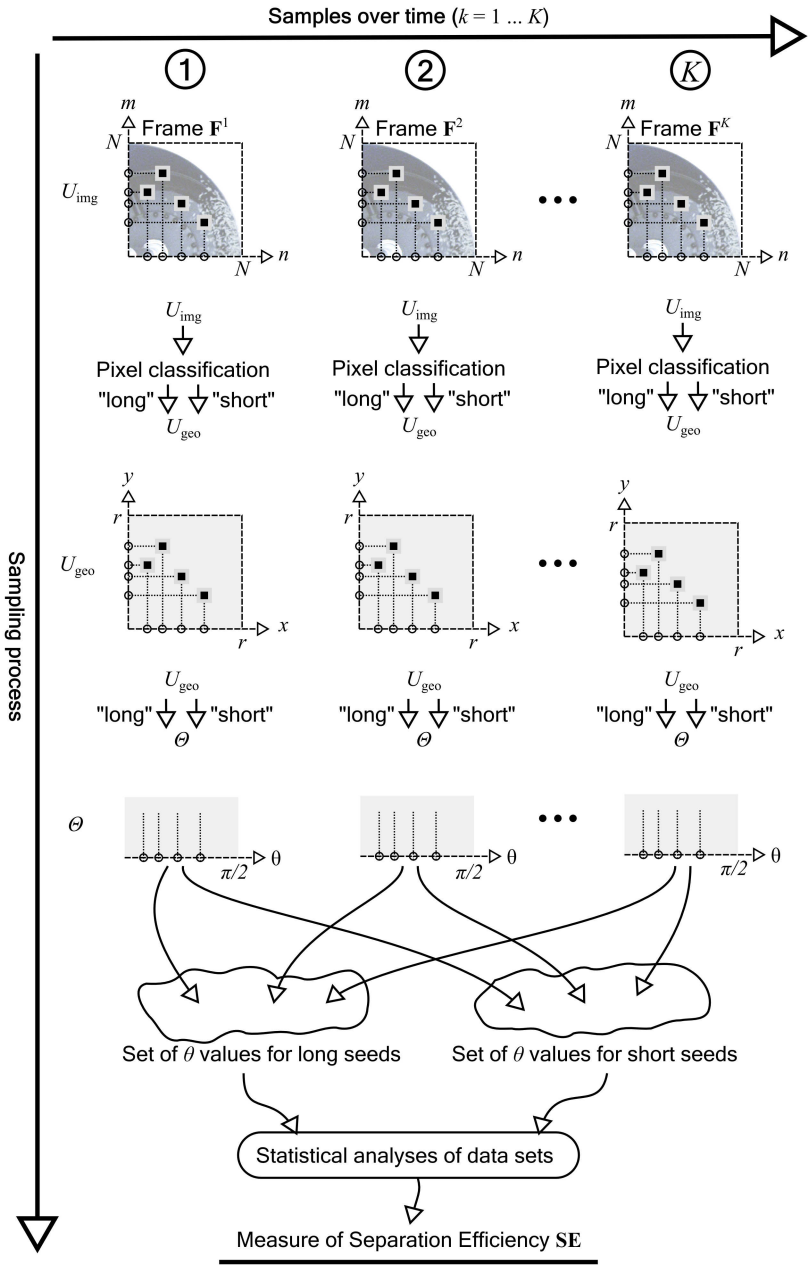

Figure 15: An overview of the sampling process applied in Paper III to get discrete estimates of the **SE** measure.

ground", and stored in a training set $D_c = D_1$ with a label index $c = 1$. The sampling itself will be trivial as no other content other than background exists. In Paper III, background pixels were sampled directly in a three-dimensional normalized RGB space, or more generally $\mathbb{R}^3$, but the features came directly from RGB colour components.

Consider now the k-th "foreground-frame" $\mathbf{F}^k_{\text{unary}}$ from any unary sequence. The possible content of such a frame will be either background or a combination of background and one of the three seed species used. Such a frame does represent a source of training examples for either "cannabis"

($c = 2$), "rice" ($c = 3$), or "wheat" ($c = 4$) – although they cannot be as easily sampled as before. The sampling of these three classes was solved in Paper III as a one-class classification problem – also known more generally as novelty or anomaly detection (Markou and Singh, 2003a; Chandola et al., 2009). The exact method was based on classical statistical techniques. Background pixels in frame $\mathbf{F}^k_{\text{unary}}$ and in D_1 were all assumed normally and similarly distributed in $\mathbb{R}^3$. The population statistics of the pixels in D_1 could therefore be used to arrive at parameters for a representative normal distribution for background pixels. Pixels in $\mathbf{F}^k_{\text{unary}}$ not similarly distributed in RGB space, were thus considered anomalies. By method of exclusion, such anomalous pixels could be considered as pixels that could potentially be labelled as either "cannabis", "rice", or "wheat". The measure of novelty was the Mahalanobis distance (Mahalanobis, 1936). The threshold was defined as 3 times the standard deviation from the estimated background pixel average. The sampled foreground pixels were stored in three separate sets D_2, D_3, and D_4.

The last type of frame to consider here is the k-th frame $\mathbf{F}^k_{\text{binary}}$ originating from any of the binary sequences. The possible content of such a frame will either be background or a combination of background and cannabis and rice seeds – or cannabis and wheat seeds – depending on what specific binary sequence is being processed. In any case, the contents of frame $\mathbf{F}^k_{\text{binary}}$ represents a trinary classification problem. In Paper III, this problem was solved using QDA (quadratic discriminant analysis; Fisher, 1936; Martinez and Kak, 2001) by again assuming that the RGB pixels in training sets D_1, D_2, D_3 (or D_1, D_2, D_4) were normally distributed in $\mathbb{R}^3$.

Certainly other techniques exist besides the classic Mahalanobis distance and discriminant analysis. For example, artificial neural networks (ANNs) and support vector machines (SVMs) have both been used extensively for general classification, and also for image segmentation posed as a classification problem (Wen et al., 2009; Sowmya and Rani, 2011; Yu et al., 2011; Wang et al., 2011, 2012). The one-class classification problem, and clustering in general, has also been addressed, both by the use of ANNs (Markou and Singh, 2003b; Du, 2010; De et al., 2012), and by the use of SVMs (Schölkopf et al., 2001; Wu and Chung, 2009; Junejo et al., 2011). Although the processing was never supposes to happen in real time, the reason for using such standard methods was their simplicity and speed. Such considerations were important since the full processing of the imagery data from the second set of experiments involved close to one million (i.e. $2600 \cdot 4 \cdot 10 \cdot 9 + 2600 \cdot 10 = 962\,000$) individual high-speed RGB frames of pixel dimensions 175×175. Such a single frame consists of $\sim$90 KiB of data – resulting in a total raw data size of $\sim 90\,\text{KiB} \cdot 962\,000 = \sim 83\,\text{GiB}$.

Chapter 4

Results and Discussion

4.1 Results

4.1.1 Paper I

This paper is the first internationally published work that successfully analysed the behaviour of the indented cylinder by the use of basic methods from image analysis and statistical inference. The details of the experiments and the methods are described in detail in Section 3.3.2 and Section 3.3.3.

The following are the specific results/highlights of Paper I:

1. The combined use of (classic) image processing techniques was successful in achieving a binary segmentation of the high speed frames – thereby separating the imaged barley kernels from the background. The methods applied were: (1) RGB minimum variance quantisation, (2) grayscale conversion, (3) Gaussian filtering (convolution with a 5-by-5 Gaussian kernel), (4) static background modelling using image averaging, (5) background subtraction, (6) image distance transform (see Maurer et al., 2003), regional maxima transform, and morphological shrinking of connected components to single pixels (see, for instance, Hall et al., 1996; Lam et al., 1992, p. 879; and Guo and Hall, 1989).

2. This segmentation allowed the estimation of the two-dimensional (i.e. camera projected) real world location for each seed available/detected in each frame. Any pixel coordinate $\boldsymbol{p}$ was transformed into a real world coordinate by the use of a function $f_{r,N}(\boldsymbol{p}) = r(\boldsymbol{p} - 0.5)/N$. Here N is the square image size (in pixels) and r the radius of the indented cylinder ($r = 0.2\,\mathrm{m}$ in all experiments).

3. Given that a seed's trajectory is assumed parabolic, the problem of estimating angle of escape θ from two-dimensional locations on such a trajectory can be posed as a minimisation problem in $\mathbb{R}$. Paper I shows that this is true. To solve this minimisation problem, the residual function was evaluated in the range $\theta \in [0, \pi/2)$ with a step size of

$10^{-3}\pi/2$. No stopping criteria was used. This allowed a full analysis of all 1000 residual values.

4. The statistical behaviour of angle of escape θ was analysed by the use of frequency histograms with normal fits. Generally, for a higher cylinder rotational speed ω there seems to be a higher probability for larger values of angle θ. Moreover, for the highest applied rotational speed ω the histograms (for both indent working diameters d) seem to become slightly multi-modal (see Figure 5 in Paper I).

5. The number of seed locations extracted over time (5 s) from each high speed frame is shown (graphically) to be stationary. The average number is shown to be approx. 700 seeds at the lowest cylinder rotational speed $\omega_1 = 26.03\,\mathrm{r/min}$ and approx. 300 at the highest cylinder rotational speed $\omega_{10} = 49.08\,\mathrm{r/min}$. The number of points extracted at higher rotational speeds seems to be less than for lower speeds (see Figure 6a in Paper I).

6. Angle of escape θ is shown graphically to be stationary over time. The estimated time series of angle θ show a horizontal trend at approx. 0.425 rad at ω_1 and approx. 0.625 rad at ω_{10} (see Figure 6b in Paper I).

7. A linear regression was estimated ($\beta_1 = 0.16, \beta_2 = 0.01, R^2 = 0.99$) and indicates the possibility of a linear relationship between the rotational speed ω and angle of escape θ (see Figure 7 in Paper I).

8. A final conclusive result: It was in general shown to be possible to extract information about the probabilistic nature of angle of escape θ using methods from image analysis.

4.1.2 Paper II

Paper II is part one of two companion papers and represents part of an extension on the work and results published in Paper I. Again, see Section 3.3.2 and 3.3.3 for details on materials and methods. The paper primarily establishes all details on the setup of the second set of experiments. The paper also presents results on the use of classic image segmentation techniques applied on the sequences recorded using only the unary mixtures (i.e. the sequence contained only one kind of seed). These segmentation techniques resulted in some interesting plots of signals carrying information about the amount of seeds visible in quadrant I over time (see Figure 12a on page 35).

The following are the specific results/highlights of Paper II:

1. The primary result is the open source release of the high speed image data. It is being released as a cite-aware database than can be used in future collaborative research efforts. The data is currently available at `http://olebuus.info/research`.

2. The secondary result comes from the segmentation trials mentioned above. These trials resulted in some plots of signals carrying information about the amount of seeds visible in quadrant I over time (see Figure 11 in Paper II). These signals indicate a oscillatory behaviour (seasonality) of rice seeds when manipulated by the inner cylinder surface. A one-sided frequency power spectrum of two of such signals are shown in Figure 12 in Paper II. These spectra are shown to have a peak between 1.1 Hz and 1.2 Hz.

4.1.3 Paper III

Paper III is part two of two companion papers and again represents part of an extension on the work and results published in Paper I. The paper begins with a detailed set of arguments for the model of observation described in Section 3.2. Please note that Paper III does not apply the exact term "**SE** measure". Instead it describes the exact same same concept using use a slightly more technical nomenclature than the one used in these introductory and summarising chapters. The paper hereafter focuses on (elaborately) presenting the methods applied to detect and classify the visible seeds in any frame as being either a cannabis, wheat, or a rice seed (see Section 3.1 and Section 3.3).

The following are the specific results/highlights of Paper III:

1. The **SE** measure is introduced and given a mathematical definition.

2. The binary segmentation of cannabis, rice, and wheat seeds from the background was successfully achieved by combining the use of novelty detection (Mahalanobis distance; Mahalanobis, 1936) and supervised learning techniques (quadratic discriminant analysis; QDA; Fisher, 1936). As in Paper I, this allowed the estimation of the two-dimensional real world location for each seed available/detected in each frame (by using the same linear interpolation technique described in result 2 of Paper 1).

3. The problem of estimating angle of escape θ from two-dimensional locations is revisited. The paper derives and uses a closed-form solution solve the minimisation problem.

4. Two time series of angle of escape θ where estimated acquired for a set of cylinder rotational speeds $\omega_i, \ldots, \omega_{10}$, four indent working diameters $d_1, \ldots, d_4$, three mixture ratios of rice ("long") and cannabis ("short"), and three mixture ratios of wheat ("long") and cannabis ("short").

5. The **SE** measure was estimated from the aggregation of all θ estimates from all times – resulting in two resulting sets of θ values. The distribution of both of these two sets of aggregated values were assumed to be univariate normal. Two statistical distance metrics were used for the **SE** measure: (1) the numerical distance between the means of the

two normal distributions, and (2) the Hellinger distance between the two normal distributions.

6. Interpretations of the estimated values of the **SE** measure for each value of $\omega_1, \ldots, \omega_{10}$ and $d_1, \ldots, d_4$ resulted in the following conclusions about the most optimal ranges of ω and d (a summary of Table 4 in Paper III):

   a) For the three binary cannabis/rice mixtures used in the experiments, the optimal value for d is found to be in the range from 6.5 mm to 7.0 mm. Similarly, the optimal value for ω is found to be in the range from 36.71 r/min to 42.60 r/min.

   b) For the three binary cannabis/wheat mixtures, the optimal value for d is found to be 6.5 mm and the optimal range for ω is 36.71 r/min to 39.73 r/min.

7. The six histogram plots shown in Figure 9 (in Paper III in Appendix C) show similar standard deviations of angle θ for both short and long seeds. This standard deviation for long and short seeds is in the range 10.60° to 11.8° and 10.50° to 11.2°, respectively.

8. The zero contours seen in Figure 7 (in the paper) indicate that the separation behaviour is reversed for ω values below 33.96 r/min. In such a situation, long material is lifted higher than short material. This observation is tentative and further experiments should be conducted to validate it.

9. The estimated mean of angle of escape θ, calculated from and aggregation of data from each 25 time-steps (resulting in 104 data points), is shown graphically to be stationary over time. (see Figure 11 in Paper III). This result correlates nicely with result 3 in Paper I (see Section 4.1.1).

Regarding the assumption of normality

Figure 9 in Paper III shows six examples of histograms of data from $\boldsymbol{\theta}^{\text{long}}$ and $\boldsymbol{\theta}^{\text{short}}$ – modelled as being the realisations of normally distributed univariate random variables $\Theta_{\text{A}}^{\text{long}}$ and $\Theta_{\text{A}}^{\text{short}}$ (see Section 3.2.3), respectively. The estimated normal densities are superimposed onto each corresponding histogram and their parameters are given in the figure legends. The results of Paper I and Paper III are all based on the assumption that these sample data were normally distributed.

They might in fact not be: A Lilliefors test (Lilliefors, 1967) was later performed on all pairs of $\boldsymbol{\theta}^{\text{long}}$ and $\boldsymbol{\theta}^{\text{short}}$ at the 5 % significance level. The result of these tests was the rejection of the null hypothesis that the data comes from a normal, an exponential, or an extreme value distribution. The lowest tabulated value $p = 0.001$ at the 5 % significance level was the result from all these tests.

The most important assumption about the attempted statistical modelling, was the difference in location, or mean, of the two normal distributions for "long" and "short" seeds. The estimated mean from the data available in $\boldsymbol{\theta}^{\text{long}}$ was naturally expected to be lower than the estimated mean from the data available in $\boldsymbol{\theta}^{\text{short}}$. A two-sample left-tailed t-test was performed on all available pairs of $\boldsymbol{\theta}^{\text{long}}$ and $\boldsymbol{\theta}^{\text{short}}$. The null hypothesis, that the vectors contain data from normal distributions with equal means, was tested against the alternate hypothesis that the mean of $\boldsymbol{\theta}^{\text{long}}$ is less than than the mean of $\boldsymbol{\theta}^{\text{short}}$ (the situation that we would normally expect). Equality of variances was not assumed. The result for most values of ω and d, was the rejection of the null hypothesis ($p = 0$, 5 % significance level). This is interesting, and it could mean that one can then accept the alternate hypothesis. The results from the Lilliefors tests however, indicate that the rejection of the t-test null hypothesis emphasises yet again that the original data vectors are not normally distributed.

From these investigations, it is safe to conclude that the statistical analyses need more work. Perhaps other distributions would be better models or perhaps nonparametric techniques would suffice. However, the contour plots presented in Figure 7 and Figure 8 in Paper III are still useful as indicators of the most optimal ranges of parameters ω and d.

4.1.4 Posters I and II

Beyond the three papers available in Appendix A, B, and C, this thesis also contains two posters: (1) Poster I available in Appendix D and (2) Poster II available in Appendix E.

Poster I

This poster shows some early results of some tracking experiments using the Kalman filter algorithm (Kalman, 1960). The poster was displayed at Visionday 2010 at the Technical University of Denmark in May 2010. The image data used for tracking originates from early preliminary experiments carried out prior to the first set of experiments described in Section 3.3.2. The seed material was polished rice (same variety used later in the second set of experiments). The geometry of the scene recorded was similar to the one depicted in Figure 13a on page 39 – although only quadrant I in the scene model was processed. The main idea was to take advantage of the imaged area in which the seeds can be seen to leave the cylinder inner surface. A Kalman filter tracking algorithm was initialised with a location of an individual seed from the point at which it would leave the cylinder inner surface. By keeping track of the two-dimensional location of the seed and assuming a parabolic trajectory, the Kalman filter was assumed able to update correctly at each time step and track the seed's location until it would exit the recorded scene.

No conclusive results were drawn. This was likely due to the following facts:

- The preliminary experiments suffered slightly from the lack of established experimental protocols for correct illumination, direction of view of the camera, uncertainty with focus, etc. This introduced issues with general image quality.
- There was a difficulty with properly updating the current state of the Kalman filter, i.e. estimating the seed's current location. This update step required the local re-detection of the tracked seed which was found difficult to achieve due to occlusion from other rice seeds and the general low image quality. Moreover, it was also found difficult to find an initial location for a rice seed leaving the cylinder inner surface.

Poster II

This poster graphically depicts certain key aspects of the research published in Paper I. The conclusions that it draws are therefore the same as those already summarised in Section 4.1.1.

4.2 Discussion

The content of this PhD thesis seems to represent the very first published research effort where it was attempted to analyse the behaviour of both unary (single-component) and binary (two-component) seed mixtures being manipulated in a laboratory scaled indented cylinder. This work analysed distribution of a very important local parameter of a seed in an indented cylinder, namely the angle of escape θ. Statistical inference was used used to conclude on the overall behaviour of this parameter. The development of a new measure of "separation efficiency" – or **SE** measure – as well as the use of methods from computer vision and image analysis to acquire such a measure by empirical means, are the main highlights of the work summarised in this PhD thesis.

The laboratory scaled indented cylinder have been investigated in a few previous works, but none of them have attempted to formalise how one might automatically observe a measure of performance. Grochowicz (1980, chp. 7) presents a full analysis of the motions of the seeds. This work is a summary of a number of Polish works – all apparently published in Polish in the years from 1950 to 1970. Besides the basic mechanics, Grochowicz also presents a theoretical differential equation for the sorting process in an indented cylinder. The work is generally highly theoretical without much or any experimental validation.

The work by Churchill et al. (1989) show results from experiments with sorting wheat using a laboratory scaled indented cylinder. Interestingly, the brand and model of the indented cylinder was similar to the one used in this work. They also used similar rotational speeds and indent working diameters (although fewer of them – a key point addressed in the next section). In the following 20-year span between 1989 to 2009, is seemed that no one

were interested in (open) research regarding the indented cylinder. Choon-Ki et al. (2009) then publishes on experiments with a laboratory scaled indented cylinder and 41 varieties of rice. This work did not apply image analysis. The works by Churchill et al. (1989) and Choon-Ki et al. (2009) are both important since they report on practical experiments with the indented cylinder. They are therefore further discussed in the next section.

The use of digital imaging and methods from computer vision for this kind of analysis of the indented cylinder has been previously done only by Sorica et al. (see 2012). That work is particularly important since it establishes a mathematical model for the angle of escape θ and compares this model to reality. However, the authors did not attempt to achieve an empirical analysis of a performance measure. Their work is still very relevant as it verifies a number of assumptions made in the work of this thesis and is therefore also discussed in some detail in the following section.

4.2.1 On Previous Approaches

Sorting/cleaning of wheat – Churchill et al. (1989)

Churchill et al. (1989) made some interesting and early attempts at achieving a reproducible set of rules (a "decision-support system") for length separation using a laboratory scaled indented cylinder. Interestingly, the model used (a Kamas-Westrup LA-T) is similar in brand and model to the one used in the experimental work for the three papers. The authors used three different rotational speeds ω (22 r/min, 36 r/min, 50 r/min), three different indent working diameters d (5.0 mm, 6.0 mm, and 7.0 mm), and three different collecting-bin working angles α ($-20°$ and $20°$) – resulting in a total of 27 experiments. An early computer vision system (Intellidex V-200) was used to measure the lengths of precleaned Stevens wheat. Image analysis was not used to analyse the behaviour of seeds while in motion.

Churchill et al. concluded that all three operating parameters of the indented cylinder had a significant impact on the length distribution of seeds in the lifted fraction ("short" seeds) and no significant impact in the length distribution of seeds in the unlifted ("long" seeds) fraction. The authors also concluded that the indented cylinder "... does not appear to be a perfect discriminator of length for wheat seed." Their findings indicate that to achieve close separation, the working indent diameter d will need to be approximately equal to or slightly less that the average particle length.

Both Paper I and Paper II present details on experiments with a similar laboratory scaled indented cylinder. The crucial difference lies in the number of rotational speeds applied in both Paper I and Paper III. Churchill et al. applied only three speeds and the current work applied a total of ten speeds. Paper I+III thus achieves more information about the dynamics between the rotational speeds that Churchill et al. investigated. This is especially true for speeds between 36 r/min and 50 r/min.

The authors interestingly conclude that a higher rotational speed ω seemed to result in less length difference between the lifted and unlifted

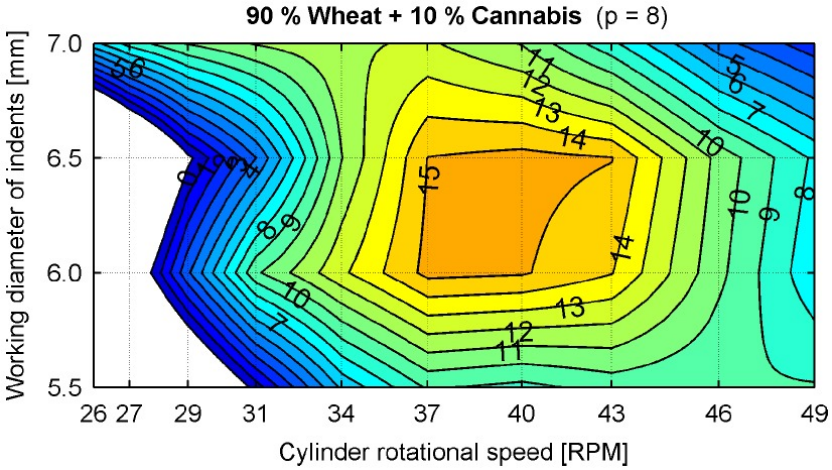

(a)

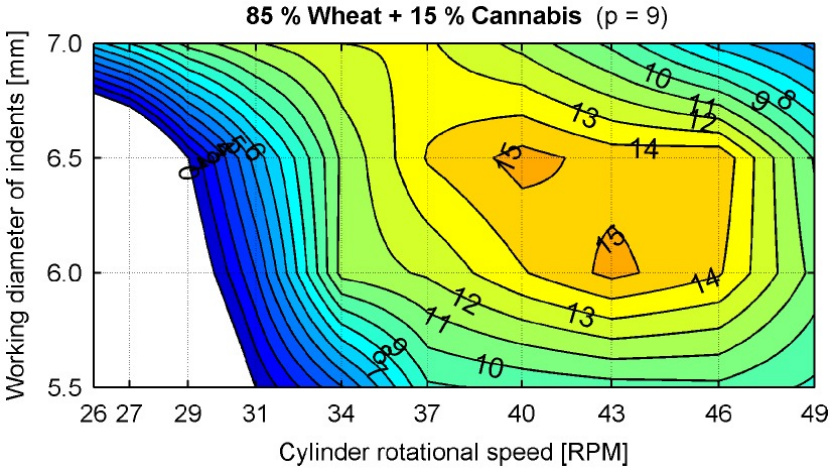

(b)

Figure 16: Two linearly interpolated contour maps of numerical distances between averages (see the figure caption of Figure 7 in Paper III for more information): (a) Contour map generated using data from experiments using a binary (two-component) mixture containing 90 % wheat and 10 % cannabis; (b) similar but for a mixture containing 85 % wheat and 15 % cannabis.

fraction. The results of Paper III is not directly able to confirm this conclusion. Figure 16 shows two linearly interpolated contour maps of numerical distances between averages (please see the figure caption of Figure 7 in Paper III for more information). These maps give an explicit overview of the ability of the inner cylinder surface to separate binary (two-component) cannabis/wheat mixtures. The contours and tones of the map are scaled in the range from 1° to 20° – representing the separation of the two components in the input mixture on the cylinder circumference.

From these contour plots, it is evident that it is generally at higher values of ω where high length difference is observed – and not the other way around as the authors conclude. Importantly, the best separation is observed in the

range of rotational speed ω between 36 r/min and 50 r/min. Churchill et al. did not analyse this range.

Sorting/cleaning of rice – Choon-Ki et al. (2009)

Choon-Ki et al. (2009) reports on investigations into optimum operation conditions for a laboratory-scaled indented cylinder for removing broken rice from non-broken rice. Image analysis was not used. The authors used 41 different varieties of rice, three different indent working diameters r (3.5 mm, 3.8 mm, and 4.2 mm), and three different settings of the working angle α of the collecting-bin (5°, 15°, and 30°). The rotational speed ω was apparently not varied.

Besides recommendation on the most optimal angle α, which was between 5° and 15°, Choon-Ki et al. also give recommendations on the indent working diameter d that led to the best separation between broken and non-broken rice seed. This depended on the different rice varietal characteristics. For example, for rice varieties with a 1000-kernel weight of more than 22.3 g, a width larger than 2.9 mm and a length larger than 5.2 mm, the recommended value for d was a working diameter larger than 4.2 mm. For varieties with the smallest and thinnest kernels observed, the recommended size was 3.8 mm and for the varieties with short to middle sized kernels the recommended range for d was between 3.8 mm and 4.2 mm.

Binary (two-component) mixtures of milled (polished) rice and cannabis where used in Paper II and Paper III. The 1000-kernel weight for rice was measured to be ∼13.98 g (see Table 1 in Paper II). Much needed data from sample measurements of the dimensions of the seeds involved in the experiments of Paper II+III, is unfortunately missing in either of the three papers. This would have been very useful as a physical source of validation. Lack of technical equipment did unfortunately not allow for such experimental data to be gathered in due time.

The intent here, is only to compare the optimal ranges of parameters ω and d given as results of Paper III in Section 4.1.3 to those given by Choon-Ki et al. The geometrical data that can be visually interpreted from Figure 4 in Paper II can therefore suffice as a source of sample statistics. The length and width of the single rice kernel in that figure is close to ∼8.0 mm and ∼2 mm, respectively. The data presented by Choon-Ki et al. seem to indicate that, for rice mixtures of the aforementioned lengths, widths, and 1000-kernel weights, the use of an indent working diameter larger than 3.8 mm is not recommended. It might therefore be better for future work to attempt similar analyses using a range of smaller indent working diameters than the ones used in the three papers (here four sizes were used – from 5.5 mm to 7.0 mm – with an interval of 0.5 mm).

A mathematical model – Sorica et al. (2012)

The aim of the work by Sorica et al. was to develop a mathematical model for angle of escape θ (referred to as the "critical angle of detachment" in

the text). A set of equations similar to those derived by Grochowicz (1980, chp. 7, pp. 272–278) and Huimin et al. (2011) are given. Interestingly, the work only deals with "short" seeds/particles – referred to as "impurities". These seeds have support only inside the indents. It is assumed that a parabola can describe the trajectory of a seed after it has left an indent. The mathematical model developed is dependent on constructive parameters such as details on the size and shape of the indents and the radius of the cylinder r, as well as the rotational speed ω. Besides these parameters, it is also dependent on an angle ϕ that a "short" particle/seed resting in an indent has with the horizontal. This particular variable ϕ is local to each seed and is related to the individual length of that seed. The model was simulated using MathCad 2012. The importance of the variation interval of variable ϕ is mentioned but the actual simulated range is never given.

The model is verified by experiments using digital imaging and methods from computer vision. Their experimental setup seems to be closely similar to the setup used in this work. The experiments involved the use of a high speed camera (Phantom V10) configured to record at ∼1800 frames/s. This was much faster than what achievable using the Point Grey Grashopper (model: GRAS-03K2C-C; maximum frame rate at 8-bit 240×480 "format 7" pixel resolution, i.e. with half the sensor lines disabled, was ∼260 frames/s). The light source was also more powerful as it consisted of four projectors (manufacturer and model unspecified) with an aggregate power of 2000 W. In comparison, for the the first set of imaging experiments, illumination was provided by a 150 W halogen modelling light (SOLO 1600 B) placed between camera and cylinder (see Section 3.3.2).

The authors are able to conclude that a good correlation exists between model and reality. This thesis also assumed a parabolic motion model would suffice and the work by Sorica et al. therefore verifies the validity of this assumption. The image analysis was done by the use of special software (TEMA Automative by Image Systems AB, Sweden). The work does not provide any details on the choices of tracking algorithms or other kinds of details. The presentation in the paper also lacks any information of the kind of particles used in the indented cylinder. The manufacturer and model of the indented cylinder itself is also not given. A laboratory scaled indented cylinder was used in the experiments, although this fact is evident only from an included photo of the experimental setup.

This work by Sorica et al. is comparable to the work in all three papers – especially Paper I and Paper III. The work in those two papers involved the development of algorithms to extract the location of each seed in each high speed frame. This is in direct contrast to the work by Sorica et al. that used special software to track the seeds – thereby hiding these important details. The comparison between model and reality is also of great relevance to the overall aim of this thesis.

Chapter 5

Conclusions and Perspectives

As mentioned in Section 1.1, the processes involved in the sorting of seeds are generally complicated. The outcomes of such processes are likely dependent on a countless number of systemic parameters of the mechanical and biological kind. It would be highly beneficial for the seed industry in general, if this complexity and the difficulties that arise because it, could somehow be minimised.

The overall aim therefore became to achieve an insight into the relationship between input and output of the process in an indented cylinder – thereby helping to minimise the difficulty that exists in optimally configuring the sorting process inside an indented cylinder – specifically a laboratory scaled version. Achieving such an aim required the use of concepts from the area of empirical model development, especially system (i) identification and (ii) experimentation (see Section 1.4.1).

Identification deals with the estimation of mathematical models from observed dynamic states of known input and corresponding output. This task relies on the availability of preexisting methods that can acquire a relevant output from the physical system under investigation. Thus, for actual system identification to be possible, the technical difficulties related to defining relevant output variables and correctly sampling these, had to be addressed and solved first.

5.1 Conclusions

In regards to the indented cylinder, a natural choice of relevant variables would be variables that carry information about the machine's performance, i.e. how efficient it is at separating any given input mixture. Experimental methodologies to achieve a sampling of such output variables, did not exist at the time when the PhD project was initiated in May 2009. Neither did a formal definition of a measure of separation efficiency that could somehow be derived from the raw variable(s) sampled.

As a direct consequence of the work in this thesis, such methods and formal definitions do indeed exist now. The following are the main conclusions:

- The work contributes with a novel technical solution based on digital imaging techniques and methods from computer vision. This solution makes it practically possible to observe and sample a measure of separation efficiency of a laboratory scaled indented cylinder.
  - A separation efficiency – or **SE** – measure (a mathematical metric) was developed on the basis of what was already known about the operational characteristics of the indented cylinder. A definition is given in Section 1.4.3.
  - High speed imaging experiments were designed for the purpose of sampling the **SE** measure. These experiments made possible the acquisition of high speed image sequences of seeds caught in mid-air while being manipulated by a laboratory scaled indented cylinder.
  - The choice of camera placement in front of the cylinder opening, made it possible – by the use of methods from computer vision – to detect/segment, approximately locate, and classify each individual seed visible in each recorded high speed frame (see the technical hypotheses in Section 2.3). In return, this made possible the sampling of time series of angle of escape θ.
- Imaging experiments were carried out for ten cylinder rotational speeds $\omega_1, \ldots, \omega_{10}$, for (up to) four indent working diameters $d_1, \ldots, d_4$, and for a (varying) number of different mixtures of seeds – of both the "unary" (single-component) and "binary" (two-component) kind.
  - A magnitude for the **SE** measure was estimated for each of these experiments by the use of data from time series of angle of escape θ for both "long" and "short" seeds.
  - These experiments, along with the **SE** measure estimations, made possible the determination of optimal ranges of the two most important input variables: (i) cylinder rotational speed ω and (ii) indent working diameter d (see Section 4.1.3 for the specific ranges).
- Paper I makes freely available a cite-aware body of image data from the second set of experiments, and thereby attempts to enable future research into analysing the behaviour and performance of a laboratory scaled indented cylinder. The data set is available at `http://olebuus.info/research`.

5.2 Perspectives

5.2.1 Toward Control of the Indented Cylinder

In a general system control situation, for instance in a standard control loop feedback mechanism, the essential goal is usually to regulate the observed

output according to some reference value. The regulation is done by dynamically adjusting the input so that any deviation from the output reference is minimised. To do this, one must achieve an understanding of how the input influences the output. Such an understanding can be represented by a set of equations, i.e. a mathematical model. As also explained in Section 1.4, the goal of system identification is to establish such a model by the use of observations of inputs and outputs from a physical system (Ljung, 1999; Pearson, 2006).

Any reason for any dynamical regulation during the continuous operation, would primarily arise from the input mixture itself. The various characteristics of this input mixture might fluctuate and give rise to a need for change in rotational speed ω and working angle α of the collecting bin. The indent working diameter d is a physical parameter of the steel cylinder mantle. According to the industry itself, it can take considerable time and effort to change these mantles on the industrial-scale machines. It is therefore likely that d would have to be considered as a fixed parameter of the system since it is not possible to automatically manipulate.

Continuous analysis of input

Consider an experimental scenario in which the single input and two output mixtures of a laboratory indented cylinder are all recorded using a machine vision camera. The seed mixture enters and leaves the system on small conveyor belts and each of the cameras installed over the three belts acquires a still image at a fixed time interval. These images are analysed and various individual features are measured from each visible seed, e.g. length, width, coefficient of sphericity, etc. The univariate distribution of the individual seed lengths measured in the single input mixture would be assumed multimodal or perhaps bimodal, i.e. a univariate mixture distribution of (at least) two gaussian components with different location and scale parameters.

The univariate distributions for the individual seed lengths, similarly measured in the images taken of the two output mixtures, would be assumed unimodal (univariate gaussian). Such probabilistic measurements of input and output seed lengths, combined with other inputs such as the value of rotational speed ω, indent working diameter d, and the working angle α of the collecting bin, all represent a useful set of observations that can be used to continuously control the indented cylinder's performance through the adjustment of rotational speed ω and the working angle α of the collecting bin.

Input mixture as a fixed parameter

Alternatively, it might be more practical (as in simpler) to consider the characteristics of the input mixture as being fixed parameters. Dynamic control of the indented cylinder would in this case not be necessary. The governing parameters ω, d and α would be instead be adjusted just once to achieve an optimal sorting outcome.

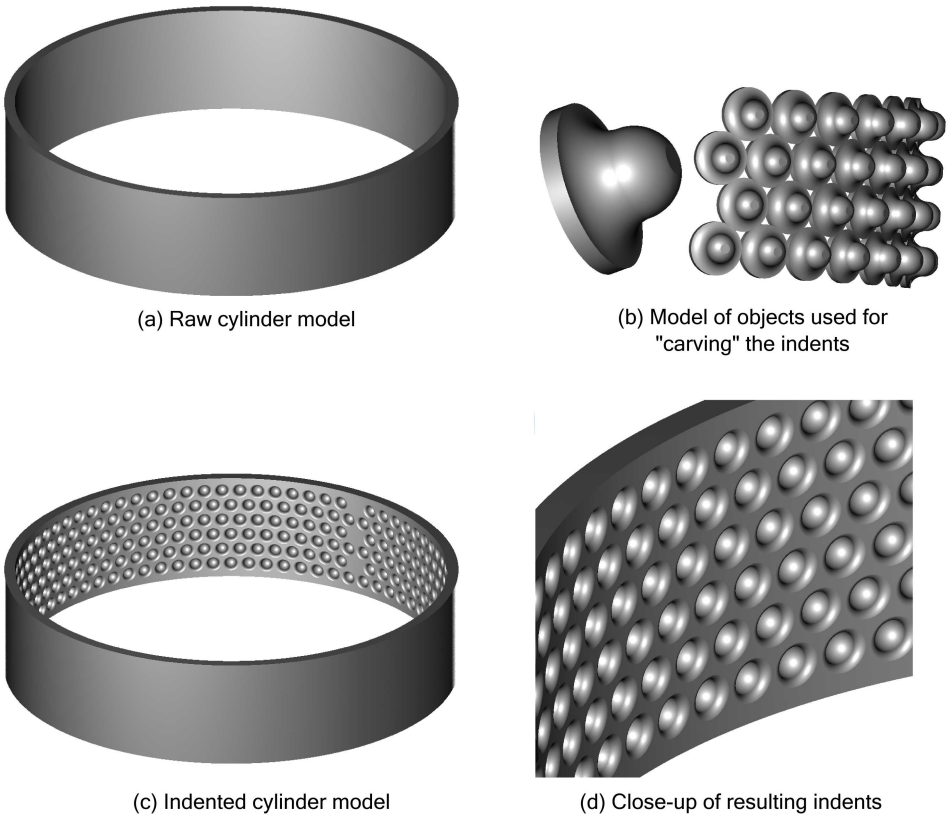

Figure 17: Computer-aided design (CAD) models of the indented cylinder.

5.2.2 Computer Simulations

It would be useful to have software that would make it possible to carry out two- or three-dimensional visualisations of the internal process in the indented cylinder. Such software would most likely be based on the discrete element method (DEM) introduced by Cundall and Strack (1979). By using open-source DEM-based simulation software[1] it would be possible to carry out synthetic seed separation experiments and also visualise them in three dimensions. By taking advantage of computational hardware acceleration, such as general-purpose graphical units (GPGPU), it would possible to run such simulations in real-time using a realistic high number of individual granular objects.

DEM-based simulations would require a computerised model of the inner surface of the indented cylinder. There are many ways in which such a model could be constructed. This section reports on a preliminary attempt at designing a model of the inner cylinder surface using computer aided design (CAD) software. The software used was the free BRL-CAD[2].

[1] One example of simulation software could be Yade (Yet Another Dynamic Engine). Yade is an open source toolkit of DEM algorithms written in C++. These toolkits are integrated with Python to give easy access to description and control of a simulation scenario (Šmilauer et al., 2010).

[2] Available at `http://brlcad.org/` for various major operating systems.

In BRL-CAD, one use concepts from constructive solid geometry (CSG) to design complex solid models by combining three-dimensional solid primitives. The combinations are based on simple set-theoretical rules: (1) union, (2) intersection, and (3) subtraction of primitives such as cylinders, spheres, toruses, and general polyhedrons (Requicha, 1980; Ghali, 2008).

Figure 17 shows ray-traced version of some of the CSG-based sub-elements involved in the design. These models were created using BRL-CAD. Figure 17a shows a raw cylinder model with no indents in its inner surface. This model was created by subtracting a small cylinder primitive from a larger cylinder primitive – thereby creating a hole in the larger cylinder. Shown in the left side of Figure 17b is the solid object used to "carve" out the indents of the raw cylinder model. This object, itself being a combination of solid primitives, represents the spatial inverse of an indent. Shown in the right side of the same figure is a combined set of these objects. They are positioned relatively to each other in such a way that they will each carve one indent in the raw cylinder inner surface at the correct location. The resulting cylinder model is depicted in Figure 17c and a close-up is shown in Figure 17d. It is likely that DEM-based computer simulations would benefit from such models of the indented cylinder.

5.2.3 Final Thoughts

The research summarised in this thesis should be seen as an important step towards future research in system identification of the indented cylinder. Computer vision techniques were developed to extract a measure of the separation efficiency of a laboratory indented cylinder. Such technical solutions are currently novel and represent an ideal platform for future applied research into empirical model development.

Such research should focus specifically on sampling time series of the inputs and outputs of the indented cylinder – both laboratory-scaled and industrial-scaled versions. The short-term vision could be an automated indented cylinder that adjusts itself after having been given some initial data.

The long-term vision could be a new form of seed sorting device based on the original indented cylinder. The operations of such a device would most likely involve technologies such as computer vision, artificial intelligence, and probably also borrow from the field of robotics. This long-term vision will most likely require a technological paradigm shift.

References

Abdel-Salam, M., Ahmed, A., El-Kishky, H., 2004. Seeds sorting by electrostatic separation: an experimental study, in: Electrical Insulation and Dielectric Phenomena, 2004. CEIDP '04. 2004 Annual Report Conference on, pp. 377–380.

Alexandratos, N., Bruinsma, J., 2012. World agriculture towards 2030/2050: the 2012 revision. ESA Working Paper No. 12–03. FOA (Food and Agriculture Organization of the United Nations).

Balascio, C.C., Misra, M.K., Johnson, H.P., 1987a. Particle movement and separation phenomena for a gravity separator: I. development of a markov probability model and estimation of model parameters. Transactions of the American Society of Agricultural Engineers 30, 1834–1839.

Balascio, C.C., Misra, M.K., Johnson, H.P., 1987b. Particle movement and separation phenomena for a gravity separator: Ii. experimental data and performance of distance-transition markov models. Transactions of the American Society of Agricultural Engineers 30, 1840–1847.

Balascio, C.C., Misra, M.K., Johnson, H.P., 1988. Stochastic modeling of granular flow in seed sorting. Mathematical and Computer Modelling 11, 523–527.

Berlage, A.G., Bilsland, D.M., Brandenburg, N.R., Cooper, T.M., 1984a. Experimental indent cylinder for separating seeds. Transactions of the American Society of Agricultural Engineers 27, 358–361.

Berlage, A.G., Churchill, D.B., Cooper, T.M., Bisland, D.M., 1989. The application of new technologies to seed conditioning. Journal of Agricultural Engineering Research 42, 193–202.

Berlage, A.G., Cooper, T.M., Carone, R.A., 1984b. Seed sorting by machine vision. Agricultural engineering 65, 14–17.

Besl, P.J., Jain, R.C., 1985. Three-dimensional object recognition. ACM Comput. Surv. 17, 75–145.

Bharathi, P.T., Subashini, P., 2011. Optimization of image processing techniques using neural networks: a review. WSEAS Trans. Info. Sci. and App. 8, 300–328.

Bhattacharyya, A., 1943. On a measure of divergence between two statistical populations defined by their probability distributions. Bulletin of the Calcutta Mathematical Society 35, 99–109.

Bishaw, Z., Niane, A.A., Gan, Y., 2007. Quality seed production, in: Yadav, S.S., McNeil, D.L., Stevenson, P.C. (Eds.), Lentil. Springer Netherlands, pp. 349–383.

Braidwood, R.J., Çambel, H., Watson, P.J., 1969. Prehistoric investigations in southeastern turkey. Science 164, 1275–1276.

Brandenburg, N.R., 1977. The principles and practice of seed cleaning: separation with equipment that senses dimension, shape, density, and terminal velocity of seeds. Seed science and technology 5, 173–186.

Brandenburg, N.R., Harmond, J.E., 1966. Separating Seeds by Length With Special Indent Cylinders. Technical Bulletin 88. Agricultural Experiment Station, Oregon State University, Corvalis.

Bridgwater, J., 2012. Mixing of powders and granular materials by mechanical means – a perspective. Particuology 10, 397–427.

Bruzzone, L., Roli, F., Serpico, S.B., 1995. An extension of the jeffreys-matusita distance to multiclass cases for feature selection. Geoscience and Remote Sensing, IEEE Transactions on 33, 1318–1321.

Butunoi, T., Buda, G., Dragos, C., Samuila, A., Neamtu, V., Morar, R., Dascalescu, L., Iuga, A., 2011. Wheat seeds separation in high-intensity electric field, in: Advanced Topics in Electrical Engineering (ATEE), 2011 7th International Symposium on, pp. 1–6.

Buus, O.T., Jørgensen, J.R., Carstensen, J.M., 2011. Analysis of seed sorting process by estimation of seed motion trajectories, in: Heyden, A., Kahl, F. (Eds.), Image Analysis. Springer Berlin / Heidelberg. volume 6688 of *Lecture Notes in Computer Science*, pp. 273–284.

Campbell, C.S., 2006. Granular material flows – an overview. Powder Technology 162, 208–229.

Căsăndroiu, T., Popescu, M., Voicu, G., 2009. A developing a mathematical model for simulating the seeds separation process on the plane sieves. UPB Scientific Bulletin, Series D: Mechanical Engineering 71, 17–28.

Chandola, V., Banerjee, A., Kumar, V., 2009. Anomaly detection: A survey. ACM Comput. Surv. 41, 15:1–15:58.

Chatfield, C., 2004. The Analysis of Time Series – An Introduction. Texts in Statistical Science, Chapman & Hall. 6 edition.

Chhabra, M., Reel, P.S., 2011. Morphology based feature extraction and recognition for enhanced wheat quality evaluation, in: Aluru, S., Bandyopadhyay, S., Catalyurek, U.V., Dubhashi, D.P., Jones, P.H., Parashar, M., Schmidt, B. (Eds.), Contemporary Computing. Springer Berlin Heidelberg. volume 168 of *Communications in Computer and Information Science*, pp. 41–50.

Choon-Ki, L., Song, J., Yun, J.T., Seo, J.H., Lee, J.E., Kim, J.T., Jeong, G.H., Kim, C.K., 2009. The optimum operating conditions of indented-cylinder length grader to remove broken rice based on varietal characteristics. Korean Journal of Crop Science 54, 366–374.

Christ, M.C.J., Parvathi, R.M.S., 2012. Segmentation of medical image using k-means clustering and marker controlled watershed algorithm. European Journal of Scientific Research 71, 190–194.

Churchill, D.B., Berlage, A.G., Bilsland, D.M., Cooper, T.M., 1989. Decision-support system development for conditioning seeds with indent cylinder. Transactions of the American Society of Agricultural Engineers 32, 1395–1398.

Cooper, T.M., Berlage, A.G., 1985. Machine vision for monitoring seed conditioning. ASAE Paper 85-3036. American Society of Agricultural Engineers, St. Joseph, MI 49085.

Cooper, T.M., Berlage, A.G., 1986. Integrating database and machine vision seed measuring process. ASAE paper 86-3062. American Society of Agricultural Engineers, St. Joseph, MI 49085.

Cundall, P.A., Strack, O.D.L., 1979. Discrete numerical model for granular assemblies. Geotechnique 29, 47–65.

De, S., Bhattacharyya, S., Chakraborty, S., 2012. Color image segmentation using parallel optimusig activation function. Applied Soft Computing 12, 3228–3236.

Dell'Aquila, A., 2007. Towards new computer imaging techniques applied to seed quality testing and sorting. Seed Science and Technology 35, 519–538.

Dell'Aquila, A., 2009. Digital imaging information technology applied to seed germination testing. a review. Agronomy for Sustainable Development 29, 213–221.

Delouche, J.C., Cabrera, E.R., Keith, B.C., 1995. Strategies for improving physiological seed quality. Bulletin 1029. Mississippi Agricultural and Forestry Experiment Station.

Demagh, Y., Moussa, H.B., Lachi, M., Noui, S., Bordja, L., 2012. Surface particle motions in rotating cylinders: Validation and similarity for an industrial scale kiln. Powder Technology 224, 260–272.

Desai, B.B., 2004. Drying, cleaning, and upgrading, in: Seeds Handbook: Processing And Storage. CRC Press, pp. 477–511.

Ding, Y.L., Forster, R.N., Seville, J.P.K., Parker, D.J., 2001. Scaling relationships for rotating drums. Chemical Engineering Science 56, 3737–3750.

Dinneen, G.P., 1955. Programming pattern recognition, in: Proceedings of the Western Joint Computer Conference, pp. 94–100.

Douik, A., Abdellaoui, M., 2010. Cereal grain classification by optimal features and intelligent classifiers. International Journal of Computers, Communications and Control 5, 506–516.

Du, K., 2010. Clustering: A neural network approach. Neural Networks 23, 89–107.

Egmont-Petersen, M., de Ridder, D., Handels, H., 2002. Image processing with neural networks – a review. Pattern Recognition 35, 2279–2301.

Ekstrand, B., 2012. Some aspects on filter design for target tracking. Journal of Control Science and Engineering 2012, 1–15.

El-Awady, M.N., Yehia, I., Ebaid, M.T., Arif, E.M., 2009. Development of rice cleaner for reduced impurities and losses. AMA, Agricultural Mechanization in Asia, Africa and Latin America 40, 15–20.

Farkas, I., 2003a. Artificial intelligence in agriculture. Computers and Electronics in Agriculture 40, 1–3. Editorial.

Farkas, I., 2003b. Control aspects of postharvest technologies, in: Handbook of Postharvest Technology. CRC Press, pp. 845–866.

Farkas, I., 2005. Modelling and control in agricultural processes. Computers and Electronics in Agriculture 49, 315–316. Editorial.

Fisher, R.A., 1936. The use of multiple measurements in taxonomic problems. Annals of Eugenics 7, 179–188.

Forsyth, D.A., Ponce, J., 2011. Computer Vision, A Modern Approach. Prentice Hall.

Forterre, Y., Pouliquen, O., 2008. Flows of dense granular media. Annual Review of Fluid Mechanics 40, 1–24.

Fouad, H.A., 1980. The effect of cell configuration on length grading of beans. Journal of Agricultural Engineering Research 25, 391–406.

Frühwirth-Schnatter, S., 2006. Finite Mixture and Markov Switching Models. Springer Series in Statistics, Springer New York.

Ghali, S., 2008. Constructive solid geometry, in: Introduction to Geometric Computing. Springer London, pp. 277–283.

Gorman, C.F., 1969. Hoabinhian: A pebble-tool complex with early plant associations in southeast asia. Science 163, 671–673.

Gregg, B., Billups, G., 2010a. Seed Conditioning, Volume 1: Management. Science Publishers.

Gregg, B., Billups, G., 2010b. Seed Conditioning, Volume 2: Technology. Science Publishers.

Grochowicz, J., 1980. Machines for cleaning and sorting of seeds. Department of Agriculture. Translated from Polish.

Guberac, V., Martinčić, J., Marić, S., 1998. Influence of seed size on germinability, germ length, rootlet length and grain yield in spring oat [einfluss der samengrosse auf die keimfahigkeit, keimlings- und wurzellange und auf den ertrag von sommerhafer]. Bodenkultur 49, 13–18.

Guerrero, J., Pajares, G., Montalvo, M., Romeo, J., Guijarro, M., 2012. Support vector machines for crop/weeds identification in maize fields. Expert Systems with Applications 39, 11149 –11155.

Guevara-Hernandez, F., Gomez-Gil, J., 2011. A machine vision system for classification of wheat and barley grain kernels. Spanish Journal of Agricultural Research 9, 672–680.

Guo, Z., Hall, R.W., 1989. Parallel thinning with two-subiteration algorithms. Commun. ACM 32, 359–373.

Hajra, S., Khakhar, D., 2011. Radial segregation of ternary granular mixtures in rotating cylinders. Granular Matter 13, 475–486.

Hall, R.W., Kong, T.Y., Rosenfeld, A., 1996. Shrinking binary images, in: Kong, T.Y., Rosenfeld, A. (Eds.), Topological Algorithms for Digital Image Processing. North-Holland. volume 19 of *Machine Intelligence and Pattern Recognition*, pp. 31–98.

Hampton, J.G., 2002. What is seed quality? Seed Science and Technology 30, 1–10.

Harmond, J.E., Brandenburg, N.R., Jensen, L.A., 1965. Physical properties of seed. Transactions of ASAE 8, 30–32.

Harper, J.L., Lovell, P.H., Moore, K.G., 1970. The shapes and sizes of seeds. Annual Review of Ecology and Systematics 1, 327–356.

Heimann, T., Meinzer, H., 2009. Statistical shape models for 3d medical image segmentation: A review. Medical Image Analysis 13, 543–563.

Hellinger, E., 1909. Neue begründung der theorie quadratischer formen von unendlichvielen veränderlichen. Journal für die reine und angewandte Mathematik 136, 210–271.

Huimin, W., Mingliang, W., Lun, T., Yong, L., Ping, D., 2011. Dynamic analysis to the seeds in indent of the indent cylinder separator, in: International Conference on Intelligent Computation Technology and Automation (ICICTA) 2011, pp. 66–70.

Jaeger, H.M., Nagel, S.R., Behringer, R.P., 1996. The physics of granular materials. Physics Today 49, 32–38.

Jayadevappa, D., Murty, D., Kumar, S., 2011. Medical image segmentation algorithms using deformable models: A review. IETE Technical Review 28, 248–255.

Jayas, D.S., Cenkowski, S., 2006. Grain property values and their measurement, in: Mujumdar, A.S.. (Ed.), Handbook of Industrial Drying. CRC Press, pp. 575–603.

Johnson, H.L., 1938. Grain separators. U.S. Patent 2,135,343, filled September 30, 1935, and issued November 1, 1938.

Junejo, I., Bhutta, A., Foroosh, H., 2011. Single-class svm for dynamic scene modeling. Signal, Image and Video Processing 5, 1–8. 10.1007/s11760-011-0230-z.

Kalkan, F., Kara, M., 2011. Handling, frictional, and technological properties of wheat as affected by moisture content and cultivar. Powder Technology 213, 116–122.

Kalman, R.E., 1960. A new approach to linear filtering and prediction problems. Journal of Basic Engineering 82, 35–45.

Karaj, S., Müller, J., 2010. Determination of physical, mechanical and chemical properties of seeds and kernels of jatropha curcas l. Industrial Crops and Products 32, 129–138.

Karasulu, B., Balli, S., 2010. Image segmentation using fuzzy logic, neural networks and genetic algorithms: survey and trends. Machine Graphics & Vision International Journal 19, 367–409.

Karimi, M., Kheiralipour, K., Tabatabaeefar, A., Khoubakht, G.M., Naderi, M., Heidarbeigi, K., 2009. The effect of moisture content on physical properties of wheat. Pakistan Journal of Nutrition 8, 90–95.

Ke, Y., Zhang, G., 2011. An improved image segmentation algorithm using support vector machines, in: Computer Science and Service System (CSSS), 2011 International Conference on, pp. 185–188.

Keil, T., 2010. Separator for sorting of granules. Patent WO 2010/125528 A2, filed 28 April 2010, and issued 4 November 2010.

Kurth, H., 1877. Improvement in grain-separators. U.S. Patent 188,641, filled March 10, 1877, and issued March 20, 1877.

Lam, L., Lee, S.W., Suen, C.Y., 1992. Thinning methodologies-a comprehensive survey. Pattern Analysis and Machine Intelligence, IEEE Transactions on 14, 869–885.

Lampeter, W., 1965. Die saatgutaufbereitung. VEB Deutscher Landwirtschaftsverlag, Berlin.

Langkilde, N.E., Nydam, J., 1973. Seed cleaning in the laboratory. Technical report.

Leadbeater, T.W., Parker, D.J., 2011. A modular positron camera for the study of industrial processes. Nuclear Instruments and Methods in Physics Research Section A: Accelerators, Spectrometers, Detectors and Associated Equipment 652, 646–649.

Leadbeater, T.W., Parker, D.J., Gargiuli, J., 2012. Positron imaging systems for studying particulate, granular and multiphase flows. Particuology 10, 146–153.

Lilliefors, H.W., 1967. On the kolmogorov-smirnov test for normality with mean and variance unknown. Journal of the American Statistical Association 62, 399–402.

Ljung, L., 1999. System Identification – Theory for the user. Prentice Hall.

Ljung, L., 2010. Perspectives on system identification. Annual Reviews in Control 34, 1–12.

MacNeish, R.S., 1964. Ancient mesoamerican civilization. Science 143, 531–537.

Madsen, E., Langkilde, N.E. (Eds.), 1987a. ISTA handbook for cleaning of agricultural and horticultural seeds on small-scale machines – Part 1. International Seed Testing Association.

Madsen, E., Langkilde, N.E. (Eds.), 1987b. ISTA handbook for cleaning of agricultural and horticultural seeds on small-scale machines – Part 2. International Seed Testing Association.

Mahalanobis, P., 1936. On the generalized distance in statistics. Proceedings of the National Institute of Sciences of India 2, 49–55.

Markou, M., Singh, S., 2003a. Novelty detection: a review – part 1: statistical approaches. Signal Process. 83, 2481–2497.

Markou, M., Singh, S., 2003b. Novelty detection: a review – part 2: neural network based approaches. Signal Process. 83, 2499–2521.

Martinez, A.M., Kak, A., 2001. Pca versus lda. Pattern Analysis and Machine Intelligence, IEEE Transactions on 23, 228–233.

Martre, P., Bertin, N., Salon, C., Génard, M., 2011. Modelling the size and composition of fruit, grain and seed by process-based simulation models. New Phytologist 191, 601–618.

Matusita, K., 1955. Decision rules, based on the distance, for problems of fit, two samples, and estimation. The Annals of Mathematical Statistics 26, 631–640.

Matusita, K., 1956. Decision rule, based on the distance, for the classification problem. Annals of the Institute of Statistical Mathematics 8, 67–77.

Maurer, C.R., J., Qi, R., Raghavan, V., 2003. A linear time algorithm for computing exact euclidean distance transforms of binary images in arbitrary dimensions. Pattern Analysis and Machine Intelligence, IEEE Transactions on 25, 265–270.

McCarthy, J., Minsky, M.L., Rochester, N., Shannon, C.E., 1955. A proposal for the dartmouth summer research project on artificial intelligence.

Mjolsness, H., 1939. Apparatus for separating grain. U.S. Patent 2,182,638, filled February 4, 1935, and issued December 5, 1939.

Mobius, M.E., Lauderdale, B.E., Nagel, S.R., Jaeger, H.M., 2001. Brazil-nut effect: Size separation of granular particles. Nature 414, 270–270.

Nikulin, M.S., 1989. Hellinger distance, in: Hazewinkel, M. (Ed.), Encyclopedia of Mathematics. Kluwer Academic Publishers. volume 4, p. 400.

Nobbe, F., 1876. Handbuck der Samenkunde. Verlag von Wiegand, Hempel, und Parey, Berlin.

Obregón, L., Realpe, A., Rinaldi, C., Velázquez, C., 2010a. Mixing of granular materials. part i: Effect of periodic shear. Powder Technology 197, 9–16.

Obregón, L., Realpe, A., Velázquez, C., 2010b. Mixing of granular materials, part ii: effect of particle size under periodic shear. Powder Technology 201, 193–200.

Ogunnaike, B., Ray, W.H., 1994. Process Dynamics, Modeling, and Control. Topics in Chemical Engineering, OUP USA.

Olsen, C., Hansen, P., 1980. Høsttid i vinterhvede, vårhvede og vinterrug. Tidskrift for Planteavl 84, 89–100.

Ottino, J.M., Khakhar, D.V., 2000. Mixing and segregation of granular materials. Annual Review of Fluid Mechanics 32, 55–91.

Öztürk, T., Esen, B., 2008. Physical and mechanical properties of barley. Agricultura tropica et subtropica 41, 117–121.

Pal, N.R., Pal, S.K., 1993. A review on image segmentation techniques. Pattern Recognition 26, 1277–1294.

Panasiewicz, M., Sobczak, P., Mazur, J., Zawiślak, K., Andrejko, D., 2012. The technique and analysis of the process of separation and cleaning grain materials. Journal of Food Engineering 109, 603–608.

Parker, D., Broadbent, C., Fowles, P., Hawkesworth, M., McNeil, P., 1993. Positron emission particle tracking - a technique for studying flow within engineering equipment. Nuclear Instruments and Methods in Physics Research Section A: Accelerators, Spectrometers, Detectors and Associated Equipment 326, 592–607.

Parker, D.J., Dijkstra, A.E., Martin, T.W., Seville, J.P.K., 1997. Positron emission particle tracking studies of spherical particle motion in rotating drums. Chemical Engineering Science 52, 2011–2022.

Pearson, R., 2003. Control systems, identification, in: Meyers, R.A. (Ed.), Encyclopedia of Physical Science and Technology (Third Edition). Academic Press, New York, Third edition edition. pp. 687–707.

Pearson, R.K., 2006. Nonlinear empirical modeling techniques. Computers & Chemical Engineering 30, 1514–1528.

Pearson, T., 2009. Hardware-based image processing for high-speed inspection of grains. Computers and Electronics in Agriculture 69, 12–18.

Pearson, T., Brabec, D., Haley, S., 2008. Color image based sorter for separating red and white wheat. Sensing and Instrumentation for Food Quality and Safety 2, 280–288.

Pedersen, J.B. (Ed.), 2011. Oversigt over Landsforsøgene 2011. Forsøg og undersøgelser i Dansk Landbrugsrådgivning, Videncentret for Landbrug, Planteproduktion.

Pereira, G., Sinnott, M., Cleary, P., Liffman, K., Metcalfe, G., Šutalo, I., 2011. Insights from simulations into mechanisms for density segregation of granular mixtures in rotating cylinders. Granular Matter 13, 53–74.

Pöschel, T., Buchholtz, V., 1995. Complex flow of granular material in a rotating cylinder. Chaos, Solitons and Fractals 5, 1901–1905,1907–1912.

Rajchenbach, J., 2000. Granular flows. Advances in Physics 49, 229–256.

Requicha, A.G., 1980. Representations for rigid solids: Theory, methods, and systems. ACM Comput. Surv. 12, 437–464.

Riahi, E., Ramaswamy, H.S., 2003. Structure and composition of cereal grains and legumes, in: Handbook of Postharvest Technology. CRC Press, pp. 17–40.

Ristow, G., 2000. Rotating drum, in: Pattern Formation in Granular Materials. Springer Berlin / Heidelberg. volume 164 of *Springer Tracts in Modern Physics*, pp. 81–124.

Robert, C., Noriega, A., Tocino, Á., Cervantes, E., 2008. Morphological analysis of seed shape in arabidopsis thaliana reveals altered polarity in mutants of the ethylene signaling pathway. Journal of Plant Physiology 165, 911–919.

Sablani, S.S., Ramaswamy, H.S., 2003. Physicial and thermal properties of cereal grains, in: Handbook of Postharvest Technology. CRC Press, pp. 17–40.

Salti, S., Cavallaro, A., Di Stefano, L., 2012. Adaptive appearance modeling for video tracking: Survey and evaluation. Image Processing, IEEE Transactions on 21, 4334–4348.

Schmidt, L., 2007. Seed processing, in: Tropical Forest Seed. Springer Berlin Heidelberg, pp. 67–142.

Schölkopf, B., Platt, J.C., Shawe-Taylor, J., Smola, A.J., Williamson, R.C., 2001. Estimating the support of a high-dimensional distribution. Neural Computation 13, 1443–1471.

Seiden, G., Thomas, P.J., 2011. Complexity, segregation, and pattern formation in rotating-drum flows. Rev. Mod. Phys. 83, 1323–1365.

Selfridge, O.G., Neisser, U., 1960. Pattern recognition by machine. Scientific American 203, 60–68.

Shapiro, L.G., Stockman, G.C., 2001. Computer Vision. Prentice Hall.

Siddiqui, F., Mat Isa, N.A., 2012. Optimized k-means (okm) clustering algorithm for image segmentation. Opto-Electronics Review 20, 216–225.

Simonyan, K.J., Mudiare, O.J., El-Okene, A.M., Yiljep, Y.D., 2010. Development of a mathematical model for predicting the cleaning efficiency of stationary grain threshers using dimensional analysis. Applied Engineering in Agriculture 26, 189–195.

Sinha, P.K., 2012. Scene illumination, in: Image Acquisition and Preprocessing for Machine Vision Systems. SPIE, pp. 75–102.

Sologubik, C., Campañone, L., Pagano, A., Gely, M., 2013. Effect of moisture content on some physical properties of barley. Industrial Crops and Products 43, 762 –767.

Sonka, M., Hlavac, V., Boyle, R., 2008. Image Processing, Analysis, and Machine Vision. Cengage Learning.

Sorica, C., Pirna, I., Bracacescu, C., Marin, E., Postelnicu, E., 2012. Cinematic analysis of particle of impurity in conditioning process of grains into indented cylinder separators, in: Engineering for Rural Development, pp. 60–66.

Sowmya, B., Rani, B.S., 2011. Colour image segmentation using fuzzy clustering techniques and competitive neural network. Applied Soft Computing 11, 3170–3178.

Studman, C.J., 2001. Computers and electronics in postharvest technology – a review. Computers and Electronics in Agriculture 30, 109–124.

Szczypiński, P.M., Zapotoczny, P., 2012. Computer vision algorithm for barley kernel identification, orientation estimation and surface structure assessment. Computers and Electronics in Agriculture 87, 32–38.

Szeliski, R., 2010. Computer Vision: Algorithms and Applications. Springer.

Tabatabaeefar, A., 2003. Moisture-dependent physical properties of wheat. Int. Agrophysics 17, 207–211.

Tang, M., Peng, X., 2012. Robust tracking with discriminative ranking lists. Image Processing, IEEE Transactions on 21, 3273–3281.

Tavakoli, M., Tavakoli, H., Rajabipour, A., Ahmadi, H., Gharib-Zahedi, S.M.T., 2009. Moisture-dependent physical properties of barley grains. International Journal of Agricultural and Biological Engineering 2, 84–91.

The Economist, 2011. The 9 billion-people question – a special report on feeding the world.

Third, J.R., Scott, D.M., Müller, C.R., 2011. Axial transport within bidisperse granular media in horizontal rotating cylinders. Phys. Rev. E 84, 041301.

Vavilov, N.I., 1926. Studies on the origins of cultivated plants. Bulletin of applied botany and plant breeding 16, 1–245.

Šmilauer, V., Gladky, A., Kozicki, J., Modenese, C., Stránskỳ, J., 2010. Yade Using and Programming, in: Šmilauer, V. (Ed.), Yade Documentation. The Yade Project, 1st edition. Http://yade-dem.org/doc/.

Wang, X.Y., Wang, Q.Y., Yang, H.Y., Bu, J., 2011. Color image segmentation using automatic pixel classification with support vector machine. Neurocomputing 74, 3898–3911.

Wang, X.Y., Zhang, X.J., Yang, H.Y., Bu, J., 2012. A pixel-based color image segmentation using support vector machine and fuzzy -means. Neural Networks 33, 148–159.

Ward, T., Hourigan, W., 2012. Granular segregation in a tilted-rotating drum. Powder Technology 215–216, 227–234.

Wen, X.B., Zhang, H., Wang, F.Y., 2009. A wavelet neural network for sar image segmentation. Sensors 9, 7509–7515.

Wu, R.S., Chung, W.H., 2009. Ensemble one-class support vector machines for content-based image retrieval. Expert Systems with Applications 36, 4451–4459.

Xun, Y., Zhang, J., Li, W., Cai, W., 2006. Automatic system of seeds refined grading based on machine vision, in: Intelligent Control and Automation, 2006. WCICA 2006. The Sixth World Congress on, pp. 9686 –9689.

Yang, H., Wang, X., Wang, Q., Zhang, X., 2012. Ls-svm based image segmentation using color and texture information. Journal of Visual Communication and Image Representation 23, 1095–1112.

Yilmaz, A., Javed, O., Shah, M., 2006. Object tracking: A survey. ACM Comput. Surv. 38, 1–45.

Yu, Z., Wong, H.S., Wen, G., 2011. A modified support vector machine and its application to image segmentation. Image and Vision Computing 29, 29–40.

Yuan, J., Yu, T., Wang, K., 2006. A hybrid intelligent approach for optimal control of seed cleaner. IFIP International Federation for Information Processing 207, 780–785.

Zhang, H., Fritts, J.E., Goldman, S.A., 2008. Image segmentation evaluation: A survey of unsupervised methods. Computer Vision and Image Understanding 110, 260–280.

Zhang, K., Song, H., 2013. Real-time visual tracking via online weighted multiple instance learning. Pattern Recognition 46, 397–411.

Zhu, H., Zhou, Z., Yang, R., Yu, A., 2007. Discrete particle simulation of particulate systems: Theoretical developments. Chemical Engineering Science 62, 3378–3396.

Zhu, H., Zhou, Z., Yang, R., Yu, A., 2008. Discrete particle simulation of particulate systems: A review of major applications and findings. Chemical Engineering Science 63, 5728–5770.

Appendix A

Paper I – Analysis of Seed Sorting Process by Estimation of Seed Motion Trajectories

Buus O.T., Carstensen J.M., Jørgensen, J.R., 2011. **Analysis of Seed Sorting Process by Estimation of Seed Motion Trajectories**, in: Heyden, A., Kahl, F. (Eds.), Image Analysis. Springer Berlin / Heidelberg. volume 6688 of Lecture Notes in Computer Science, pp. 273–284.

Submitted December 20th 2010 and accepted as poster paper at the Scandinavian Conference in Image Analysis (SCIA), 23-27 May 2011, Ystad, Sweden. The accompanying poster (Poster II) is available in Appendix E.

Analysis of Seed Sorting Process by Estimation of Seed Motion Trajectories

Ole Thomsen Buus[1], Johannes Ravn Jørgensen[1], and Jens Michael Carstensen[2]

[1] Aarhus University, Faculty of Agricultural Sciences, Department of Genetics and Biotechnology, 4200 Slagelse, Denmark
{Ole.Buus,Johannes.Jorgensen}@agrsci.dk
[2] Informatics and Mathematical Modelling, Technical University of Denmark, Building 321, DK-2800 Lyngby, Denmark
jmc@imm.dtu.dk

Abstract. Seed sorting is a mechanical process in which the goal is to achieve a high level of purity and quality in the final product. Prediction and control of such processes are generally considered very difficult. One possible solution is a systems identification approach in which the seeds and their movement are directly observed and data about important process parameters extracted. Image analysis was used to extract such data from the internal sorting process in one particular seed sorting device - the so-called "indented cylinder". Twenty high speed image sequences were recorded of the indented cylinder in action, sorting a batch of barley with both whole and broken kernels. The motion trajectories and angle of escape for each seed in each frame were estimated. Motion trajectories and frequency distributions for the angle of escape are shown for different velocities and pocket sizes. A possible linear relationship is shown to exist between velocity and the angle. The temporal stability of certain parameters in the sorting process were also analysed and is shown to be quite stable for lower velocities.

Keywords: Seed sorting, indented cylinder, system identification, motion trajectories, image analysis

1 Introduction

When seeds are harvested from fields they contain a number of larger impurities (for example stones, leaves, branches, insects) that need to be removed. When these impurities have been removed using various preprocessing machinery all that remains are particles of generally the same size. If necessary this relatively clean seed material can now be processed further. This later step is known as *seed sorting* and is the industrial application that we have focused on in this work. In seed sorting the task is to further sort or *divide* the preprocessed seed material into at least two individual sets of particles.

Different types of seed sorting machines are used in the industry today. By physically manipulating the seed material in a way that takes advantage of various individual physical distinguishing characteristics of the seeds (usually one

for each type of machine) these machines are able to sort the material. Typical examples of such characteristics are (1) *mass* (density), (2) surface *texture* (friction with surfaces), (3) *length*, (4) general *size*, and (5) *shape* (for example round, prolonged, egg-shaped, flat).

The *prediction* and *control* of the process in these machines is generally considered very difficult. This is primarily due to the biological variations in the physical characteristics of the individual seeds. This is where the application of image analysis becomes relevant. There is a need for a systems identification approach wherein (parts of) the mechanical particle manipulation process is directly observed and useful information about important process parameters extracted. Image analysis is a natural tool for this.

In this paper we show results from experiments wherein image analysis was used to extract information from the internal process in the *indented cylinder* (laboratory scale). The indented cylinder is a *length* sorter that divides the incoming seed material into two subsets: (1) *long* and (2) *short* seeds. This is necessary for some seed species for which sorting based on other characteristics is not possible. The machine consists of a rotating cylinder lying down. The seed material is fed from one side. The inner surface of this cylinder is equipped with small pockets (indented into the metal). Due to the rotation of the cylinder these pockets carry the seeds up to a certain angle. This angle is dependent on the individual length of the seeds. In principle: Shorter seeds will be carried further than longer seeds. A catch-pan mounted at the centre of the cylinder will catch the shorter seeds while the longer seeds fall down to the bottom of the cylinder again. Due to a small tilt of the cylinder itself the longer seed material advances to the other side due to gravity. The shorter material is advanced using vibration of the catch-pan. Most of these basic principles are also depicted graphically in Figure 1(a).

Berlage et al. [2–4] are some of the earliest examples on the use of image analysis to analyse and improve seed sorting using prototypical machines (not indented cylinders). Dell'Aquila [7] is an example of a recent review on the subject of automated inspection of seed sorting for quality testing. On the modelling aspect again early work by Berlage et al. [1] and Churchill et al. [6] are mentionable. The analysis, modeling and simulation of the flow of particles in rotating cylinders has been done to great extent. But mostly for use in chemical, pharmaceutical, and matallurgical industries. Positron emission particle tracking (PEPT) [10, 11] and particle image velocimetry (PIV) [5] are examples of specialised technologies which have been applied for various purposes. Sandidi et al. [12] used a CCD camera for analysing the flow in a rotating drum used for coating tablets. Lastly we mention the summarised work in Grochowich [8] – one of the earliest full analyses of various types of seed sorting machines and their inherent complexity.

In this work we have specifically focused on deducing the *angle of escape* θ (with horizontal) of the individual seeds from recordings of the indented cylinder during an actual sorting process. The distribution of this important process pa-

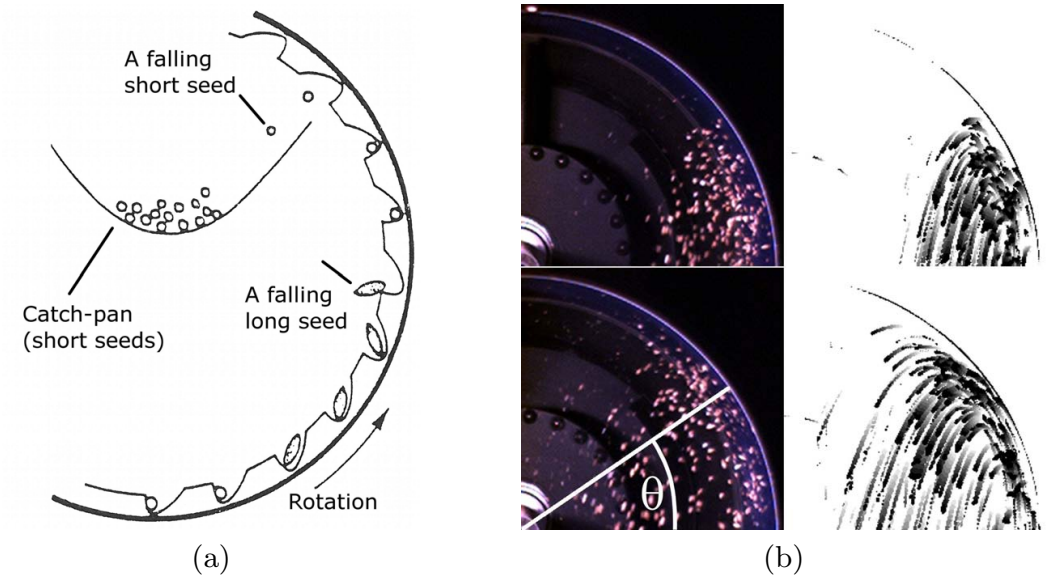

Fig. 1. A graphic and four examples of frames from the imaging data. Figure 1(a): The basic principles of the sorting process in the indented cylinder (modified from [9]). Figure 1(b): Four examples on frames acquired in the experiments. The two rows each show a situation from two different angular velocities of the cylinder (top: 26 rpm [revolutions per minute], bottom: 34 rpm). To the left we see the original version and to the right we see examples on accumulated seed segmentations (accumulated of over 10 frames starting from the one on the left). The *angle of escape* θ is shown graphically in the lower left original version.

rameter over time says something about the machines current ability to process and sort the material given to it.

We placed a colour CCD camera in front of the active cylinder (it was in motion with material in it) with the catch-pan removed. Each image frame (taken at 260 frames/sec) was then segmented and the (approximate) location of each seed (or particle) in the image plane was extracted. Using a combination of these locations and the laws of motion (no drag included) we were able to deduce the most likely parabolic escape trajectories and thus also an estimate for the angle of escape θ for each particle. Figure 1(b) shows two examples of the images recorded for two different rotational speeds of the cylinder.

Section 2 describes in more detail the experiments, seed material (barley), and the acquired data (20 image sequences). Section 3 explains the basic methods used for extracting the seed locations and for estimating the angle of escape θ. Section 4 presents the results and Section 5 concludes.

2 Materials and Data

2.1 Experimental Setup

We used a laboratory-sized indented cylinder (Westrup L-AT *LAT-0801*) that supports cylinders with a radius of 200 mm and a depth of 500 mm. The cylinder

had a (fixed) inclination with horizontal of 0.7°. A CCD colour camera (Point Grey Grasshopper *GRAS-03K2C-C*) was placed in front of the cylinder with the direction of sight aligned with the plane containing the cylinder's axis of rotation. The end of the cylinder closest to the camera was slightly lower due to the small inclination angle.

It was placed at a distance such that the width of the image corresponded to the apparent width of the cylinder. The monofocal lens used had a focal length of 25 mm and a horizontal and (deduced) vertical angle of view of 10.97° and 8.24°, respectively. The camera was also rotated 180° to use sub-sampling of the sensor lines and achieve a higher framerate. Using these parameters, the correct camera-to-cylinder distance was estimated to be 2.7 m.

Illumination was provided by a 150 W halogen modelling light (*SOLO 1600 B*) placed between camera and cylinder. The angle of light was such that all the seed material inside the cylinder received the same amount of illumination. Note that the catch-pan was removed to give room for visual inspection with the camera.

2.2 The Seed Material

The seed material used was barley (*Hordeum vulgare L.*). The indented cylinder is particularly suitable for filtering *broken* (usually half) non-useful barley kernels from *whole* useful barley kernels.

The barley used was filtered manually using the indented cylinder. This allowed us to create a modelled seed batch with a known per particle distribution of whole and broken kernels. The modelled batch consisted of 50 % whole and 50 % broken barley kernels. The mixed batch had a total mass of 2 kg which was more than enough for the experiments.

2.3 Experiments and Acquired Data

The cylinder was fed with the modelled seed batch and configured to run with different settings of two important system variables. These were: (1) the cylinder rotational speed and (2) the diameter of the pockets in the cylinder. We recorded the sorting process of the cylinder for *ten* different rotational speeds and for *two* different pocket diameters. The speed was sampled in the range from 26 rpm (*revolutions per minute*) to 49 rpm with an average step of 2.56 rpm (corresponding to angular frequencies of 2.73 rad/s to 5.14 rad/s with an average step of 0.27 rad/s). We used two different cylinders with pocket diameters of 6.0 mm and 7.0 mm.

A total of $2 \times 10 = 20$ image sequences were recorded at approximately 260 frames/sec for a total of ten seconds. After recording all sequences were temporarily synchronized such that the position of the cylinder circumference was the same in the first frame. This resulted in *five* seconds (1300 frames) of useful data in all 20 sequences (26000 frames in total). Each frame is of active dimensions 240×240 pixels and contains the *upper right quadrant* of the imaged cylinder circumference.

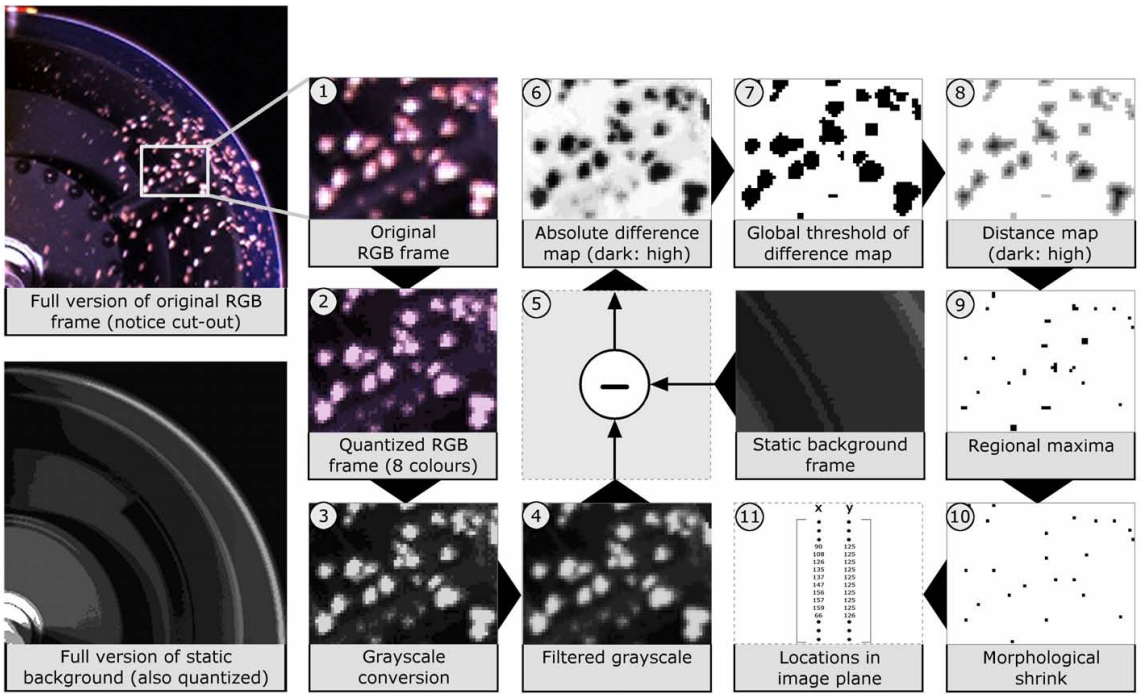

Fig. 2. The 11 image processing steps used to extract the seed locations (in the image plane). In the top-left part an example of a full frame is seen (cylinder velocity is 36 rpm [revolutions per minute]). Step 10 mentions the process of "morphological erosion". It is a continued erosion that shrinks objects without holes to single points (holes in objects are removed prior to the operation).

Let $K = 1300$ be the number of frames in each sequence, $V = 10$ the number of velocity steps, and $D = 2$ the number of pocket diameters. One can then define integer indexes $k = 1, \ldots, K$, $v = 1, \ldots, V$, and $d = 1, \ldots, D$ (where $d = 1$ and $d = 2$ corresponds to pocket diameter 6.0 mm and 7.0 mm, respectively). Any frame in any of the 20 sequences can now be described as a matrix $\mathbf{F}^{(k)}_{(v,d)} \in \mathbb{R}^{N \times N}$, where $N = 240$. Each sequence has also been given a mathematical name: $\mathcal{S}_{(v,d)} \in \mathbb{R}^{N \times N \times K}$. Finally, the following shorthand notations are defined: $\mathbf{F}^{(k)}$ is the k'th frame in any sequence $\mathcal{S}_{(v,d)}$ and $\mathbf{F}$ is any frame in any sequence. One final sequence exists: $\mathcal{B}$. This is a background sequence with no seeds in the scene – just the empty cylinder ($d = 2$) rotating at velocity step $v = 5$.

3 Methods

3.1 Estimation of Seed Locations

Figure 2 shows the 11 image processing steps used to extract the locations of the seeds in each frame $\mathbf{F}^{(k)}_{(v,d)}$. The average $\mathbf{B}_{ref}$ of sequence $\mathcal{B}$ is the static background frame mentioned in step 5. This is used for background subtraction to acquire a global segmentation and to remove certain problematic areas of the image. The resulting absolute difference map was scaled to range $[0, 1]$ and

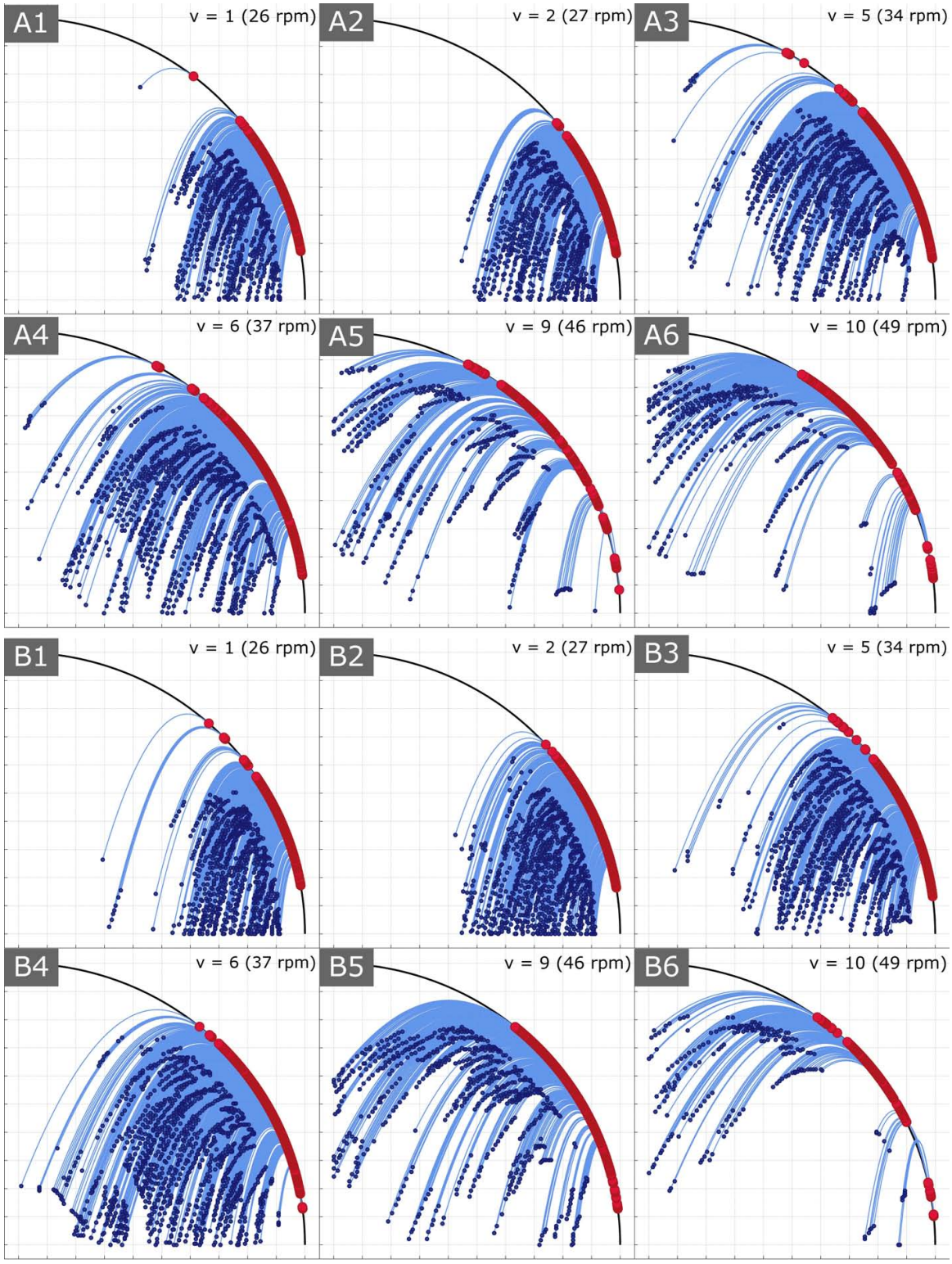

Fig. 3. Twelve "trajectory plots": In the top part (markings "A1" to "A6") they are shown for six velocities $v = 1$, 2, 5, 6, 9, and 10; for pocket size d = 1 (6.0 mm). In the lower part (markings "B1" to "B6") they are shown for the same velocities but for pocket size $d = 2$ (7.0 mm). The points shown correspond to the extracted point locations in $\mathbb{R}^2$. The markings on the circumference depict the estimated θ values.

a global threshold (step 7) of 0.4 was used (everything above that level was considered part of foreground/seed). Various morphological tools are then used to produce binary map containing approximate seed locations in the image plane. Finally these locations in the image plane are transformed to a 2-dimensional *world space* in $\mathbb{R}^2$ by a linear interpolation.

3.2 Estimating the Angle of Escape θ

We have estimated the angle of escape θ and calculated the corresponding parabolic trajectory for all twenty configurations of the indented cylinder. Figure 3 show six such "trajectory plots" for rotational speeds $v = 1$, 2, 5, 6, 9, and 10; and for both pocket sizes $d = 1$ and 2. Note the visible difference in trajectories due to change in speed. The points shown are the ones extracted from the recorded frames using the methods described above.

The estimation of θ was done for all points extracted from all frames $\mathbf{F}$ using the processing steps just described (one estimate per point). To minimize data representation complexity, the seed locations from every 10 frames were combined into a single set of points. That is, for any sequence $\mathcal{S}_{(v,d)}$ we generate $L = K/10 = 1300/10 = 130$ *accumulated* point sets $A^{(l)}$ containing $I^{(l)}$ points $(x_i, y_i) \in \mathbb{R}^2$. These accumulated point sets are then analysed for $l = 1, \ldots, L$ resulting in a solution set $\Theta^{(l)}$ containing $I^{(l)}$ scalars $\theta_i \in \mathbb{R}$.

The specific number of points $I^{(l)}_{(v,d)}$ available in each $A^{(l)}_{(v,d)}$ varies only slightly over l but expectedly varies more over index v and d. Especially for d since the 1 mm difference in pocket diameter has the effect that different amounts of seeds are caught by the pockets.

During sorting, a seed or particle moves with the cylinder up to a certain angle θ. This angle is dependent on the radius r and current angular frequency ω of the indented cylinder. We model the movement of each such particle as a point (x_i, y_i) moving in $\mathbb{R}^2$ in its own local time domain, starting at time $t_i = 0$ when a force equilibrium (explained in great detail in Grochowich [8, Chp. 7]) accelerates the particle off the cylinder wall and (in our model, influenced now only by gravity) into a parabolic trajectory.

At that time the particle modelled as the point (x_i, y_i) will have the following *initial* velocity and position components:

$$\begin{aligned} \dot{x}_0(\theta, \omega, r) &= -r\omega \sin\theta \\ \dot{y}_0(\theta, \omega, r) &= r\omega \cos\theta \\ x_0(\theta, r) &= r \cos\theta \\ y_0(\theta, r) &= r \sin\theta \ . \end{aligned} \tag{1}$$

The parabolic time-dependent motion of a single particle (x_i, y_i) is described by components:

$$x_i(t, \theta, \omega, r) = \dot{x}_0(\theta, \omega, r)t_i + x_0(\theta, r) \tag{2a}$$

$$y_i(t, \theta, \omega, r) = -(g/2){t_i}^2 + \dot{y}_0(\theta, \omega, r)t_i + y_0(\theta, r) \ , \tag{2b}$$

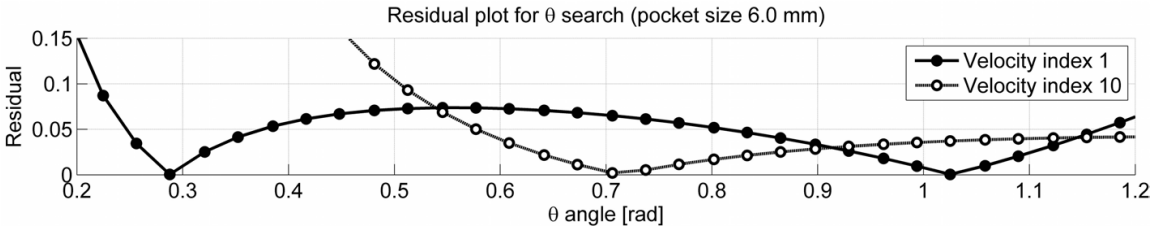

Fig. 4. Two residual curves for two distinct points: (x_{100}, y_{100}) from $A^{(65)}_{(1,1)}$ and (x_{160}, y_{160}) from $A^{(65)}_{(10,1)}$. That is, for both the slowest rotational speed $v = 1$ ("Velocity index 1") and the fastest $v = 10$ ("Velocity index 10"), though only for one pocket diameter $d = 1$. On the curve for $v = 1$ there are two minima at (1) $\theta = 0.29$ rad [16.49°] and (2) $\theta = 1.03$ rad [58.83°]. On the other curve ($v = 10$) there is only one minima at $\theta = 0.71$ rad [40.90°].

where $g = 9.82\ \mathrm{m/s^2}$ is the gravity acceleration constant. Solving for t in (2a) and substituting into (2b) we get the following function (dropping the point index i for generality):

$$\tilde{y}_{\omega,r}(\theta, x) = G_\omega \frac{1}{r^2} \csc^2\theta [r\cos\theta - x]^2 + \cot\theta\,[r\cos\theta - x] + r\sin\theta \ , \qquad (3)$$

where the constant $G_\omega = -(g/2)\omega^{-2}$ is the only factor involving gravity acceleration constant g and ω. The problem is now to solve (3) for θ for each point (x_i, y_i). This was done numerically. First we defined a residual function:

$$e_{\omega,r}(\theta, x_i, y_i) = |\tilde{y}_{\omega,r}(\theta, x_i) - y_i| \ , \qquad (4)$$

which naturally makes it a minimization problem in $\mathbb{R}$:

$$\theta_i = \arg\min_\theta e_{\omega,r}(\theta, x_i, y_i) \ . \qquad (5)$$

We chose to do a full numerical search in the entire range from 0 to $\pi/2$ with a step size of $h = 10^{-3}\pi/2$ (1000 divisions). No stopping criteria was used, resulting in a list of 1000 residual values for each point (x_i, y_i) to analyse further.

Figure 4 shows two plots for the residual value calculated for two points for the slowest and fastest rotational speed (see figure caption for details). When looking at the residual curve for $v = 1$, there are two solutions for the angle θ (two minima exist). This is a mathematical detail easily dealt with. For current point (x, y) only θ values for which the following is true can possibly be member of the solution set Θ_l: $\theta < \arccos(x/r)$, where $x \leq r$. In the current example we have $x = 0.17$, meaning that the upper θ limit is $\arccos(0.17/0.2) = 0.56$ rad [31.90°]. Thus only the lower θ value in the current example would be considered. Finally, we notice that for the residual from motion at velocity step $v = 10$ there is only one minima at a higher angle than for the $v = 1$ curve.

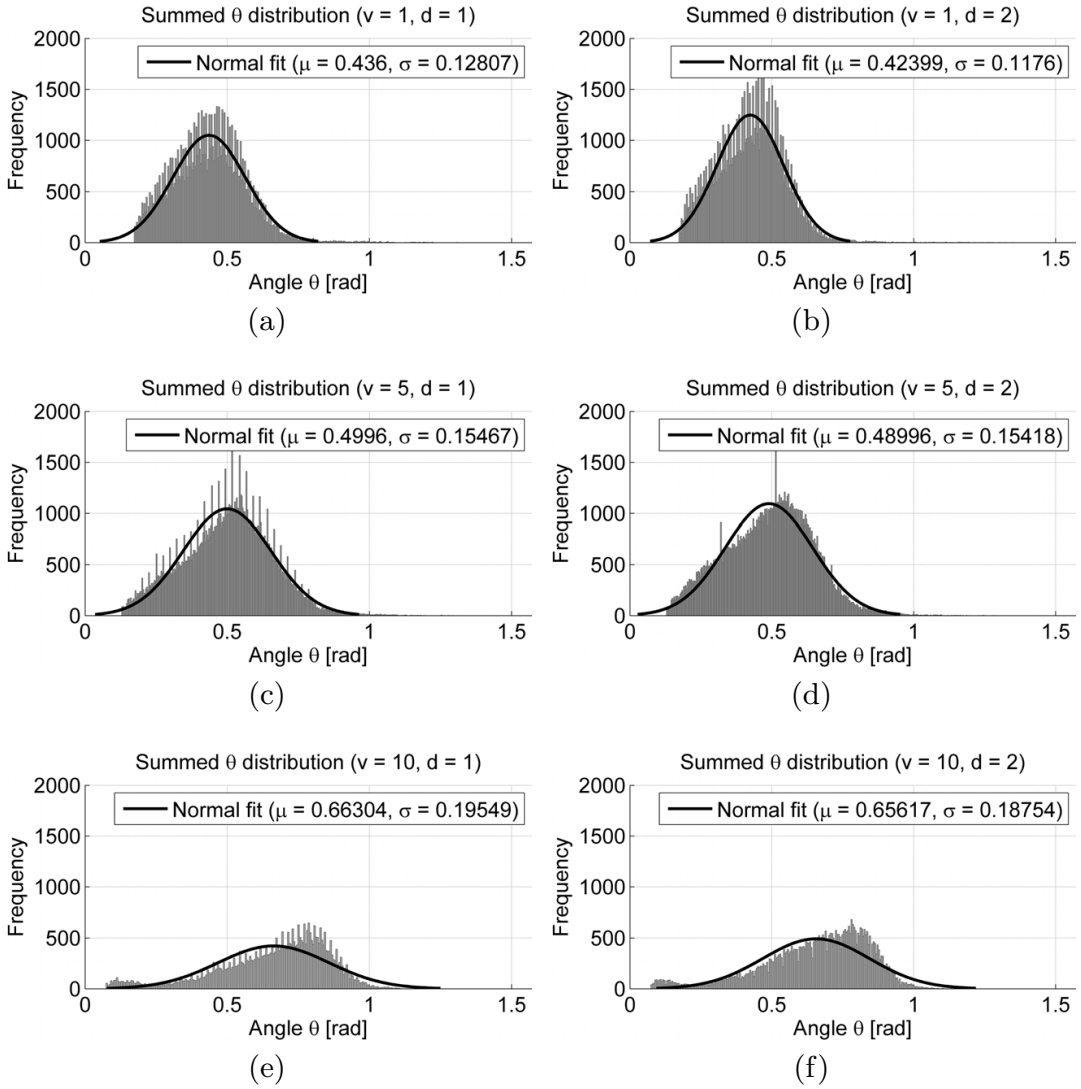

Fig. 5. Six θ frequency distributions with fitted normal density superimposed. Fig. 5(a), 5(c) and, 5(e) show the distributions and normal fit for velocities $v = 1$, 5, and 10; for pocket diameter $d = 1$ (6.0 mm). Fig. 5(b), 5(d) and, 5(f) show the distributions and normal fit for the same three velocities, but now instead for pocket diameter $d = 2$ (7.0 mm).

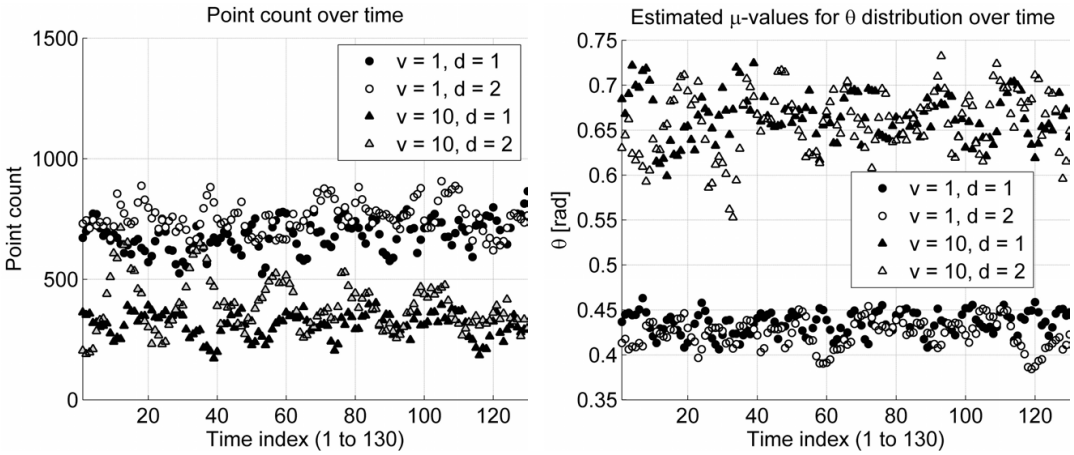

(a) (b)

Fig. 6. Two scatter plots showing different variables gathered over time: Figure 6(a) shows a scatter plot of point counts $I^{(l)}_{(d,v)}$ over $l, \ldots, L$ for $v = 1, 10$ and $d = 1, 2$. In other words: The number of points accumulated for every ten frames, for the slowest and fastest velocity and for both pocket sizes. Figure 6(b) shows a scatter plot of estimated normal μ-parameter from frequency distributions generated from solution sets Θ_l over the same index ranges as in Figure 6(a).

4 Results and Discussion

The methods presented in Section 3 made it possible to analyse for what angle with horizontal the seeds are thrown off the cylinder wall. For each solution set Θ_l available at each time index l in any sequence, we created a frequency distribution h_l over θ and estimate a normal fit with parameters μ_l and σ_l. Beyond this, all distributions h_l for each sequence were also summed and a normal density fitted as well. This made it possible to statistically describe the behaviour of θ for each full sequence using only two parameters (we refer to it specifically as the *summed* distribution).

In Figure 5 we see examples of the summed frequency distributions with the corresponding normal fit superimposed. They are specifically shown for three velocity steps: (1) slowest, middle ($d = 5$), and fastest; for both pocket sizes. Not much difference in appearance of the distribution over pocket sizes can be observed directly – mostly the difference is within changes in rotational speed. Generally, for a higher speed there seems to be a higher probability for larger values of θ. Also, for the highest speed the distribution also seems to become slightly multi-modal. Two modes are observable in figures 5(e) and 5(f) and also in the trajectories plotted in Figure 3 (for that particular rotational speed).

Figure 6(a) show a scatter plot of number of points available in each time step l. The values are shown for both slowest and fastest velocity step, as well as for both pocket sizes. The system seems to have some stability over time. It is also evident that for the fastest velocity step, fewer seeds are extracted than for the slowest velocity step. Figure 6(b) show for the same velocity steps and pocket

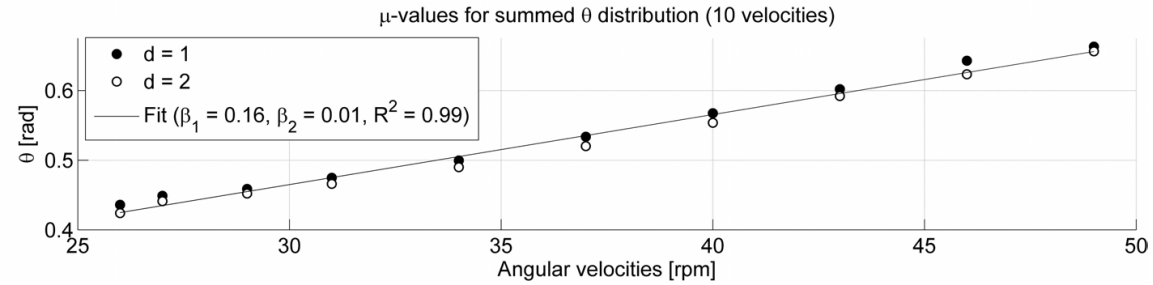

Fig. 7. Scatter plot and a linear regression fit of the μ-parameter estimated from the summed (accumulated over time) frequency distributions under the assumption that the distribution is normal. The data are shown for all ten angular velocities and for both pocket sizes. The linear fit was done using all 20 data points (with rpm values as predictors).

sizes the estimated μ_l parameter for the frequency distributions generated over time. Again we observe stability. On top of this, we observe that θ is generally larger for the fastest velocity step than for the slowest velocity step. Also, the number of points extracted is fewer for the fastest velocity step than for the slowest.

Figure 7 show the estimated μ-parameter for the summed frequency distributions over all ten rotational speeds and for both pocket sizes. The regression fit indicates the possibility of a linear relationship between the rotational speed of the indented cylinder and the angle of escape θ.

5 Conclusions

In this work we have experimentally verified a certain behaviour of the sorting process in the indented cylinder. First and foremost, at least for the 5 seconds of recording that we have dealt with, we show that the process has some stability (but mostly for the lower velocity steps). Secondly, we show a linear relation between rotational speed and angle of escape θ. As mentioned in the introduction there is a need for a systems identification approach in where the indented cylinder is analysed to acquire information about important parameters. Thus a third results is a more tentative one: We have shown that image analysis can be used for flow analysis of particles moving in an indented cylinder. This is a novel step toward the goal of predicting and controlling the sorting process in these machines.

One final important remark: Our choice of using a seed batch with 50 % whole and 50 % broken barley kernels will undoubtedly have had an impact on the distribution of the angle of escape θ. Had the kernel size distribution been more realistic, for instance, with 10 % broken, and 90 % whole or opposite, then we would likely have observed a multi-modal frequency destribution of θ. That would be interesting to try in the future.

Acknowledgements

We would very much like to acknowledge the support and guidance received from Westrup A/S, Denmark.

References

1. Berlage, A.G., Bilsland, D.M., Brandenburg, N.R., Cooper, T.M.: Experimental indent cylinder for separating seeds. Transactions of the American Society of Agricultural Engineers 27(2), 358–361 (1984)
2. Berlage, A.G., Churchill, D.B., Cooper, T.M., Bisland, D.M.: The application of new technologies to seed conditioning. Journal of Agricultural Engineering Research 42(3), 193–202 (1989)
3. Berlage, A.G., Cooper, T.M., Aristazabal, J.F.: Machine vision identification of diploid and tetraploid ryegrass seed. Transactions of the American Society of Agricultural Engineers 31(1), 24–27 (1988)
4. Berlage, A.G., Cooper, T.M., Carone, R.A.: Seed sorting by machine vision. Agricultural engineering 65(10), 14–17 (1984)
5. Buchhave, P.: Particle image velocimetry–status and trends. Experimental Thermal and Fluid Science 5(5), 586 – 604 (1992), special Issue on Experimental Methods in Thermal and Fluid Science
6. Churchill, D.B., Berlage, A.G., Bilsland, D.M., Cooper, T.M.: Decision-support system development for conditioning seeds with indent cylinder. Transactions of the American Society of Agricultural Engineers 32(4), 1395–1398 (1989)
7. Dell'Aquila, A.: Towards new computer imaging techniques applied to seed quality testing and sorting. Seed Science and Technology 35(3), 519–538 (2007)
8. Grochowicz, J.: Machines For Cleaning And Sorting Of Seeds. Department of Agriculture (1980), (Translated from Polish)
9. Lampeter, W.: Die saatgutaufbereitung. VEB Deutscher Landwirtschaftsverlag, Berlin (1965)
10. Parker, D.J., Dijkstra, A.E., Martin, T.W., Seville, J.P.K.: Positron emission particle tracking studies of spherical particle motion in rotating drums. Chemical Engineering Science 52(13), 2011 – 2022 (1997)
11. Pianko-Oprych, P., Nienow, A., Barigou, M.: Positron emission particle tracking (pept) compared to particle image velocimetry (piv) for studying the flow generated by a pitched-blade turbine in single phase and multi-phase systems. Chemical Engineering Science 64(23), 4955 – 4968 (2009)
12. Sandadi, S., Pandey, P., Turton, R.: In situ, near real-time acquisition of particle motion in rotating pan coating equipment using imaging techniques. Chemical Engineering Science 59(24), 5807 – 5817 (2004)

Appendix B

Paper II – Analysis of the Indented Cylinder Part 1: Preliminary Image Analysis Experiments

Buus O.T., Jørgensen, J.R., Carstensen J.M., 20xx. **Analysis of the Indented Cylinder Part 1: Preliminary Image Analysis Experiments**. Second revision to be resubmitted in 2013 to Computers and Electronics in Agriculture.

Working draft of second revision - updated April 2013

Analysis of the Indented Cylinder Part 1: Preliminary Image Analysis Experiments

Ole Thomsen Buus[a,*], Jens Michael Carstensen[b], Johannes Ravn Jørgensen[a]

[a]*Aarhus University, Science and Technology, Department of Agroecology, Forsøgsvej 1, DK-4200 Slagelse, Denmark.*
[b]*Technical University of Denmark, Informatics and Mathematical Modelling, Building 321, DK-2800 Lyngby, Denmark*

Abstract

This paper is Part 1 of an empirically based study of the indented cylinder. We investigated the seed sorting process that takes place inside a laboratory-scaled indented cylinder (diameter was 400 mm and depth was 500 mm). The indented cylinder uses mainly the length of seeds as the physical distinguishing characteristic. The main focus was on identifying factors leading to an optimized length-based separation. High-speed imaging (260 frames/s) and offline image analysis was used to record and analyse the behaviour of seeds while they were being manipulated inside the indented cylinder. The imaging experiments were carried out for 10 increasing rotational speeds and 4 indent working diameters. We used mixtures of cannabis seeds (*Cannabis sativa* L.), polished basmati rice seeds (*Oryza sativa* L.), and wheat seeds (*Triticum aestivum* L.). In this paper we present full details on the imaging experiments. Considerations on setup of camera and illumination were of great importance. The final body of image data consists of more than 900 000 individual frames, recorded at various input settings for the laboratory-scaled indented cylinder. We present part of this data and make it available at `http://olebuus.info/research` as a cite-aware annotated and freely available image database to facilitate further research. Results from preliminary image segmentation experiments are also presented. In these experiments we analysed the amount of seed material visible in each frame over time. The oscillation of rice-material visible

*Corresponding author

Email addresses: `ole.buus@agrsci.dk` (Ole Thomsen Buus), `jmc@imm.dtu.dk` (Jens Michael Carstensen), `johannes.jorgensen@agrsci.dk` (Johannes Ravn Jørgensen)

Preprint submitted to Computers and Electronics in Agriculture *April 22, 2013*

in the recorded scene was investigated using Fourier spectrum analysis. This oscillation is shown to have a frequency between 1.1 Hz and 1.2 Hz.
Keywords: seed processing, indented cylinder, high-speed imaging, image analysis, rice, wheat

1. Introduction

In this work we present imaging experiments applied to continuously observe and extract information from the sorting process that takes place inside a laboratory-scaled indented cylinder. This particular type of seed sorting device uses the length of the individual seeds as the distinguishing physical characteristic. It is therefore generally said that the indented cylinder sorts seeds into two main sub-groups: (1) long and (2) short seeds.

The goal with the machine is to generate a separation between long and short seeds that results in a minimum "overlap" between the two sub-groups. This is the "optimality criterion". Overlap is here defined as the amount of short seeds that ended up in the division that ideally should contain only long seeds plus the amount of long seeds that ended up in the division that ideally should contain only short seeds. The ability of the process to meet this optimality criterion is expectedly dependent on a number of system input parameters.

For modelling and control purposes it would be very useful to have a concrete empirically deduced overview of this relationship between input and output – expressed in one or more relevant variables. This was our overall objective. To achieve this, we carried out several high-speed (260 frames/s) recordings of seeds while they were being manipulated by the indented cylinder and therefore in motion. The experiments involved the use of real seeds – not coloured or coated. We used species that, by their individual physical dimensions, represented generic examples of long and short seeds. These experiments were carried out for a set of input parameters introduced later.

1.1. On the use of Image Analysis

The resulting image sequences from the experiments were analysed using various segmentation and statistical classification techniques. The purpose of analysing such image sequences was

to extract the values of certain variables. The assumptions were: (1) that the value of such variables can be extracted solely through the apparent motion of the individual seeds and (2) that the extracted values of the variables can tell us something about the machine's current ability to meet the aforementioned optimality criterion.

These basic assumptions introduce the concept of apparent motion. A trivial prerequisite for knowing about the apparent motion of a moving object is knowing the location of that object over time. The overall image analysis task was therefore to extract the location of each long and short seed detected in each frame in each sequence recorded. The methodologies and theoretical assumptions are given in Buus et al. (201x) – Part 2 of this study. In short, solving the overall image analysis task involved the use of connected component analysis, watershed segmentation, novelty detection using Mahalanobis distance, and supervised classification using linear discriminant analysis. An actual definition of the variables mentioned above is given in Section 2.2.

1.2. Objectives

The work in Part 1 was focused on five separate objectives or issues: (1) the indented cylinder and its functionality, (2) choices of species of seeds for the imaging experiments, (3) the imaging experiments and the generation of a useful body of image data, (4) a preliminary image segmentation used to get a first time-dependent estimate of the amount of seeds available in each image frame, and (5) a frequency analysis of the previous time-dependent estimate/signal to investigate and verify the oscillatory behaviour of one of the seed species used.

The work in Part 2 was focused on four separate objectives or issues: (1) on the observability using image analysis of the indented cylinder's ability to meet the criteria of optimality, (2) on a chosen set of image analysis methods to make such observations possible, (3) on using the observed variables to estimate an empirical overview of the indented cylinder's ability to meet the criteria of optimality, (4) and on the presentation of parts of such an empirical overview as the overall result.

1.3. Problem Scope and Motivation

When seeds are harvested from fields they contain a number of impurities, e.g. stones, leaves, branches, insects, etc. Between receiving the raw unprocessed material and up until seeds can

be utilised or stored, the material is sent through several processing steps where removal of these impurities is attempted. Seed sorting involves the separation of seed material into one or more sub-divisions. At the stage where seed sorting is applicable most non-seed material will have been removed using other types of machinery and what usually remains is seed-only material. However there might still be more than one species or seeds of weeds, or there might be suboptimal seeds of low quality or broken seeds.

Equipment used for sorting is designed to take advantage of the physically distinguishing characteristics of the individual seeds. Besides individual seed length, other important characteristics are the individual seed weight, surface texture, and general size. Sorting based on length is necessary for some seed species for which physical sorting based on density, surface texture, or general size gives a suboptimal result. The indented cylinder is for instance widely used for cleaning/separation of agricultural seeds (Schmidt, 2007).

The underlying intent with sorting seeds is related to the necessity of achieving a high seed quality in the resulting material. There is always an inherent goal to minimise the loss of good seeds. Seed quality is a complicated concept involving physical, physiological, and genetic aspects (Bishaw et al., 2007). Earlier work (summarised in Delouche et al., 1995) shows that there is a positive correlation between, for instance, seed size and seed quality parameters (such as germination ability and seed vigour). For reasons like this, seed cleaning/sorting equipment, such as the indented cylinder, are very important tools for ensuring that we have seeds of high quality in the end result.

The process of sorting seeds is influenced by many physical and biological variables, and it can therefore be considered quite complex. In practice, it takes several years of training and knowledge for technicians in the industry to control the process in an optimal way. The underlying problem is that the relationship between the input (machine adjustments and seeds) and the output (a separation of a certain quality) is generally unknown. A mathematical model, relating input and output, would allow an automatic control of the separation process.

Such an automated control would be aimed at maximising the general efficiency of the sorting process. This would be of high benefit to the industry. Taking it a bit further, it could make possible a more formally optimized cleaning process – in sharp contrast to the current paradigm

that involves many "rules-of-thumb" about how to carry out the best cleaning or sorting of various species of seed. Besides the ability to separate between long and short seeds, as is the sole focus of this work, the concept of efficiency of course also involves the feeding capacity – an important practical and economical consideration.

1.4. Previous Work

This work expands on the work by Buus et al. (2011). The basis for this earlier work was a preliminary set of experiments with the indented cylinder and broken and whole barley kernels. At the time of writing, this work by Buus et al. still represents the only work in which the indented cylinder was directly investigated using image analysis. The work by Berlage et al. (1984b) and Cooper and Berlage (1985) are examples on earlier work on the application of image analysis to improve the accuracy of seed sorting and conditioning in general. The methods applied are simple but effective. Cooper and Berlage (1986) devised an early vision system making it possible to create a database of physical properties of seeds. Here Cooper and Berlage interestingly concluded that "data can be gathered on about three seeds per minute". Berlage et al. (1989) investigated the general problem and need for applying new technologies to seed sorting and cleaning – machine vision was of primary focus.

Brandenburg and Harmond (1966) made an early attempt to improve the indented cylinder by developing a new prototype. Some twenty years later, Berlage et al. (1984a) continued the effort to improve it once again. Churchill et al. (1989) carried out a set of experimental cleaning trials using a laboratory-scaled indented cylinder – quite similar in model to the one used in this work (though certain important physical details vary). Churchill et al. investigated the machine's ability to separate between long and short seeds by varying the settings of input control parameters (these parameters are introduced in Section 2.1). The result was a set of decision support rules. This was in essence the first work towards a model of the indented cylinder.

From this point on, the digital computer and its ability to make decisions had an impact on later work. The automated modelling and control aspects of post-harvest technologies have been investigated most intensely for seed drying systems and sorting of fruits (see reviews, e.g. Farkas, 2003b; Studman, 2001). There has recently been much interest in applying artificial intelligence

techniques to control such processes (e.g. Farkas, 2005, 2003a). Much early Polish and Russian literature exist. Here various kinds of seed cleaning machinery were investigated – including the indented cylinder. Some of this important work was later collected by Grochowicz (1980).

El-Awady et al. (2009) investigated the improvement of a winnowing and cleaning machine for rice with the goal of reducing impurities and losses of good seed. They developed a winnowing prototype and interesting regression models. Moreover, they concluded on choices of governing parameters such as air speed, moisture content, and feeding rate. Yuan et al. (2006) investigated how to control an air screen cleaner to get the most optimal result. They applied a hybrid intelligent approach involving the use of an artificial neural network and genetic algorithms. Balascio et al. (1988) modelled the granular flow on a gravity separator table. The particle movement was modelled as a stochastic process. Simonyan et al. (2010) developed a mathematical model of the cleaning efficiency of a stationary grain thresher. The model applied the principles from dimensional analysis as the theoretical foundation. Dimensional analysis was also used by Căsăndroiu et al. (2009) to mathematically model the cleaning process on plane sieves. A pneumatic separator was designed by Panasiewicz et al. (2012) and analysed using crushed mixtures of three lupine varieties. They determined correlations between separation process parameters and separation process efficiency.

Understanding the behaviour of granular material in rotating cylinders and kilns is important for modelling segregation and mixing of industrial particles. Hajra and Khakhar (2011) investigated the radial segregation of ternary mixtures in a rotating cylinder and Ward and Hourigan (2012) looked at the general segregation of binary mixtures in a tilted rotating cylinder. In other works (e.g. Pöschel and Buchholtz, 1995; Pereira et al., 2011) the movement of granular material in rotating cylinders has been computationally simulated – usually by applying the discrete element method proposed by Cundall and Strack (1979).

2. Materials and Methods

2.1. The Indented Cylinder

The most basic component of the machine is a sloped steel cylinder indented with similarly sized and shaped tightly located indents on its inner surface. The purpose of the indented cylinder

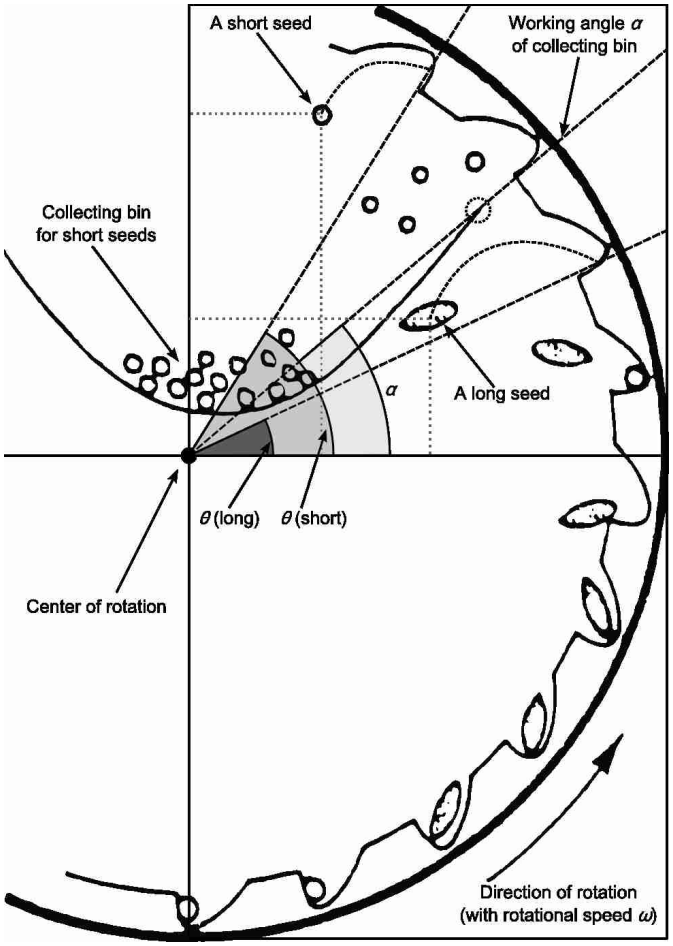

Figure 1: Conceptual drawing of the indented cylinder seen from the front The overlay graphics show the angles θ^{long} and θ^{short} for two seeds having left the cylinder wall in a parabolic-like trajectory. Modified from Lampeter (1965).

is basically to remove everything from the input material that will fit in these indents. Figure 1 gives an overview of the geometry and parameters. While the cylinder is rotating with a constant rotational speed ω, seeds are fed continuously into the cylinder from the elevated end (e.g. by using a vibrational feeder). The seeds land in the bottom of the cylinder from where they are caught by the indents and carried up along the circumference of the cylinder due to its continuous rotation.

Short seeds will generally fit in the indents and will therefore be carried up to a certain angle θ^{short} with the horizontal. Here they leave the support of the indents and are thrown into a collecting bin mounted on the cylinder's axial support. From here they are transferred away and out from

the system. Long seeds will generally not fit in the indents and will therefore have lesser support inside the indents, or alternatively, be influenced solely by friction with the surface between the indents. As a result of this, they will leave the cylinder surface at an angle with the horizontal θ^{long}. This happens earlier than for short seeds which means that θ^{long} is generally lower than angle θ^{short}. Long seeds are therefore not caught by the collecting bin and will instead fall out of the lower end of the cylinder and exit the system from there. The collecting bin is also adjustable and has a working angle α with the horizontal.

2.1.1. The Indents and Their Importance

The shape and size of the indents are very important parameters of the indented cylinder. Usually a cylinder is produced from a steel plate which has had the indents stamped into its surface. The plate is hereafter shaped into a cylinder and welded at the seam. The cylinders used in the experiments had indents with a geometry identical or at least closely similar to what is depicted in Figure 2. The indents have a working diameter d - also seen in Figure 2. This measure will be used as the single governing parameter of the indents. Fouad (1980) carried out an elaborate experimental analysis of the effects of the shape of the indents and also concluded on certain optimal shape parameters.

(Grochowicz, 1980) presented relatively simple models for the behaviour of the seeds in an indented cylinder. In these models, a seed is modelled as a dimensionless body. Furthermore, the modelling is carried out in two dimensions only – assuming that the motion of a seed is constrained to a plane perpendicular to the cylinder's axis of rotation. Usually two primary variations are used: Free-body diagrams of forces acting on a seed (1) between the indents and (2) inside the indents. The active element of the indents is simplified to a small piece of an increasingly inclined surface. The event for when a seed leaves the surface or an indent is expressed through trivial force equivalences involving friction forces and forces of normal pressure (dependent on the cylinder's rotational velocity ω and gravity acceleration g). The work by Huimin et al. (2011) represents a recent overview of the mechanics involved.

Grochowicz (1980, chp. 7) presented a more elaborate model for both a long and a short seed inside an indent. This model takes into account the points of support in the indent that would differ

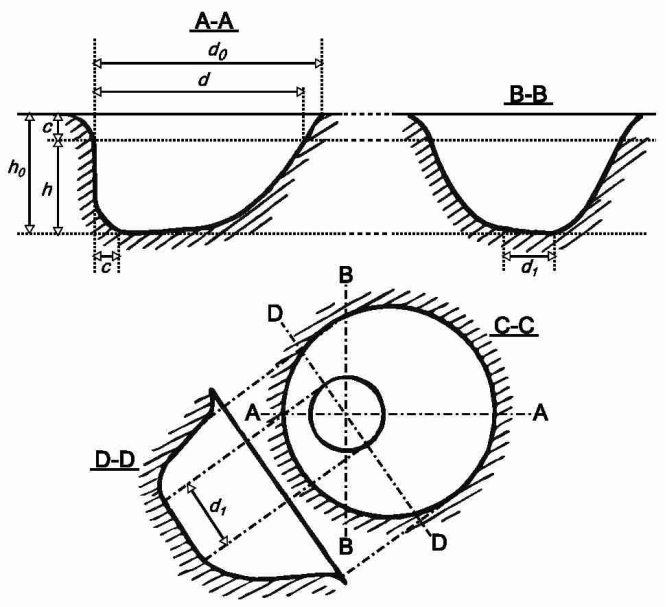

Figure 2: Geometry of the stamped indents in the indented cylinders used in the experiments. This figure also defines the working indent parameter d. Modified from Grochowicz (1980, chap. 6).

for both kinds of seeds. These models give expressions for θ^{long} and θ^{short}. Moreover given the fact that they depend on local biological parameters (seed length, friction coefficient, moisture content, etc.), the ranges of θ^{long} and θ^{short} are likely to verlap, making a complete separation difficult.

2.2. Methodology in the Experiments

We recorded the apparent motion of both long and short seeds while they were being manipulated inside an operating laboratory-scaled indented cylinder. We generated several high-speed recordings for different choices of ω and d – but not α. To minimise problems with the image analysis the collecting bin was removed in the experiments.

We initially planned to keep the collecting bin mounted, but it was found to be too large an obstacle for the imaging experiments. Removing the collecting bin obviously disabled the machine's ability to do any actual sorting. This in turn had an effect on the type of results obtained. We thus focused entirely on the indented inner cylinder surface and its ability to carry out the separation given choices of ω and d.

In this regard we find it necessary to introduce a distinction between (1) separation and (2)

sorting in the indented cylinder. It should be noted that the inner surface of the cylinder and the indents make up the parts of the machine that are solely responsible for the actual separation between long and short seeds. The ability to separate is thus completely independent of the existence of the collecting bin that mainly functions as a form of "memory" for the cylinder surface (though still an adjustable memory).

The primary objective of this work was thus solely to analyse the ability of the cylinder surface to (1) separate long and short seeds. The ability to (2) sort, which is dependent on the collecting bin (without it the separation is quickly "forgotten"), thus had a reduced focus in these particular experiments. Of the adjustable parameters that we have introduced so far, only two of them can thus be said to take part in governing the optimality of the seed separation: (1) the rotational speed ω and (2) the working diameter d of the indents. The working angle α governs only the final sorting result and can be adjusted fully independently of ω and d.

2.2.1. Toward a Measure of Separation Ability

Assume that the location of individual seeds can be extracted from the individual images recorded. If we then apply a plausible physical model for the trajectory that both kinds of seed generate in the images over time, it is possible to estimate the angles θ^{long} and θ^{short} for each individual long and short seed detected in each discrete time step. This will result in two time series of θ^{long} and θ^{short} for each coordinate in a discrete (ω, d)-parameter space.

These two time series represent the variables mentioned in the assumptions given in 1.1. Statistical analysis on these time series can directly lead to a quantifiable measure of separation ability for a particular choice of ω and d. Part 2 of this study presents the involved theory and methods used to achieve this.

2.3. Overview of Materials

The following material was used in the imaging experiments:

- **An indented cylinder (the machine):** A Westrup L-AT (model LAT-0801) was used (a laboratory-scaled model). See figure 3. This model supports attachable cylinders with a radius of 200 mm and a depth of 500 mm. When mounted, the cylinders will have a fixed

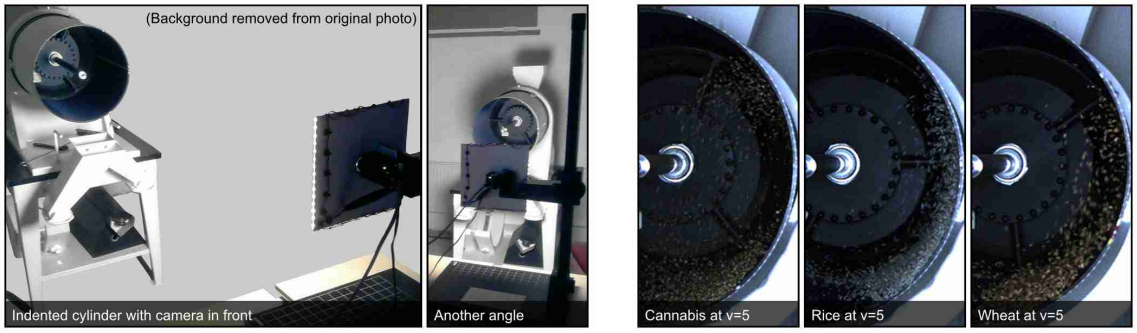

(a) (b)

Figure 3: Experimental setup and examples of the resulting imagery: (a) The indented cylinder and camera with illumination LED-plate in the configuration used in the experiments; (b) three examples of resulting image data (from image sequences created using the three unary mixtures).

angle of inclination with the horizontal of 0.7°. Controlling the cylinder's rotational speed ω was possible only by adjusting the belt tension in the internal gears. Ten discrete speed settings were found to be supported and all of these were applied in the experiments. Certain parts of the machine's surface that would otherwise be visible in the recordings were painted black with a non-glossy acrylic paint.

- **Indented cylinders:** A total of four different indent working diameters d were used. This parameter was manipulated by using four different indented cylinders. They all had the same major dimensions similar as to the ones mentioned above.

- **Seeds:** As a candidate for a "short model" seed we used *Cannabis sativa L.* and as candidates for "long model" seeds we used both *Oryza sativa L.* (basmati rice) and *Triticum aestivum L.* (common wheat). Section 2.4 elaborates further on this.

- **high-speed camera:** We used a Point Grey Grashopper (GRAS-03K2C-C) CCD colour machine vision camera. The full-frame pixel resolution of this model is 640×480 – which equates to 0.3 Mpixels. In a certain configuration, where only half of the CCD sensor-rows are enabled, this model is capable of grabbing frames at 260 frames/s (progressive shutter). This resulted in an active pixel resolution of 240×480. The camera sensor gain was set to approx. 16 dB. We used a monofocal Pentax lens with a focal length of 12 mm.

- **Source of illumination:** We used a metal plate (250 mm × 250 mm) equipped with a total of 189 Light Emitting Diodes (LEDs; model HS083XW16-01) with a colour temperature of 10 000 K. The plate, having a hole in the centre for the camera lens, was mounted on a supporting structure onto which the camera was also mounted. This allowed the lens to peak through (see Figure 6). This prototype was developed by Videometer A/S, Denmark (`http://www.videometer.com`).

- **Stationary PC:** We used a stationary PC for controlling the camera and grabbing frames from it. The PC was equipped with an Intel Core i7 processor and 24GB of main memory. The camera was controlled through a Firewire 1394b cable (length was 5 m).

- **Software for grabbing frames:** A purpose-specific software utility was previously developed by the authors for controlling the camera. The application was developed using C++ and we made use of the FlyCapture SDK version 2.x developed by Point Grey Resarch Inc. This software utility made it possible to control many aspects of the high-speed recording. For instance, the software by default grabs frames directly to memory and can, after the grabbing process has terminated, be set to purge the data to disk.

2.4. Seed Material

The imaging experiments involved the use of real seeds. The choice of seed species was based on the need for "model seeds" that could represent examples of long and short seeds. We used two kinds of batches: Batches containing (1) seeds from only one species ("unary" mixtures) and (2) batches containing seeds from two species ("binary" mixtures). The binary mixtures contain both long and short seeds and involve dynamics likely to be influenced by interactions between these two kind of seeds. The unary mixtures, on the other hand – containing only either long or short seeds – represent a source of the dynamics that are not influenced by such interactions.

2.4.1. Species

Two important factors were important in making the decision on what species of seed to use:

- **The colour of the seeds:** The later image analyses rely on the colour of the seeds and not the shape or size (the resolution of the camera is too low for that). The difference or distance

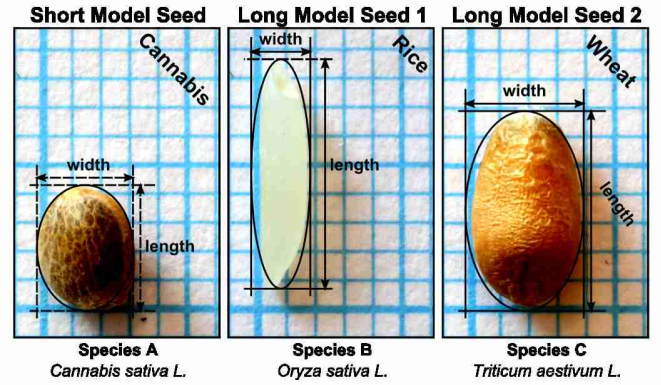

Figure 4: Photos of the three seed species used in the experiment. These seeds were chosen as representative model seeds on the basis on their length and difference in colour. An ellipse has been superimposed on each of the three seeds to indicate the dimensions for width and length. The squares in the background have dimensions 1 mm × 1 mm.

between the colour of long and short seeds must have a magnitude large enough such that statistical techniques can be used to arrive at a proper classification.

- **A need for realism**: It was important to keep the situation realistic. Coating or colouring the seeds would most likely have altered the surface characteristics of the seeds in way that would have influenced the separation dynamics observed.

It was thus important to find species that naturally had contrasting colours. As a model species for short seeds the choice fell on *Cannabis sativa L.* (from now on just *cannabis*). For long seeds we used two model species: (1) *Oryza sativa L.* (processed pusa basmati rice – from now on just *rice*) and (2) *Triticum aestivum L.* (common wheat – from now on just *wheat*). The differences in length, width, general shape, and colour in these three species are shown in Figure 4.

The shape of these three species can be modelled using an ellipse with a major and a minor axis. The length of the seed is thus represented by the size of the major axis and the width by the size of the minor axis. The two "long models", rice and wheat, represent two types of long seeds. Rice is the canonical long, thin, and also very bright, seed; on average almost twice as long as a cannabis seed. Wheat is on average a little shorter than rice but still longer than cannabis – and has a different colour. Wheat seeds also have a larger width and thus represent a median between the two extremes represented by cannabis and rice.

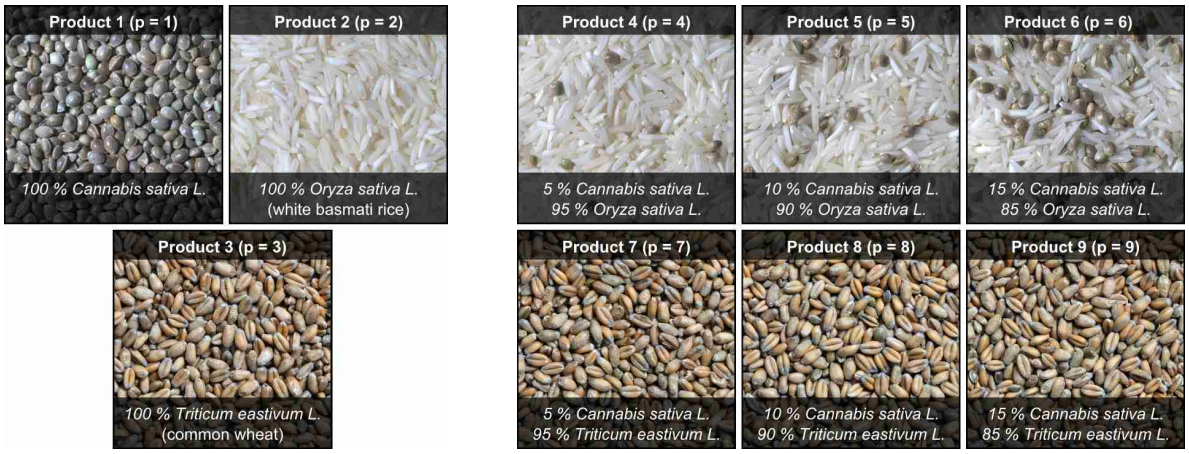

(a) (b)

Figure 5: Photos of the seed mixtures: (a) The three unary seed mixtures; (b) the six binary seed mixtures. The increasing particle-count-ratio of 5 %, 10 %, and 15 % for cannabis are evident.

2.4.2. Mixtures

We used $P = 9$ different mixtures of seeds. These are depicted graphically in Figure 5. Table 1 lists relevant data about them. The first three mixtures ($p = 1, 2, 3$) are unary mixtures (one for each seed species) and the remaining six ($p = 4, 5, \ldots, 9$) are binary mixtures. The first three binary mixtures ($p = 4, 5, 6$) contain both cannabis and rice seeds and the last three ($p = 7, 8, 9$) contain cannabis and wheat seeds. With the intent of standardizing the mixtures, the percentage of long and short seeds in each mixture were based on seed counts of each species.

We defined three different particle-count-ratios for long (q_1 in table 1) and short (q_2) seeds. By using the 1000-seed weight (w_1, and w_2), it was possible to estimate the mass ratios for long (r_1) and short (r_2) seeds. The formula used for the mass ratios were: $r_1 = \frac{q_1 w_1}{(q_1 w_1 + q_2 w_2)}$ and $r_2 = \frac{q_2 w_2}{(q_1 w_1 + q_2 w_2)}$. The final individual masses for long (m_1) and short (m_2) seeds were calculated using: $m_1 = r_1 2000\,\mathrm{g}$ and $m_2 = r_2 2000\,\mathrm{g}$. These individual masses were used to design the binary mixtures using a digital scale.

2.5. Imaging Setup

The physical configuration of the camera and illumination was based on a set of requirements. Figure 7 illustrates the choices made in this regard. Looking in from the outside, the separation

Mixture	p	q_1	q_2	w_1 (g)	w_2 (g)	r_1	r_2	m_1 (g)	m_2 (g)
Cannabis (*unary*)	1	–	1.00	–	14.39	–	1.0000	–	2000.00
Rice (*unary*)	2	1.00	–	13.98	–	1.0000	–	2000.00	–
Wheat (*unary*)	3	1.00	–	44.63	–	1.0000	–	2000.00	–
Rice + Cannabis (*binary*)	4	0.95	0.05	13.98	14.39	0.9486	0.0514	1897.20	102.80
Rice + Cannabis (*binary*)	5	0.90	0.10	13.98	14.39	0.8974	0.1026	1794.71	205.29
Rice + Cannabis (*binary*)	6	0.85	0.15	13.98	14.39	0.8463	0.1537	1692.52	307.48
Wheat + Cannabis (*binary*)	7	0.95	0.05	44.63	14.39	0.9833	0.0167	1966.63	33.37
Wheat + Cannabis (*binary*)	8	0.90	0.10	44.63	14.39	0.9654	0.0346	1930.83	69.17
Wheat + Cannabis (*binary*)	9	0.85	0.15	44.63	14.39	0.9462	0.0538	1892.33	107.67

Table 1: Data for the $P = 9$ seed mixtures used in the experiments. The mathematical quantities in the columns are (from the left): seed-count-ratio for long seeds (q_1); seed-count-ratio for short seeds (q_2); 1000-seed weight for long seeds (w_1); 1000-seed weight for short seeds (w_2); mass-ratio for long seeds (r_1); mass-ratio for short seeds (r_2); final individual mass for long seeds (m_1); and final individual mass for short seeds (m_2).

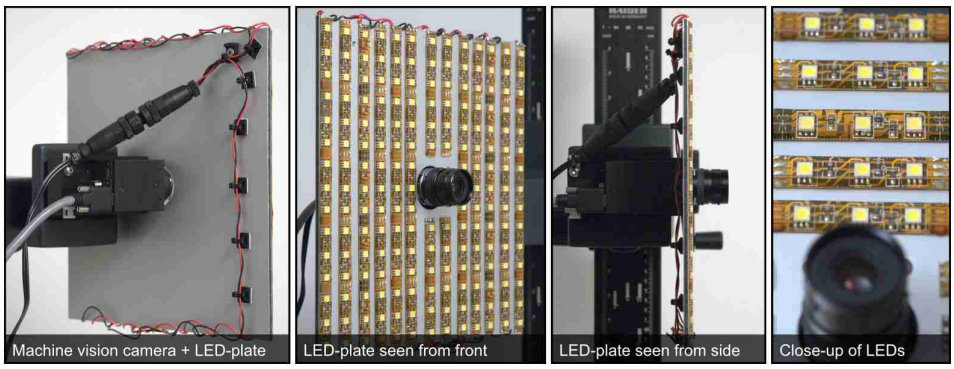

Figure 6: Camera and illumination equipment. The LED-plate is mounted into a block of plastic onto which the camera is also mounted. The LED-plate is seen from different angles.

of the seeds is solely taking place in the right side of the cylinder. The left side was therefore irrelevant and was not included in the recordings. The camera was placed in such a way that its "line-of-sight" was parallel in the horizontal plane with the right edge of the cylinder. This was done primarily to minimise the effect of perspective distortion.

The camera was also rotated 90° and half of the CCD sensor rows (now columns) were disabled to allow for a progressive sensor sampling of 260 frames/s. As a geometrical constraint, the radius of the cylinder (200 mm) had to fit the width of the recorded image. Given a horizontal field of view of 22.70° and the fact that the CCD sensor in the camera has an aspect ratio of 3/4, we used an estimate of $\frac{3}{4}22.70° \approx 17.03°$ for the angle of vertical field of view. Given this constraint and the lens geometry, it meant that the camera had to be placed at a distance of approximately 1340 mm from the cylinder.

2.6. Structure of Experiments

The experiments consisted of a number of "recording runs" – each producing a single high-speed sequence of 15 s duration which. At 15 frames/s this amounted to 3900 frames. We produced such a sequence for each choice of indent working diameter d_s where $s = 1, 2, \ldots, S$ of which we used $S = 4$ different diameters (4 different cylinders); one for each choice of cylinder rotational speed ω_v where $v = 1, 2, \ldots, V$ of which we used $V = 10$ distinct speeds; and one for each choice of seed mixture or product $p = 1, 2, \ldots, P$ of which we used $P = 9$ distinct mixtures. In addition

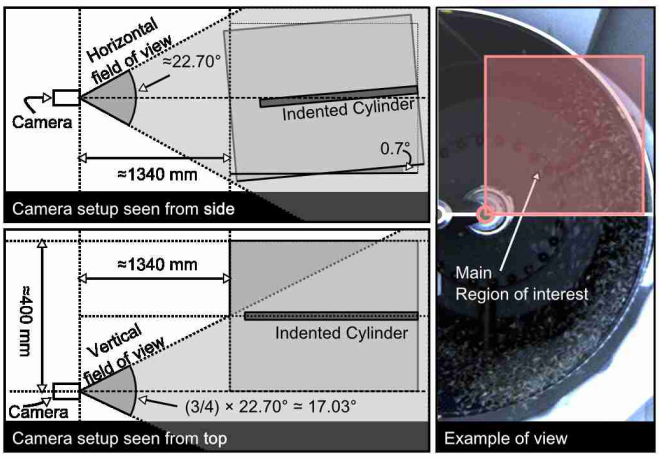

Figure 7: Geometry of camera setup. The camera's "line-of-sight" was aimed directly at the edge of the cylinder – minimising perspective distortion in that direction. The horizontal field of view of 22.70° was taken from product documentation. A "main region of interest" is emphasised in the right side of the figure (a 175×175 pixel area). Everything outside this region was not used in the later image analysis.

to this, we also created $V = 10$ recordings for each rotational speed ω_v with no material in the indented cylinder – effectively adding knowledge about the dynamics of the background. This resulted in a full total of $(S \cdot V \cdot P) + V = (4 \cdot 10 \cdot 9) + 10 = 370$ high-speed sequences. Table 2 lists the indexed values of d_s and ω_v.

The general steps of a single recording run:

1. **Preparation:** The indented cylinder is prepared with one of the $P = 9$ different seed mixtures. If this is not the first run with the current cylinder (i.e. if $1 \leq s \leq S - 1$), then the seed material having exited the cylinder is re-introduced into the feeding mechanism. In this way we cycled 2 kg of material. Since the mixtures and cylinders were clean with no foreign material present, this was deemed an acceptable trade-off to using many kilograms of material.
2. **Start cylinder rotation:** In case this is the first run with the current cylinder (i.e. if $s = 1$), the indented cylinder is started at the lowest speed ($v = 1$) and kept running for 30 seconds so that a useful amount of material from the mixture will have been fed into the cylinder. This ensures that all recording runs has comparable starting conditions. In case this is not the first run with the current cylinder (i.e. if $2 \leq s \leq S$), the cylinder is adjusted to the next

v	ω_v (r/min)	ω_v (rad s^{-1})
1	26.03	2.73
2	27.19	2.85
3	29.05	3.04
4	31.23	3.27
5	33.96	3.56
6	36.71	3.84
7	39.73	4.16
8	42.60	4.46
9	46.02	4.82
10	49.08	5.14

(a)

s	d_s (mm)
1	5.5
2	6.0
3	6.5
4	7.0

(b)

Table 2: The values for the parameters ω and d: (a) The $V = 10$ values for the cylinder rotational speed ω_v in both r/min (revolutions per minute) and rad s^{-1} (angle frequency); and (b) the $S = 4$ indent diameter values d_v in mm. The indent diameters were taken directly from product documentation but the rotational speed values were estimated using the recorded imagery and a between-frames-time of $1/260$ s ≈ 3.8 ms.

higher speed setting ($v = v + 1$).

3. **Recording:** At this stage the indented cylinder machine is continuously feeding material into the attached cylinder and manipulating the seeds. The camera is now configured to start a high-speed grabbing process of 3900 frames in total – which amounts to a duration of 15 seconds at 260 frames/s.
4. **Finishing current cylinder:** If this is not the last rotational speed step (i.e. if $1 \leq v \leq V-1$), the next recording run is carried out using steps 1-3; otherwise, if $v = V$, the indented cylinder machine is allowed to continue feeding material into the cylinder until no more material is available and the cylinder is empty (and clean). The next cylinder is hereafter attached ($s = s + 1$) and steps 1-3 repeated $V = 10$ times again. After a full recording

session ($V \cdot S = 40$ recording runs) the indented cylinder is prepared using another mixture ($p = p + 1$).

3. Primary Contribution – The Image Data

The primary contribution is the body of image data produced in the recording runs. To facilitate future comparative studies on the dynamics of the indented cylinder, the data has been made available[1] as a cite-aware annotated image database.

Prior to any processing, all 370 image sequences were temporally synchronised so that each sequence started with the indented cylinder in the same position. The number of frames available in each sequence was also reduced from 3900 to 2600. This in turn reduced the duration of each sequence from 15 seconds to 10 seconds (at 260 frames/s). Every frame was also reduced in size from 480×240 to 175×175. The region maintained is depicted in Figure 7 (the "main region of interest"). After preliminary pre-processing the entire body of image data amounted to $2600 \cdot 370 = 962\,000$ individual 8-bit Bayer-mosaic frames with a pixel resolution of 175×175.Performing analysis on such a relatively large body of data required a scripted mechanism that made possible the automated loading and subsequent processing of subsets of the full data. A processing framework for doing this was developed by the authors using MATLAB R2009b (The MathWorks, Inc.).

3.1. Mathematical Definitions

Let $k = 1, 2, \ldots, K$ be the integer index for the k'th frame and let $K = 2600$ be the total number of frames in any sequence $\mathcal{F}_{(s,v,p)} \in I^{N \times N \times K}$, where $I = [0, 1] = \{x \in \mathbb{R} : 0 \leq x \leq 1\}$ and $N = 175$. Let $\mathbf{F}^{(k)}_{(s,v,p)} \in I^{N \times N}$ be the k'th frame from the recording run that used indent diameter d_s, rotational speed ω_v, and mixture p. Some short-hand notations: Let $\mathbf{F}^{(k)}$ be the k'th frame in any sequence and $\mathbf{F}$ be any frame in any sequence. Mathematical names are also defined for the $V = 10$ background-only sequences $\mathcal{B}_{(v)} \in I^{N \times N \times K}$: Let $\mathbf{B}^{(k)}_{(v)} \in I^{N \times N}$ be the k'th background-only frame recorded using rotational speed ω_v; let $\mathbf{B}^{(k)}$ be the k'th background-only frame in any background-only sequence; and let $\mathbf{B}$ be any background-only frame in any background-only sequence.

[1] The body of image data is available for download at the `http://olebuus.info/research`.

3.2. Examples of the Image Data

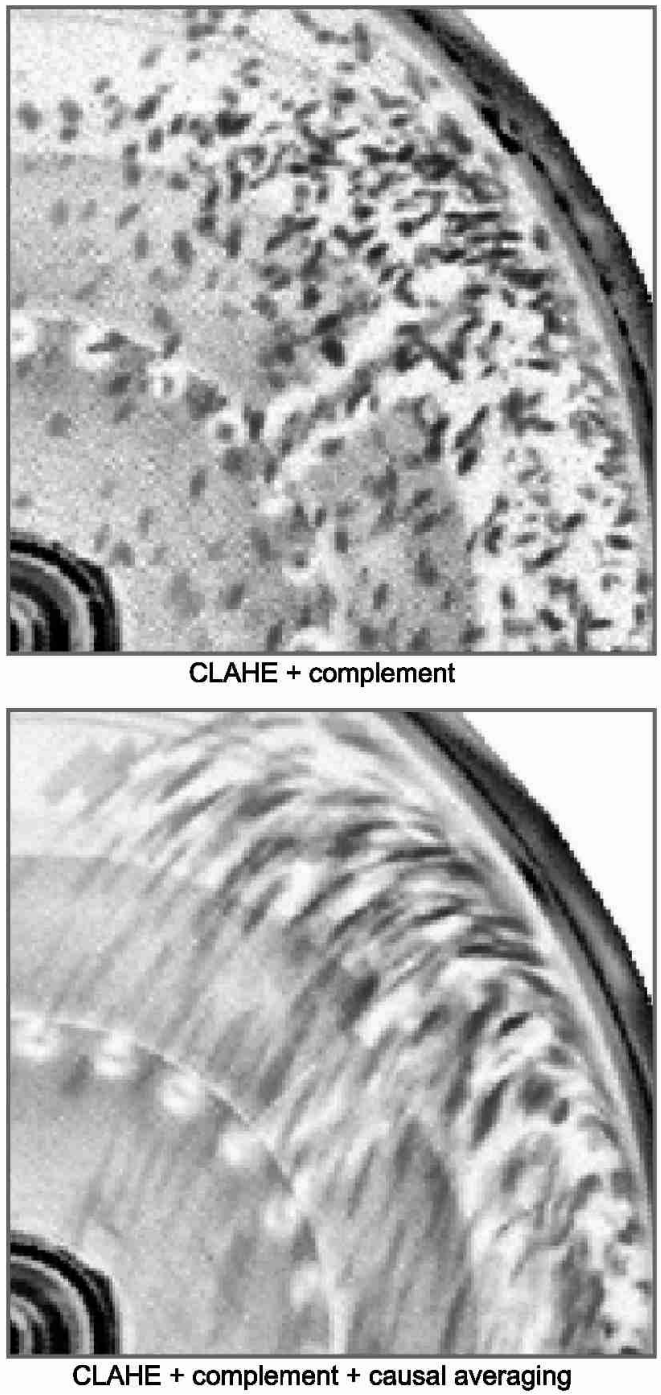

Figure 8: Two examples of a single frame with $s = 4$, $v = 7$, and $p = 5$. The frame is shown in two different pre-processed versions.

Figure 8 shows two preprocessed versions of $\mathbf{F}^{(10)}_{(4,7,5)}$, i.e. the 10th frame produced in the recording run using indent working diameter $d_4 = 7.0$ mm, rotational speed $\omega_7 = 39.73$ r/min and mixture $p = 5$ (90 % rice and 10 % cannabis).

Both versions are grey-scale versions converted from an intermediate 24-bit RGB version generated from the 8-bit Bayer-mosaic using a gradient-corrected linear interpolation (Malvar et al., 2004). The frame $\mathbf{F}^{(10)}_{(4,7,5)}$ was further preprocessed for improved visual contrast. For this we used contrast-limited adaptive histogram equalisation (CLAHE) and image grey-scale complementation (grey-scale inverse). For the CLAHE technique we used a uniform histogram distribution, a bin count of 256, a tile size of 8×8 pixels, and a clip limit of 0.01 (see e.g. Pizer et al., 1987). The result of this is seen in the top version of Figure 8. To give the illusion of motion we calculated an average of five such preprocessed frames in a causal frame-buffer centred at $k = 8$. The result of this is seen in the bottom example.

Figure 9a and 9b show further preprocessed examples of $\mathbf{F}^{(10)}_{(4,v,p)}$ and $\mathbf{B}^{(10)}_{(v)}$ for $v = 1, 4, 7, 10$ and all $P = 9$ mixtures including background-only frames. A trend in the trajectories of the seeds is clearly visible in Figure 9b: When the rotational speed is increased the trajectories change shape. This change in shape is consistent with a simple parabolic motion model in whereby each seed leaves the cylinder circumference at a certain angle and with a certain velocity. This initial velocity is dependent on the current value of rotational speed ω_v.

4. Secondary Contribution – Segmentation Trials

As a secondary contribution we present some preliminary results from the use of standard image processing techniques. The purpose with such analyses was to extract signals (or time-series) carrying useful information about the dynamics recorded in a small subset of the 360 foreground sequences. We observed that rice seeds had a tendency to "pack" together on the inner surface of the cylinder during rotation and later fall down as one large mass of granular particles. This pattern was observed throughout the recordings involving rice and introduced an oscillating pattern to the recorded granular dynamics.

We specifically focused on the sequences produced using unary mixtures only (i.e. $p = 1, 2, 3$) with $v = 1, 4, 7, 10$ and $s = 4$ (i.e. 12 sequences). Our intent was to give an estimate of the number

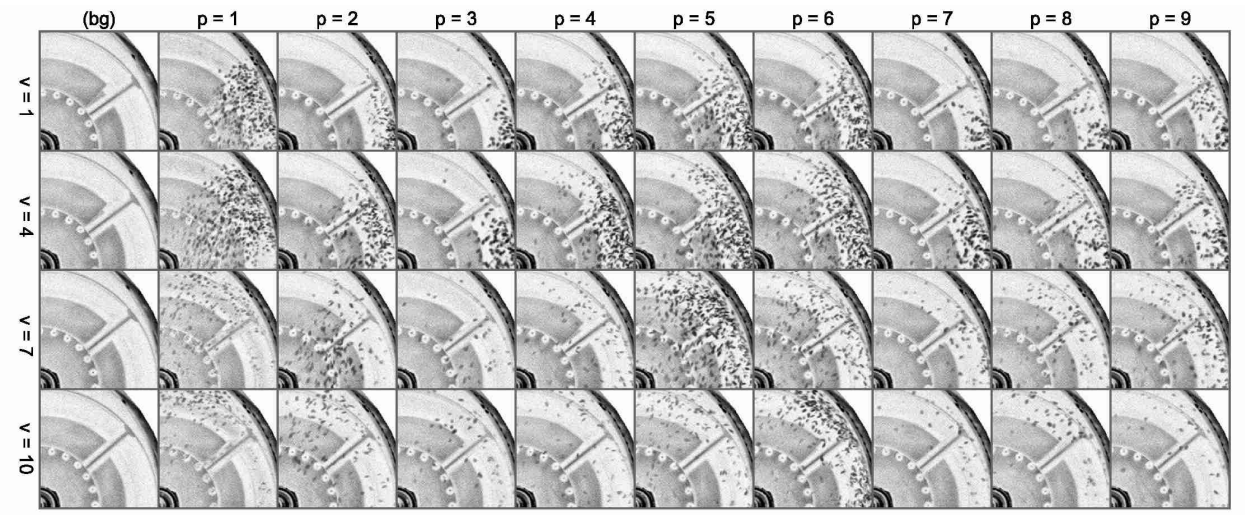

(a)

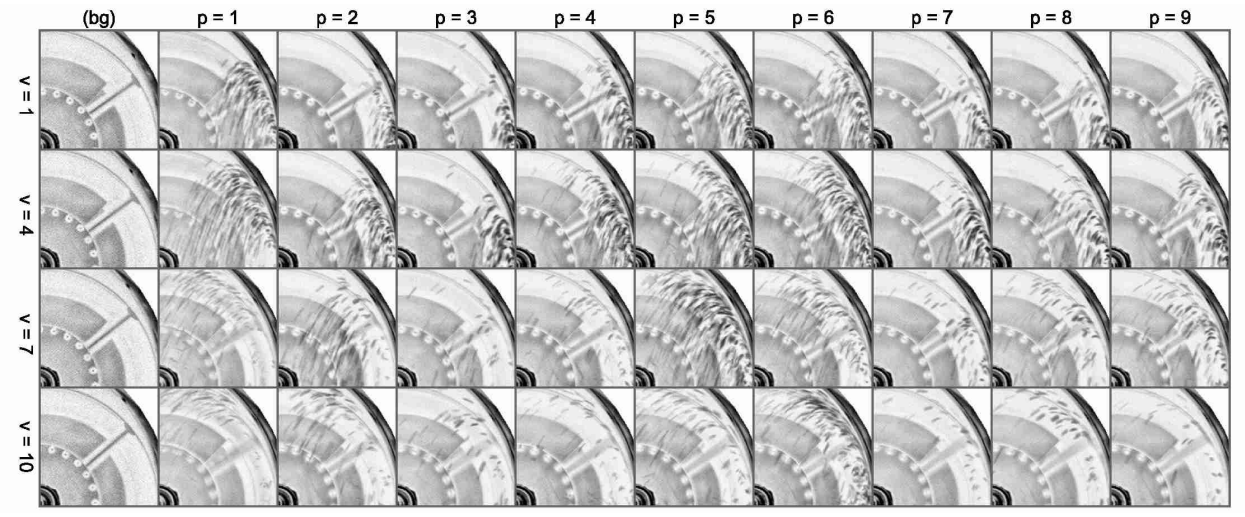

(b)

Figure 9: Examples of image data. All examples have $s = 4$ and shown only for 4 different velocities. They are all from the same time-index $k = 10$ and background-only frames are included for comparison. The examples, for both (a) and (b), are grey-scale and preprocessed for improved viewing. This preprocessing involved the use of contrast-limited adaptive histogram equalisation (CLAHE) and image grey-scale complementation (grey-scale inverse) to further improve visual contrast. The examples in (b) are the result of an averaging (arithmetic mean) of the frames in a 5-frame causal window (causal averaging) centred at $k = 8$.

of pixels in a full 175×175 frame $\mathbf{F}$ that can be considered part of the seed material. We refer to these as "seed-pixels". All other pixels in a full frame are referred to as "background-pixels".

These segmentation trials were done to analyse the apparent oscillating behaviour of rice that was observed during the experiments.

The segmentation method is based on the assumption that seed-pixels will generally have a higher pixel grey-scale intensity than background-pixels. This is generally true if ones takes the preprocessed versions in Figure 8 into account: Here, dark areas should be interpreted as pixels with high grey-scale intensity. The method was applied to the grey-scale version only and all pixels were thus represented by a floating point scalar between 0.0 (zero) and 1.0 (one).

Consider any foreground frame $\mathbf{F}$ and any background-only frame $\mathbf{B}$ and let $\mathbf{A} = f(\mathbf{F}_\mathrm{h} - \mathbf{B}_\mathrm{h})$ be the result of a function f given the difference between $\mathbf{F}_\mathrm{h} = \mathbf{h} * \mathbf{F}$ and $\mathbf{B}_\mathrm{h} = \mathbf{h} * \mathbf{B}$. Here $\mathbf{h}$ is a 5×5 Gaussian kernel and $*$ is the convolution operator. The function f processes the resulting difference between the two filtered frames and produces a final logical map $\mathbf{A}$. Pixels marked as "true" (non-zero pixels) in this map can be considered as seed-pixels.

Function f does the following:

1. nullifies all differences below zero,
2. applies a power law with $\gamma = 0.2$,
3. linearly stretches the range $[0.60, 0.65]$ to $[0.0, 1.0]$,
4. sets pixels below 0.5 to "false" (or zero) and those equal to and above 0.5 to "true" (or one).

Most of the steps in the segmentation algorithm have been visualised in Figure 10 (grey-scale inverses of originals). The top-left example (box 1) contains frame $\mathbf{F}^{(175)}_{(4,7,3)}$, box 2 contains the corresponding background-only frame $\mathbf{B}^{(175)}_{(7)}$, box 3 contains the difference between the two just prior to step 2 of function f, and box 4 contains the resulting logical map $\mathbf{A}$ (black pixels are those considered to be seed-pixels). Note that the area outside the cylinder circumference was considered irrelevant and nullified before processing started. This area was determined manually and stored as a global full-frame logical map.

As can be determined visibly in Figure 10, boxes 1 and 2, both the foreground and background-only frames features a metal arm that rotates with the cylinder. The resulting segmentation in box 4 has one particular problem: The metal arm is still present in the logical map after the segmentation; i.e it is spuriously considered to be part of the seeds. This problem is mainly a result of the

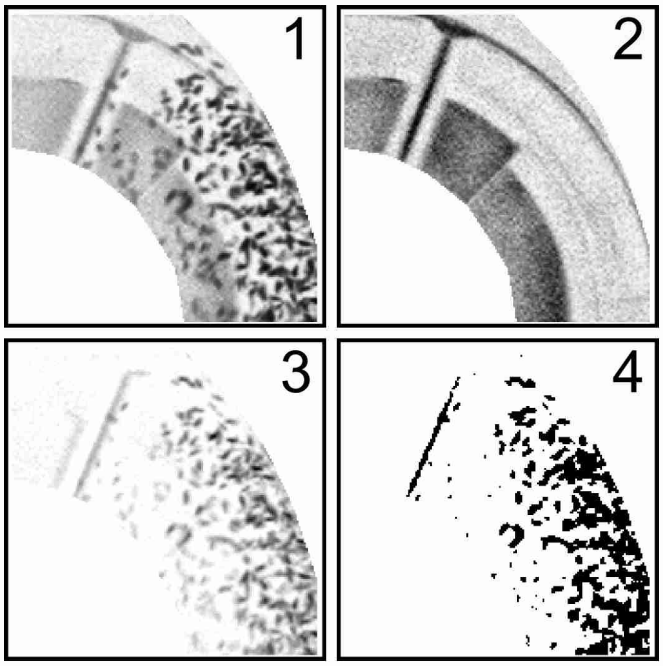

Figure 10: Visualisations of processing steps in the segmentation trials. The top-left example (box 1) contains frame $\mathbf{F}^{(175)}_{(4,7,3)}$, box 2 contains the corresponding background-only frame $\mathbf{B}^{(175)}_{(7)}$, box 3 contains the difference between the two, and box 4 contain the resulting logical map $\mathbf{A}$. Note that the area outside of the cylinder circumference was considered irrelevant and nullified before processing started. This area was determined manually and stored as a global full-frame sized logical map.

simplicity of the single-pixel processing used – especially the difference $\mathbf{A} = f(\mathbf{F}_\mathrm{h} - \mathbf{B}_\mathrm{h})$. This simplicity is an advantage in terms of reproducibility of results. Here, this simplicity also has only a minor impact on the resulting segmentation.

Let $\mathbf{A}^{(k)}$ be the k'th logical map in any sequence and let $a^{(k)}$ be the number of seed-pixels in $\mathbf{A}^{(k)}$. Let a_0 be the constant total number of pixels in a full frame ($a_0 = 175 \cdot 175 = 30\,625$). Consider a vector $\boldsymbol{a} \in \mathbb{R}^K$ estimated from any sequence (i.e. a vector with pixels counts from all frames $k = 1, \ldots, K = 2600$). The k'th value of $\boldsymbol{a}$ holds the full-frame seed-pixel percentage $100\, a^{(k)}/a_0$. We estimated such a vector for each of the 12 sequences analysed. These 12 vectors have been plotted in Figure 11. The resulting signals were further smoothed using the Savitzky-Golay filtering technique (see e.g. Savitzky and Golay, 1964) with a polynomial order of 0 (zero) and a frame width of 15.

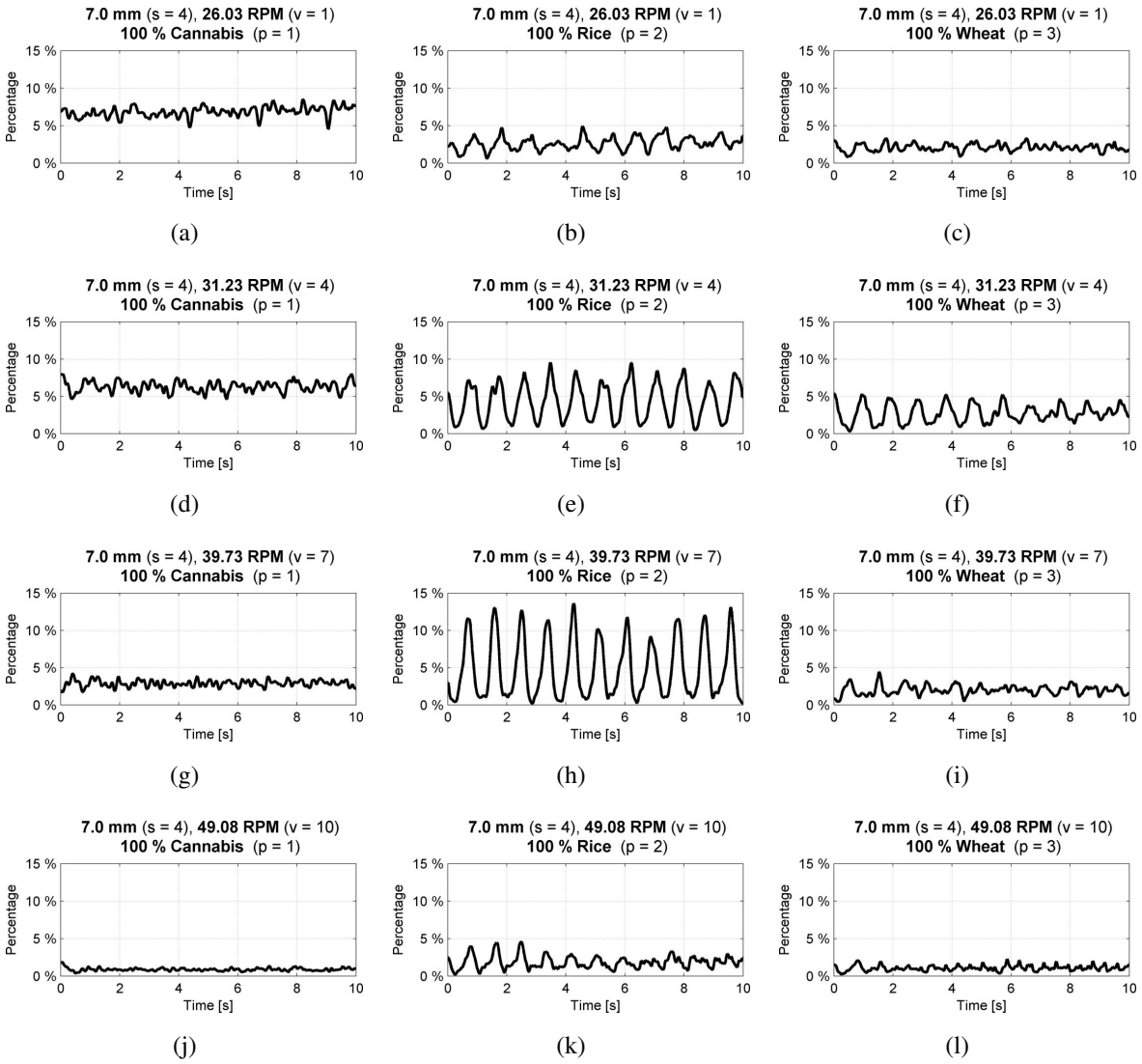

Figure 11: Full-frame seed-pixel percentages over time. Let $\mathbf{A}^{(k)}$ let be the k'th logical segmentation-map in any sequence and let $a^{(k)}$ be the number of seed-pixels in $\mathbf{A}^{(k)}$. Let a_0 be the constant total number of pixels in a full frame ($a_0 = 175 \cdot 175 = 30\,625$). The 12 plots from (a) to (l) each show an estimate of vector $\boldsymbol{a} \in \mathbb{R}^K$ in which the k'th value holds the full-frame seed-pixel percentage $100\,a^{(k)}/a_0$. The Savitzky-Golay filtering technique with a polynomial order of 0 (zero) and a frame width of 15 was used for smoothing the signals.

The 12 preprocessed full-frame seed-pixel percentage vectors shown in Figure 11 can be used directly as signals that carry information on the amount of cannabis, rice, and wheat available over time in each full frame (the main region of interesting depicted in Figure 7).

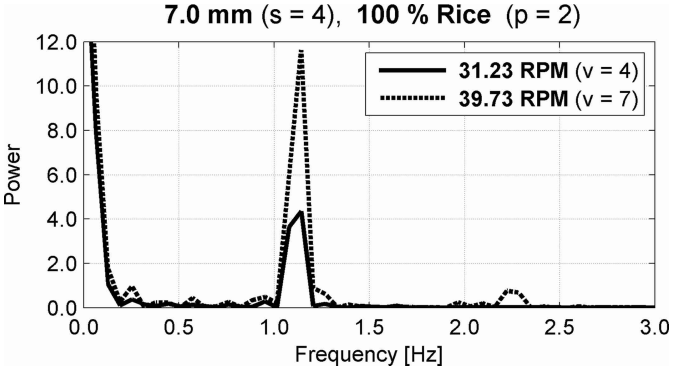

Figure 12: One-sided power spectra of two signals. These two signals are plotted in 11e and 11h and show a tendency of rice to oscillate when being manipulated in the indented cylinder. These spectra have a peak between 1.1 Hz and 1.2 Hz which can be assumed to correspond to the oscillatory behaviour of rice.

Figure 11 shows the oscillating behaviour of all three seed species. When comparing the plots of full-frame seed-pixel percentages for rice with those for cannabis and wheat, the oscillating behaviour is evidently greatest for rice. See, in particular, Figure 11e and 11h for 31.23 r/min and 39.73 r/min, respectively. We therefore carried out a spectrum analysis of the two signals in those two plots by the use of the fast Fourier transform. The one-sided power spectrum for both signals for rice are shown in Figure 12. These spectrum plots share a peak between 1.1 Hz and 1.2 Hz. This shared frequency component is an interesting result and is assumed to correspond to the oscillatory behaviour of rice.

5. Conclusions

It is of great importance to the related industries that the indented cylinder receives a fresh focus in modern research. Moreover, the general problem of modelling and controlling complex machinery involving granular mixtures represents an important basic scientific problem. In this paper, we have introduced the problem and argued that one solution is to observe/record the motion of the seeds when they are manipulated. This resulted in a relatively large set of digital image sequences holding information about the internal dynamics for different input parameter choices. This body of data has been made publicly available at `http://olebuus.info/research`. Our hope is that this data will be considered useful and also used for future comparative studies.

The segmentation trials also resulted in an interesting quantifiable observation. Rice seems to oscillate; it "packs" together on the inner surface of the cylinder and then falls down as one large mass of granular particles. It was possible to analyse this oscillatory behaviour using the time-series extracted from two 100 % rice sequences. The power spectra of these two signals have a strong peak between 1.1 Hz and 1.2 Hz. We argue that this peak corresponds to the oscillatory behaviour of rice.

References

Balascio, C.C., Misra, M.K., Johnson, H.P., 1988. Stochastic modeling of granular flow in seed sorting. Mathematical and Computer Modelling 11, 523–527.

Berlage, A.G., Bilsland, D.M., Brandenburg, N.R., Cooper, T.M., 1984a. Experimental indent cylinder for separating seeds. Transactions of the American Society of Agricultural Engineers 27, 358–361.

Berlage, A.G., Churchill, D.B., Cooper, T.M., Bisland, D.M., 1989. The application of new technologies to seed conditioning. Journal of Agricultural Engineering Research 42, 193–202.

Berlage, A.G., Cooper, T.M., Carone, R.A., 1984b. Seed sorting by machine vision. Agricultural engineering 65, 14–17.

Bishaw, Z., Niane, A.A., Gan, Y., 2007. Quality seed production, in: Yadav, S.S., McNeil, D.L., Stevenson, P.C. (Eds.), Lentil. Springer Netherlands, pp. 349–383.

Brandenburg, N.R., Harmond, J.E., 1966. Separating Seeds by Length With Special Indent Cylinders. Technical Bulletin 88. Agricultural Experiment Station, Oregon State University, Corvalis.

Buus, O.T., Carstensen, J.M., Jørgensen, J.R., 201x. Analysis of the indented cylinder part 2: Overview of length separation ability. Computers and Electronics in Agriculture (In this issue).

Buus, O.T., Jørgensen, J.R., Carstensen, J.M., 2011. Analysis of seed sorting process by estimation of seed motion trajectories, in: Heyden, A., Kahl, F. (Eds.), Image Analysis. Springer Berlin / Heidelberg. volume 6688 of *Lecture Notes in Computer Science*, pp. 273–284.

Căsăndroiu, T., Popescu, M., Voicu, G., 2009. A developing a mathematical model for simulating the seeds separation process on the plane sieves. UPB Scientific Bulletin, Series D: Mechanical Engineering 71, 17–28.

Churchill, D.B., Berlage, A.G., Bilsland, D.M., Cooper, T.M., 1989. Decision-support system development for conditioning seeds with indent cylinder. Transactions of the American Society of Agricultural Engineers 32, 1395–1398.

Cooper, T.M., Berlage, A.G., 1985. Machine vision for monitoring seed conditioning. ASAE Paper 85-3036. American Society of Agricultural Engineers, St. Joseph, MI 49085.

Cooper, T.M., Berlage, A.G., 1986. Integrating database and machine vision seed measuring process. ASAE paper 86-3062. American Society of Agricultural Engineers, St. Joseph, MI 49085.

Cundall, P.A., Strack, O.D.L., 1979. Discrete numerical model for granular assemblies. Geotechnique 29, 47–65.

Delouche, J.C., Cabrera, E.R., Keith, B.C., 1995. Strategies for improving physiological seed quality. Bulletin 1029. Mississippi Agricultural and Forestry Experiment Station.

El-Awady, M.N., Yehia, I., Ebaid, M.T., Arif, E.M., 2009. Development of rice cleaner for reduced impurities and losses. AMA, Agricultural Mechanization in Asia, Africa and Latin America 40, 15–20.

Farkas, I., 2003a. Artificial intelligence in agriculture. Computers and Electronics in Agriculture 40, 1–3. Editorial.

Farkas, I., 2003b. Control aspects of postharvest technologies, in: Handbook of Postharvest Technology. CRC Press, pp. 845–866.

Farkas, I., 2005. Modelling and control in agricultural processes. Computers and Electronics in Agriculture 49, 315–316. Editorial.

Fouad, H.A., 1980. The effect of cell configuration on length grading of beans. Journal of Agricultural Engineering Research 25, 391–406.

Grochowicz, J., 1980. Machines for cleaning and sorting of seeds. Department of Agriculture. Translated from Polish.

Hajra, S., Khakhar, D., 2011. Radial segregation of ternary granular mixtures in rotating cylinders. Granular Matter 13, 475–486.

Huimin, W., Mingliang, W., Lun, T., Yong, L., Ping, D., 2011. Dynamic analysis to the seeds in indent of the indent cylinder separator, in: International Conference on Intelligent Computation Technology and Automation (ICICTA) 2011, pp. 66–70.

Lampeter, W., 1965. Die saatgutaufbereitung. VEB Deutscher Landwirtschaftsverlag, Berlin.

Malvar, H.S., He, L., Cutler, R., 2004. High-quality linear interpolation for demosaicing of bayer-patterned color images, in: Acoustics, Speech, and Signal Processing, 2004. Proceedings. (ICASSP '04). IEEE International Conference on, pp. 485–488.

Panasiewicz, M., Sobczak, P., Mazur, J., Zawiślak, K., Andrejko, D., 2012. The technique and analysis of the process of separation and cleaning grain materials. Journal of Food Engineering 109, 603–608.

Pereira, G., Sinnott, M., Cleary, P., Liffman, K., Metcalfe, G., Šutalo, I., 2011. Insights from simulations into mechanisms for density segregation of granular mixtures in rotating cylinders. Granular Matter 13, 53–74.

Pizer, S.M., Amburn, E.P., Austin, J.D., Cromartie, R., Geselowitz, A., Greer, T., ter Haar Romeny, B., Zimmerman, J.B., Zuiderveld, K., 1987. Adaptive histogram equalization and its variations. Computer Vision, Graphics, and Image Processing 39, 355–368.

Pöschel, T., Buchholtz, V., 1995. Complex flow of granular material in a rotating cylinder. Chaos, Solitons and Fractals 5, 1901–1905,1907–1912.

Savitzky, A., Golay, M.J.E., 1964. Smoothing and differentiation of data by simplified least squares procedures. Analytical Chemistry 36, 1627–1639.

Schmidt, L., 2007. Seed processing, in: Tropical Forest Seed. Springer Berlin Heidelberg, pp. 67–142.

Simonyan, K.J., Mudiare, O.J., El-Okene, A.M., Yiljep, Y.D., 2010. Development of a mathematical model for predicting the cleaning efficiency of stationary grain threshers using dimensional analysis. Applied Engineering in Agriculture 26, 189–195.

Studman, C.J., 2001. Computers and electronics in postharvest technology – a review. Computers and Electronics in Agriculture 30, 109–124.

Ward, T., Hourigan, W., 2012. Granular segregation in a tilted-rotating drum. Powder Technology 215–216, 227–234.

Yuan, J., Yu, T., Wang, K., 2006. A hybrid intelligent approach for optimal control of seed cleaner. IFIP International Federation for Information Processing 207, 780–785.

Appendix C

Paper III – Analysis of the Indented Cylinder Part 2: Length Separation Ability

Buus O.T., Jørgensen, J.R., Carstensen J.M., 20xx. **Analysis of the Indented Cylinder Part 2: Length Separation Ability**. Second revision to be resubmitted in 2013 to Computers and Electronics in Agriculture.

Working draft of second revision - updated April 2013

Analysis of the Indented Cylinder Part 2: Length Separation Ability

Ole Thomsen Buus[a,*], Jens Michael Carstensen[b], Johannes Ravn Jørgensen[a]

[a]*Aarhus University, Science and Technology, Department of Agroecology, Forsøgsvej 1, DK-4200 Slagelse, Denmark.*
[b]*Technical University of Denmark, Informatics and Mathematical Modelling, Building 321, DK-2800 Lyngby, Denmark*

Abstract

This paper is Part 2 of an empirically based study of the indented cylinder. We investigated the seed sorting process that takes place inside a laboratory-scaled indented cylinder (diameter was 400 mm and depth was 500 mm). The indented cylinder uses mainly the length of seeds as the physical distinguishing characteristic. The main focus was on identifying factors leading to an optimized length-based separation. High-speed imaging (260 frames/s) and offline image analysis was used to record and analyse the behaviour of seeds while they were being manipulated inside the indented cylinder. The imaging experiments were carried out for 10 increasing rotational speeds and 4 indent working diameters. We used mixtures of cannabis seeds (*Cannabis sativa* L.), polished basmati rice seeds (*Oryza sativa* L.), and wheat seeds (*Triticum aestivum* L.). In this paper we present details on assumptions regarding observability, parabolic trajectories of seeds, statistical measures of separation, and methods of image analysis. The overall image analysis task was to estimate the location of each individual seed in each frame. Moreover, the task was to classify each seed into either long or short. This was solved as a two-level hierarchical segmentation problem. Here we used distance-based novelty detection (Mahalanobis distance) for preliminary segmentation, and quadratic discriminant analysis for final supervised classification of pixels as belonging to either a short or a long seed, or background (10-fold cross validation errors were all between 0.18 % and 18 %). We present parts of an empirical overview of separation ability at

*Corresponding author
Email addresses: ole.buus@agrsci.dk (Ole Thomsen Buus), jmc@imm.dtu.dk (Jens Michael Carstensen), johannes.jorgensen@agrsci.dk (Johannes Ravn Jørgensen)

Preprint submitted to Computers and Electronics in Agriculture *April 22, 2013*

different cylinder rotational speeds and indent diameters. For the cannabis/rice mixtures the highest separation happened for a rotational speed between 37 r/min and 43 r/min and indent diameter between 6.5 mm and 7.0 mm. For cannabis/wheat the best rotational speed was between 37 r/min and 40 r/min and the best indent diameter was found to be 6.5 mm.
Keywords: seed processing, image analysis, novelty detection, discriminant analysis, wheat, rice

1. Introduction

This paper is part 2 of a larger study wherein we analysed the seed sorting process inside a laboratory-scaled indented cylinder. The indented cylinder mainly uses the length of the individual seeds as the distinguishing physical characteristic. It is generally used to separate an incoming seed mixture into two sub-mixtures: (1) long and (2) short seeds. This is also why the indented cylinder is usually known as a "length sorter". The process that it carries out is likewise known as "length sorting". An optimal separation is naturally one where there will be a minimum "overlap" between the long and short sub-mixtures. This is the "criterion of optimality". Overlap is here defined as the amount of short seeds that ended up in the division that ideally should contain only long seeds, plus the amount of long seeds that ended up in the division that ideally should contain only short seeds.

The ability of the process to meet this criterion of optimality is expectedly dependent on a number of system input parameters. It was our overall objective to create an empirical overview of the indented cylinder's ability to meet the above criterion of optimality. An analysis of the process was possible by continuously observing it by the use of a high-speed camera (260 frames/s) placed in front of an operating laboratory-scaled indented cylinder (Westrup L-AT model LAT-0801). This was done for a number of input parameters. Information on these input parameters, and details on experiments, camera, illumination, functionality of the indented cylinder are available in Buus et al. (201x) (Part 1 of this study). The reader is referred to Part 1 for such details as these are not repeated in this paper (Part 2).

1.1. Objectives

The work in Part 1 was focused on five separate objectives or issues: (1) the indented cylinder and its functionality, (2) choices of species of seeds for the imaging experiments, (3) the imaging experiments and the generation of a useful body of image data, (4) a preliminary image segmentation used to get a first time-dependent estimate of the amount of seeds available in each image frame, and (5) a frequency analysis of the previous time-dependent estimate/signal to investigate and verify the oscillatory behaviour of one of the seed species used.

The work in Part 2 was focused on four separate objectives or issues: (1) on the observability using image analysis of the indented cylinder's ability to meet the criterion of optimality, (2) on a chosen set of image analysis methods to make such observations possible, (3) on using the observed variables to estimate an empirical overview of the indented cylinder's ability to meet the criterion of optimality, (4) and on the presentation of parts of such an empirical overview as the overall result.

1.2. Resulting Body of Image Data

The imaging experiments, or "recording runs", were carried out for each choice of indent working diameter d_s where $s = 1, 2, \ldots, S$ of which we used $S = 4$ different diameters (4 different cylinders); one for each choice of cylinder rotational speed ω_v where $v = 1, 2, \ldots, V$ of which we used $V = 10$ distinct speeds; and one for each choice of seed mixture or product $p = 1, 2, \ldots, P$ of which we used $P = 9$ distinct mixtures using both unary (i.e. mixtures with only one seed species and binary mixtures (i.e. mixtures with two seeds species). Including $V = 10$ extra background-only sequences this amounted to a total of $(S \cdot V \cdot P) + V = (4 \cdot 10 \cdot 9) + 10 = 370$ digital high-speed image sequences. The values for the parameters ω and d are listed in Table 1.

Each of the 370 resulting image sequences consists of $K = 2600$ individual 8-bit Bayer-mosaic frames with a pixel resolution of 175×175 (10 s at 260 frames/s). An example of such a frame is shown in Figure 1. This particular frame is the 10th frame in the image sequence recorded using indent working diameter $d_4 = 7.0$ mm, rotational speed $\omega_7 = 39.73$ r/min, and mixture $p = 5$ (90 % rice and 10 % cannabis). To improve the presentation quality of this particular example, it was preprocessed to increase its visual contrast. For this we used contrast-limited adaptive

v	ω_v (r/min)	ω_v (rad/s)
1	26.03	2.73
2	27.19	2.85
3	29.05	3.04
4	31.23	3.27
5	33.96	3.56
6	36.71	3.84
7	39.73	4.16
8	42.60	4.46
9	46.02	4.82
10	49.08	5.14

(a)

s	d_s (mm)
1	5.5
2	6.0
3	6.5
4	7.0

(b)

Table 1: The values for the parameters ω and d: (a) The $V = 10$ values for the cylinder rotational speed ω_v in both r/min (revolutions per minute) and rad s^{-1} (angle frequency); and (b) the $S = 4$ indent diameter values d_v in mm. The indent diameters were taken directly from product documentation but the rotational speed values were estimated using the recorded imagery and a between-frames-time of $1/260$ s ≈ 3.8 ms.

histogram equalisation (CLAHE) and image grey-scale complementation (grey-scale inverse). For the CLAHE technique we used a uniform histogram distribution, a bin count of 256, a tile size of 8×8 pixels, and a clip limit of 0.01 (see e.g. Pizer et al., 1987). Note that these preprocessing methods were not used in the actual analyses.

1.3. On the Image Analysis Task

The 370 image sequences produced in the imaging experiments were analysed using various segmentation and statistical classification techniques. These methods are presented in Section 3, 4, and 5. The intent of analysing such image sequences was to extract the values of certain variables. This section will briefly account on the basic assumption regarding the observability

Figure 1: An example of a preprocessed frame. This particular frame is the 10th frame in the image sequence recorded using indent working diameter $d_4 = 7.0\,\text{mm}$, rotational speed $\omega_7 = 39.73\,\text{r/min}$, and mixture $p = 5$ (90 % rice and 10 % cannabis). To improve the presentation quality for this particular example, it was preprocessed to increase its visual contrast. For this we used contrast-limited adaptive histogram equalisation (CLAHE) and image grey-scale complementation (grey-scale inverse). Note that these preprocessing methods were not used in the actual analyses.

and applicability of such variables.

The assumptions were: (1) that the value of such variables can be deduced from the apparent motion of the individual seeds and (2) that the deduced values of the variables can tell us something about the machine's current ability to meet the aforementioned criterion of optimality.

These basic assumptions introduce the concept of apparent motion of an object and to determine that we need the location of such an object over time. The image analysis task thus involved the detection of individual seeds in each frame and then determining if they were long or short. The camera used had too low a resolution for us to use pixel geometry to ascertain the length for each seed. Instead, we used the statistical properties of the colours for each class of seeds. The imagery represented quite a challenge in general for object detection and classification.

1.4. Previous Work

Our work in this paper and its companion paper (Part 1) seems to be the first study into empirically analysing the indented cylinder using high-speed image analysis. Recent work dealing with image analysis and biological products focuses mainly on analysis of fruits, e.g. apples (Bennedsen et al., 2005; Xiao-bo et al., 2010) and oranges (Li et al., 2011; Kondo et al., 2000). Analysis of seeds using imaging has been researched for some time. Pearson et al. (2008); Pearson (2009); Dana and Ivo (2008); Szczypiński and Zapotoczny (2012) are examples on recent research in this area (see also reviews, e.g. Brosnan and Sun, 2002; Ruiz-Altisent et al., 2010). We mention these works and reviews since they revolve around the use of image analysis for analysing seeds in general. One important application is seed germination testing. Non-invasive techniques such as imaging or non-lethal X-ray techniques have recently become popular for this purpose and continues to develop (Dell'Aquila, 2007, 2009a,b).

2. Observability

Assume that the location of individual seeds (both long and short) can be extracted from the individual images recorded. If we then apply a plausible physical model for the trajectory that both kinds of seed generate in the images over time (a parabolic trajectory is assumed), it is possible to estimate the angles θ^{long} and θ^{short} for each individual long and short seed detected in each discrete time step. Details on this are given in Section 6.

This will result in two time series (or vectors) of θ^{long} and θ^{short} for each coordinate in a discrete (ω, d)-parameter space and for each of the six binary mixtures ($p = 4, 5, \ldots, 9$). Let these two time series of observations be modelled as the realizations of two normally distributed random variables Θ^{long} and Θ^{short}; each with expected values $\mu_\Theta^{\text{short}}$ and μ_Θ^{long}, and standard deviations $\sigma_\Theta^{\text{short}}$ and $\sigma_\Theta^{\text{long}}$. Statistical analyses on such time series, combined with the notion of a realistic motion model, can lead to a quantifiable measure of separation-ability for a particular choice of ω and d.

2.1. Seed Trajectories

Figure 2 graphically demonstrates the assumptions regarding the use of a parabolic motion model (only gravity, no drag). The figure depicts the region of the (x, y)-plane that corresponds to

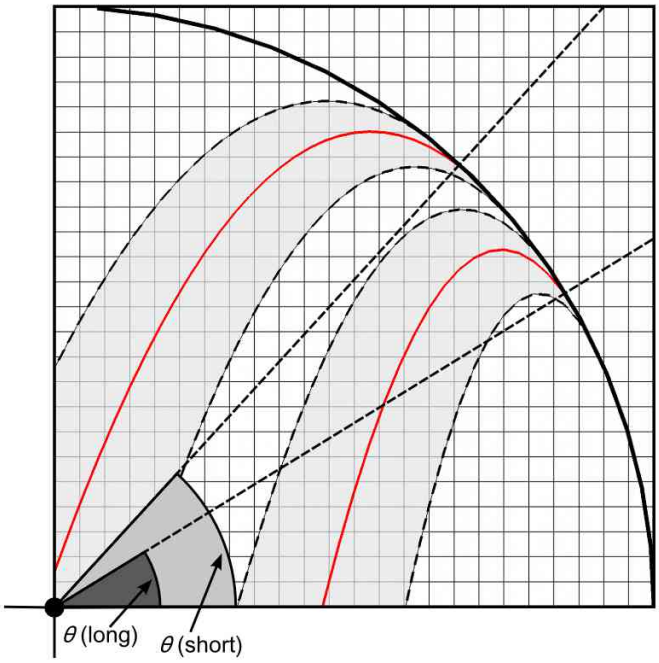

Figure 2: Examples of parabolic trajectories for long and short seeds. It is here assumed that a parabolic trajectory can be used as the motion model (only gravity, no drag). The parabolas are graphical depictions of the trajectories that a seed would most likely take when leaving the inner surface of the cylinder at an angle θ with horizontal. The parabolas are modelled as tangent to the cylinder surface at angle θ and their shape is expectedly dependent on the rotational speed ω. The lower set of parabolas represent trajectories for long seeds and the upper set does the same but for short seeds.

the (projected) volume of space imaged in the experiments. We define this geometrical universe of discourse as $U_{\text{geo}} = \{[x, y]^\top \in \mathbb{R}^2_+ : x^2 + y^2 \leq r^2\}$; i.e. a subset of the two-dimensional set of non-negative real numbers $\mathbb{R}^2_+ = \{[x, y]^\top \in \mathbb{R}^2 : x \geq 0 \wedge y \geq 0\}$. We mapped the origin $[0, 0]^\top$ to the centre of rotation of the cylinder.

Six parabolas are depicted: a set of three lower parabolas and a set of three upper parabolas. Notice the separation or "gap" between these two sets. These parabolas are graphical depictions of the trajectories that a seed would most likely take when leaving the inner surface of the cylinder at an angle θ with horizontal. The parabolas are modelled as tangent to the cylinder surface circumference at angle θ and their shape is expectedly dependent on the rotational speed ω. The lower set of parabolas represents trajectories for long seeds and the upper set represents trajectories for

short seeds.

The middle non-dotted parabola in each set represents the estimated "central tendency" in each of the two sets of parabolas. It can also be interpreted as the "average trajectory" for either a long or a short seed. The lower one of the two such central parabolas is tangent at μ_Θ^{long} while the upper one is tangent at $\mu_\Theta^{\text{short}}$. The four dotted parabolas represent the "spread" of the two sets of parabolas. The lower pair of dotted parabolas is tangent at $\pm\sigma_\Theta^{\text{long}}$ while the the upper pair is tangent at $\pm\sigma_\Theta^{\text{short}}$.

The parabolas are partially characterised by the statistical parameters of the two normally distributed continuous random variables Θ^{long} and Θ^{short}. The statistical parameters define the initial position $\boldsymbol{p}_\theta = r[\cos\theta, \sin\theta]^\top$ for a seed when it leaves the cylinder surface. The θ-domain considered for both of the related probability density functions is the interval $\theta \in [0, \pi/2]$ when angle θ is measured in degrees. The seed continues in a free fall parabolic trajectory. The shape of this parabola is solely dependent on (1) the initial position $\boldsymbol{p}_\theta$, (2) the initial velocity $\boldsymbol{v}_\theta = r[-\omega\sin\theta, \omega\cos\theta]^\top$, and (3) the gravitational acceleration $\boldsymbol{g} = [0, -9.82\,\text{m}\,\text{s}^{-2}]^\top$.

2.2. Measures of Separation

The ability to separate is geometrically characterised by the gap between the two sets of parabolas in Figure 2. A large gap will naturally correspond to a good ability to separate. A large gap can also make it easier to find an optimal working angle α for the collecting bin. Our aim was to find those values of ω and d that would correspond to the observation of two "bundles" of seed trajectories with a minimum spatial overlap between them – while at the same time having that $\mu_\Theta^{\text{long}} < \mu_\Theta^{\text{short}}$.

This notion invites us to think in terms of metric distances between such trajectory bundles. Since the shape and location of these bundles were determined using statistical estimates, any such distance would have to be a statistical distance, i.e. a distance between probability distributions or between two probability vectors drawn from such distributions. We applied two types of statistical distances: (1) a numerical distance of averages and (2) the Hellinger distance.

2.2.1. Numerical Distance Between Averages

This is simply the distance between the two averages μ_Θ^{long} and $\mu_\Theta^{\text{short}}$. We calculated the numerical quantity using $\mu_\Theta^{\text{short}} - \mu_\Theta^{\text{long}}$. This is a signed value and only for positive magnitudes will it have practical meaning. This distance can be directly applied as a numerical measure of separation between long and short seeds and represents one way of answering the question posed in the control problem defined earlier. The co-domain of this measure is $[-\pi/2, \pi/2] \in \mathbb{R}$. A large (positive) measure will geometrically correspond to a large (practically meaningful) separation between the two sets of parabolas in Figure 2.

2.2.2. Hellinger Distance

One problem with the numerical distance between averages is that the standard deviations $\sigma_\Theta^{\text{long}}$ and $\sigma_\Theta^{\text{short}}$ are entirely ignored. We propose the Hellinger distance as an alternative distance that takes both the averages and variances into consideration. This distance is also known as the Jeffreys-Matusita distance (Matusita, 1956, 1955; Bruzzone et al., 1995) and can be used to quantify the similarity between two probability distributions.

The Hellinger distance $H(f, g)$ between two probability density functions $f(x)$ and $g(x)$ is the square root of the squared Hellinger distance defined as

$$\begin{aligned} H^2(f,g) &= \frac{1}{2}\int \left(\sqrt{f(x)} - \sqrt{g(x)}\right)^2 dx \\ &= 1 - \int \sqrt{f(x)g(x)}dx \\ &= 1 - BC(f,g) \\ &= \frac{1}{2}\left\|\sqrt{f} - \sqrt{g}\right\|_2^2 \ , \end{aligned}$$

where $BC(f, g)$ is the Bhattacharyya coefficient (Bhattacharyya, 1943). The Hellinger distance is a true metric. We can see from the use of the L_2-norm that $H(f, g)$ is both non-negative, symmetric, and satisfies the triangle inequality. The distance goes from 0 (zero) to 1 (one). A distance of 0 corresponds to a complete similarity between f and g and a distance of 1 to no similarity. The closed-form expression of the squared Hellinger distance $H^2(P, Q)$ between two normal distribu-

tions $P \sim \mathcal{N}(\mu_1, \sigma_1^2)$ and $Q \sim \mathcal{N}(\mu_2, \sigma_2^2)$ will be relevant in Section 7 and is as follows:

$$H^2(P, Q) = 1 - \sqrt{\frac{2\sigma_1\sigma_2}{\sigma_1^2 + \sigma_2^2}} \exp\left(-\frac{1}{4}\frac{(\mu_1 - \mu_2)^2}{\sigma_1^2 + \sigma_2^2}\right) \quad . \tag{1}$$

For notational convenience we also define the equivalence $H^2(\mu_1, \sigma_1, \mu_2, \sigma_2) \equiv H^2(P, Q)$.

3. Image Analysis: Mathematical Notation and Software

The overall image analysis task was to estimate the location of each long and short seed detected in each frame in each sequence recorded. We are in fact talking about two sub-tasks: (1) the detection of seeds as disjoint regions in the image plane and (2) the estimation of the approximate location in U_{geo} of each such detected region. These two sub-tasks can be addressed by solving a number of specific image analysis problems. These are: (1) a two-level hierarchical segmentation problem and (2) a set of three connected component problems. Section 5 will present the overall segmentation methodology.

3.1. Notation

Let $k = 1, 2, \ldots, K$ be the integer index for the k'th frame and let $K = 2600$ be the total number of frames in any sequence $\mathcal{F}_{(s,v,p)} \in I^{N\times N\times K}$, where $I = [0, 1] = \{x \in \mathbb{R} : 0 \leq x \leq 1\}$ and $N = 175$. Let $\mathbf{F}^{(k)}_{(s,v,p)} \in I^{N\times N}$ be the k'th frame from the recording run that used indent diameter d_s, rotational speed ω_v, and mixture p. Some shorthand notations: Let $\mathbf{F}^{(k)}$ be the k'th frame in any sequence and $\mathbf{F}$ be any frame in any sequence. Mathematical names are also defined for the $V = 10$ background-only sequences $\mathcal{B}_{(v)} \in I^{N\times N\times K}$: Let $\mathbf{B}^{(k)}_{(v)} \in I^{N\times N}$ be the k'th background-only frame recorded using rotational speed ω_v; let $\mathbf{B}^{(k)}$ be the k'th background-only frame in any background-only sequence; and let $\mathbf{B}$ be any background-only frame in any background-only sequence. Similarly, we define shorthand notations for any sequence $\mathcal{F}$ and any background-only sequence $\mathcal{B}$. Finally, let $\mathbf{D}$ be any frame $\mathbf{F}$ or background-only frame $\mathbf{B}$ and let $\mathcal{D}$ be any sequence $\mathcal{F}$ or background-only sequence $\mathcal{B}$.

The following sections will use the technical notion of a "logical map". This is simply a binary frame and mathematically it is a member of $\{0, 1\}^{N\times N}$. Pixels in it can thus only take the values one (1) or zero (0). Pixels can be considered "enabled" in a logical map only when they have

the value 1. Otherwise they are "disabled". Another technical notion is that of a "label map". Mathematically, a label map is a member of $\{0, 1, \ldots, C\}^{N \times N}$, where $C \geq 0$ is some maximum integer label. A label map is not a logical map but can be converted to one using logical or morphological operations.

3.2. Software for Processing

Doing analysis on such a relatively large body of data required a scripted mechanism that made possible the automated loading and subsequent processing of subsets of the full data. A processing framework for doing this was developed by the authors using MATLAB R2009b (The MathWorks, Inc.). This framework operates on an iteration of discrete time-steps from $k = 1$ to $k = K = 2600$ (a "full run"). At each such k-iteration, the framework invokes a pre-configured callback-procedure that then iterates over all, or over a pre-configured subset, of the three-dimensional space of integer indices spanned by $s = 1, 2, \ldots, S$, $v = 1, 2, \ldots, V$, and $p = 1, 2, \ldots, P$. At each such svp-iteration, this callback-procedure invokes its local processing code with matrices $\mathbf{F}^{(k)}_{(s,v,p)}$ and $\mathbf{B}^{(k)}_{(v)}$ as input. We implemented three different callback-procedures – each with individual responsibilities. These are introduced in more detail in Section 5.2.

The main methodology is explained in the following sections. If not stated otherwise, such explanations always take place in the context of any svp-iteration in any k-iteration. When appropriate, the text will apply the mathematical shorthand notations introduced earlier.

4. Image Analysis: Preprocessing

The following preprocessing steps were applied to frame $\mathbf{D}$ in sequence $\mathcal{D}$ (i.e. to frame $\mathbf{F}^{(k)}_{(s,v,p)}$ in sequence $\mathcal{F}_{(s,v,p)}$ and frame $\mathbf{B}^{(k)}_{(v)}$ in sequence $\mathcal{B}_{(v)}$, in any svp-iteration in any k-iteration):

1. The frame is initially a raw 8-bit Bayer-mosaic frame. It is therefore converted into a 24-bit RGB colour representation using a gradient-corrected linear interpolation technique (Malvar et al., 2004).
2. The frame is filtered using a standard Gaussian 3×3 kernel with a standard deviation of 0.5 (each 8-bit colour component is filtered individually).

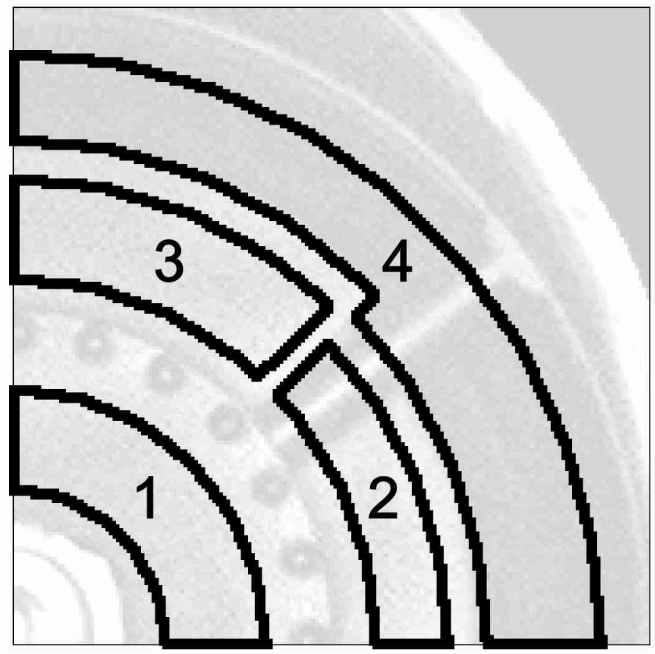

Figure 3: Main "data-ROIs" (Regions of Interest) in the image plane. The data-ROIs are numbered from 1-4. These data-ROIs were determined by manual inspection to have localized statistical properties. All later actual analyses were always applied locally inside these data-ROIs.

3. The frame is segmented into four (4) manually pre-configured "data-ROIs" referred to as $\mathbf{R}_1$, $\mathbf{R}_2$, $\mathbf{R}_3$, and $\mathbf{R}_4$. See Figure 3 for their locations in the full 175×175 pixel frame. The shorthand notation $\mathbf{R}_i$ is used for any of the four data-ROIs when applicable.

The data-ROIs introduced in step 3 above were determined by manual inspection to have localized statistical properties. The priori assumption was that these particular regions will only contain pixels that can be labelled as being either (1) part of background, (2) part of a long seed (i.e. a rice or wheat seed), and/or (3) part of a short seed (i.e. a cannabis seed). Section 5.1 further elaborates on the classification scheme applied. All later actual analyses were always applied locally inside these data-ROIs – in succession from $\mathbf{R}_1$ to $\mathbf{R}_4$. This effectively added four extra local processing iterations to any *svp*-iteration in any *k*-iteration. Pixels outside these data-ROIs were not used.

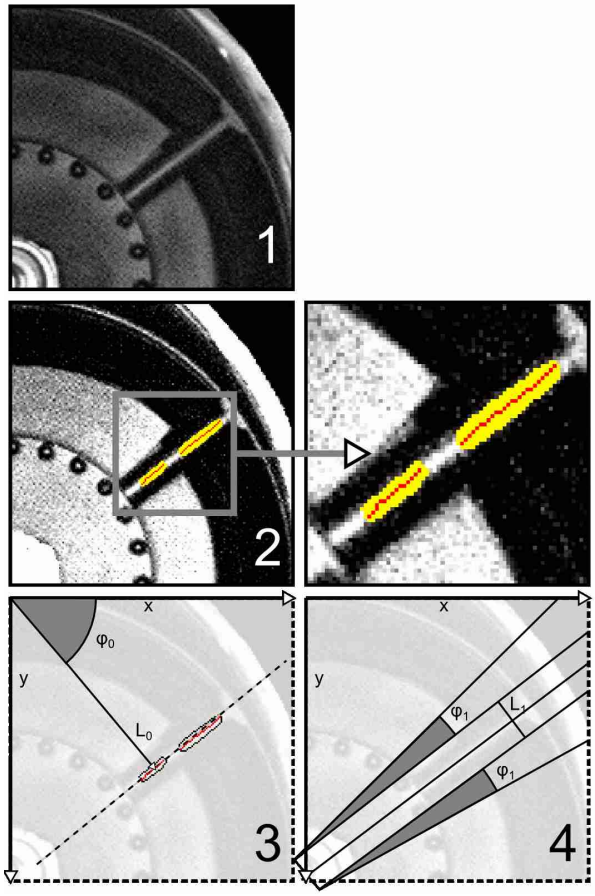

Figure 4: Steps involved in the algorithm used to remove (nullify) the metal arms in the frames. Step 1 shows a raw frame. Step 2 shows an intermediate step where a metal arm has been detected. In step 3 the data from step 2 is used as input to a standard Hough-transform for line detection. Step 4 shows the geometry of a polygonal area used to nullify the metal arm in any frame **F**. Angle φ_1 was set to 6.0°.

4.1. Removal of Rotating Metal Arms

The background in any frame **F** and **B** is unfortunately not completely static. It features rotating metal "arms". These metal arms are structural supports for the cylinder and thus rotates with it. One of these is slightly visible in the foreground frame $\mathbf{F}^{(10)}_{(4,7,5)}$ shown in Figure 1. There are three of such arms – all fixed to the centre of rotation at an angle of 120° to each other. Only one of these arms will ever be visible in any frame **D** at any k-iteration. For some k-iterations no arm will be visible. The first frame **D** at $k = 1$ always features an arm at approximately 30° with the horizontal.

These arms are dynamic disturbances and needed to be removed. We developed an algorithm that detects the presence and location of an arm in the current background-only frame **B** and hereafter removes it in both **F** and **B**. Figure 4 graphically depicts the steps involved in this algorithm. One of the metal arms is clearly visible in the top example (step 1).

The steps of the devised algorithm are as follows:

1. A logical (full frame) map with pixels enabled only at the location of a metal arm is created. See step 2 in Figure 4. This is done using various image filtering and morphological techniques applied to $\mathbf{R}_2$, $\mathbf{R}_3$, and $\mathbf{R}_4$. This logical map will be empty if no arm was found. In that case the algorithm terminates here.
2. The medial axis, or morphological skeleton, is estimated from the enabled areas in the logical map. The algorithm applied for this uses successive thinning and pruning (Lam et al., 1992; also described in Gonzalez and Woods, 2007, chp. 10). It is specifically implemented in function "bwmorph" in MATLAB R2009b Image Processing Toolbox version 6.4. This skeleton is further simplified by iteratively removing whatever branches it may have (again, by using the "bwmorph" function). The result is an updated logical map with sets of highly collinear enabled pixels.
3. The enabled pixels in the logical map are used as input to a standard Hough-transform for line detection (Duda and Hart, 1972; Hough, 1962). A single peak in the two-dimensional (L_0, φ_0) Hough-accumulator is used to determine the location of the metal arm. See step 3 in Figure 4. The resolution was 0.25 for distance L_0 and 0.25° for angle $\varphi_0 \in [0.00°, 89.75°]$.
4. The logical map is updated one final time. A rectangular area of enabled pixels is constructed at the location of the metal arm. The situation is shown in step 4 of Figure 4. The rectangle half-width L_1 was set to 20 pixels. The resulting logical map is hereafter used to nullify (set to zero) the enabled pixels in frame **B**. Nullifying the metal arm in frame **F** is less trivial since it cannot be expected to exactly line up with the line-geometry found in frame **B**. This discrepancy is a natural outcome of the fact that the raw sequences were registered manually. The rectangular area is therefore extended as also shown in step 4 of Figure 4. Angle φ_1 was set to 6.0°. This extended polygonal area is used to nullify the metal arm in frame **F**.

5. Image Analysis: Two-Level Hierarchical Segmentation

It was established in Section 2 that the overall image analysis task is the estimation of the individual location of each long and short seed detected in any frame **F**. The solution of this overall task was in this work posed as the solution to a two-level hierarchical segmentation problem.

Two aims were defined in regard to this problem:

1. Determine what pixels in any data-ROI $\mathbf{R}_i$ in any frame **F** that can be considered part of visible seeds and not background. This is the first binary segmentation in the two-level hierarchical segmentation and is covered in Section 5.3.
2. Determine what pixels in any data-ROI $\mathbf{R}_i$ in any frame **F** that can be considered part of either a single long seed or a single short seed. This is the second binary segmentation in the two-level hierarchical segmentation and is covered in Section 5.4.

The first segmentation was solved as a novelty detection problem (see reviews, e.g. Markou and Singh, 2003a,b). The method applied was a standard statistical distance measure based on the Mahalanobis distance. The second segmentation was solved as a supervised classification problem. The method applied here was a standard quadratic discriminant analysis (QDA). Both statistical methods were applied directly in the standard RGB space. Lee et al. (2010); Huang et al. (2011); Sobieranski et al. (2009) are examples of recent work where the task was image segmentation.

These methods relied on the availability of sets of pre-labelled training pixels. The extraction of such pixels was done using a straightforward hierarchical sampling method. The foundation for this method was based on a simple classification scheme that we introduce next.

5.1. Classification Scheme

Consider a region **S** in **F**. We made the basic assumption that such a region **S** will always consist solely of pairwise disjoint sub-regions (connected components) that can each be labelled as either:

- background (label index $c = 0$);

- foreground – part of a cannabis seed (label index $c = 1$);
- foreground – part of a rice seed (label index $c = 2$);
- or foreground – part of a wheat seed (label index $c = 3$).

We only considered each of these labellings when it was practical to do so. The reason for this was that some of the $P = 9$ seed mixtures involved a variation in the use of the three species of seeds in the experiments. This variation in turn gave rise to a number of different classification scenarios.

Consider the set S_p of all pixels in any given region $\mathbf{S}$ from any frame $\mathbf{F}^{(k)}_{(s,v,p)}$. In accordance with our model of image content, this set S_p will always be equal to the union of one or more pairwise disjoint pixel subsets L_c:

$$S_p = \bigcup_{c \in C_p}^{|C_p|} L_c \ ,$$

where the index set C_p defines which label indices we can practically consider for each possible p:

$$C_p = \begin{cases} \{0, p\}, & \text{if } p = 1, 2, 3 \\ \{0, 1, 2\}, & \text{if } p = 4, 5, 6 \\ \{0, 1, 3\}, & \text{if } p = 7, 8, 9 \end{cases} ,$$

and where $L_c \in S_p$ is the set of all pixels in S_p which have been given the label c.

5.2. Callback-Procedures and Pipelines

Two intermediate results and one single final result were needed:

- The first intermediate result should be a set of training pixels pre-labelled as background (label index $c = 0$) extracted from any data-ROI $\mathbf{R}_i$ in any frame $\mathbf{B}$.
- The second intermediate result should be three individual sets of training pixels pre-labelled as (1) foreground/cannabis ($c = 1$), as (2) foreground/rice ($c = 2$), and as (3) foreground/wheat ($c = 3$). These three sets should be extracted from any data-ROI $\mathbf{R}_i$ in any frame $\mathbf{F}$. These four sets of training pixels were then used in a supervised classification setting to generate the final result.

- The single final result should be a set of pixel-coordinates determined from the contents in any data-ROI $\mathbf{R}_i$ in any frame $\mathbf{F}$. One such pixel-coordinate should exist for each detected connected component classified as either a long or a short seed. This pixel coordinate should also be the approximate centre of each such connected component.

As mentioned in Section 3.2, the MATLAB processing framework took use of pre-configurable call-back procedures. We implemented three such callback-procedures:

- procedure A, used to produce the first intermediate result,
- procedure B, used to produce the second intermediate result,
- and procedure C, used to produced the single final result.

These three procedures where applied using three individual full runs (i.e. the k-iterations were from $k = 1$ to $k = K = 2600$) in succession of each other. This resulted in three individual processing phases or "pipelines":

Pipeline A: a full run using procedure A, producing a result data-structure on disk here referred to as "datastore" A.

Pipeline B: dependent on the availability and correctness of datastore A, a full run using procedure B, producing datastore B.

Pipeline C: dependent on the availability and correctness of both datastore A and datastore B, a full run using procedure C, producing datastore C.

Figure 5 presents an overview of the work carried out in these three pipelines. The schematic is read sequentially from left to right where each columns represents an individual isolated action on the image data. The titles in parentheses describe the generic action taking place in each column. There are six such actions:

1. Load (load frames from disk),
2. Initialise (image analysis step 1),

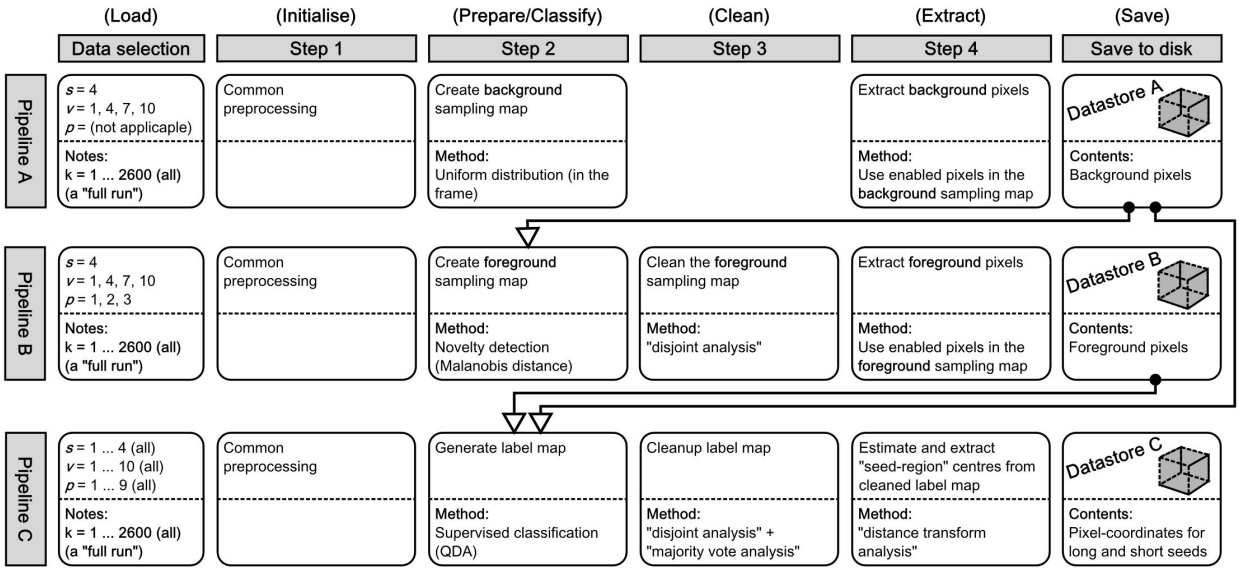

Figure 5: Overview of pipelines. The schematic is read sequentially from left to right. The set of image analysis tasks carried out in each pipeline in each *svp*-iteration in each *k*-iteration, is represented by up to four individual steps numbered from 1 to 4. The arrows leading from the final "datastore" boxes into later steps applied in pipeline A and pipeline B, indicate the reuse of previously sampled pre-labelled training data.

3. Prepare/Classify (image analysis step 2),
4. Clean (image analysis step 3),
5. Extract (image analysis step 4),
6. Save (save data to datastore on disk).

The actual image analysis taking place in each pipeline in each *svp*-iteration in each *k*-iteration is represented by four individual steps numbered from 1 to 4. To be able to refer to these individual steps, the following sections will use shorthand textual codes: For instance, step A2 is the second step of pipeline A. Also, there is no step A3.

The column entitled "Data selection" defines the subset of the *svp*-iterations for each of the three individual callback-procedures invoked in each pipeline. When compared to pipeline C that involved all 360 *svp*-iterations, Pipeline A and B, being tasked solely with the problem of sampling training-pixels for a supervised classification, involved a smaller number of *svp*-iterations: 40 for pipeline A and 120 for pipeline B.

5.3. The First Binary Segmentation

This was the task of distinguishing between background and foreground in any data-ROI $\mathbf{R}_i$ in any frame $\mathbf{F}$. Pipeline A and pipeline B were used to solve this problem.

5.3.1. Pipeline A – Sampling of Background Pixels

As explained in Section 5.2, pipeline A was responsible for generating a set, known as datastore A, holding training pixels pre-labelled as background (label index $c = 0$). Step A2 in Figure 5 introduces the concept of a "sampling map". A sampling map is a logical map in which the enabled pixels denote which pixels to sample or extract from any data-ROI $\mathbf{R}_i$ in frame $\mathbf{D}$. Generating the sampling map in step A2 is trivial since we assume that all pixels in a single data-ROI $\mathbf{R}_i$ in any frame $\mathbf{B}$ are relatively localized in the normalized RGB space, i.e. they represent a single cluster of data-points. On the basis of this assumption, a sampling map was created for each data-ROI $\mathbf{R}_i$ with up to 200 pixels enabled (all evenly distributed in the current data-ROI). A sampling count of 200 pixels represent a sampling percentage of 0.65 % in relation to the number of pixels in a full frame (30 625). This sampling map was then used in step A3 to extract up to 200 background training pixels for label $c = 0$ for for each enabled *svp*-iteration in all $K = 2600$ k-iterations.

5.3.2. Pipeline B – Sampling of Foreground Pixels

At this point, pipeline A has completed and datastore A is available on disk holding pre-labelled background pixels. Prior to invoking pipeline B, a subset of datastore A is loaded from disk into memory and prepared for fast lookup.

Step B2 produced a sampling map for foreground pixels. This was done using novelty detection: The background training examples were used to detect which pixels that could not, in accordance with a threshold on a pixel distance metric, be labelled as background pixels. By the method of exclusion, such pixels thus represented training examples that could be labelled as foreground, i.e. with label indices $c = 1$, $c = 2$, or $c = 3$. The distance metric used was the standard Mahalanobis distance. The threshold was set to three times the standard deviation in each of the three dimensions in the normalized RGB space (for all four data-ROIs $\mathbf{R}_1$ to $\mathbf{R}_4$). The use of pre-labelled background pixels is indicated graphically in Figure 5 by the arrow leading from datastore A to step B2.

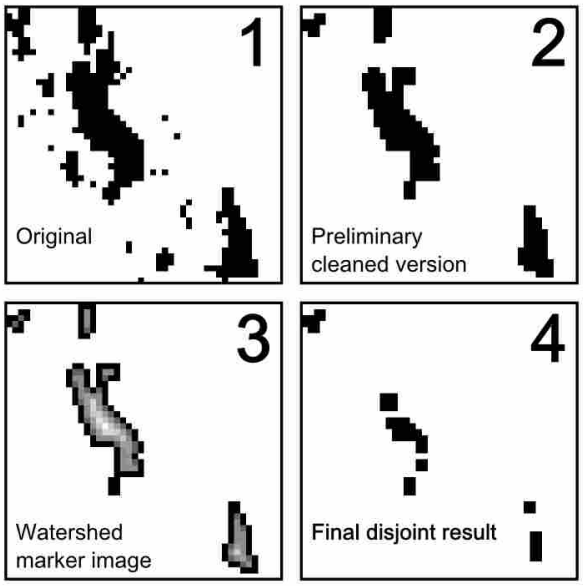

Figure 6: The main steps in the disjoint analysis procedure. Step 1 shows an unprocessed result and in Step 2 a preliminary cleaned version is shown. This was achieved using standard morphological techniques. The processing continues and takes use of watershed segmentation. The watershed segmentation was applied on a preprocessed marker image shown in step 3. This was based on the image distance transform of map in step 2. Step 4 shows the final result after watershed segmentation.

Step B2 resulted in a rudimentary sampling map suffering from statistical noise. To be useful as a sampling for foreground pixels, it had to meet more strict requirements: The enabled pixels of such a map should form disjoint connected components. Each such component (or "seed-region") should correspond (more or less) to parts of the single same seed or one whole seed. These requirements were assured in step B3 using a range of morphological operations collectively referred to as "disjoint analysis".

Figure 6 shows the main steps in the disjoint analysis procedure. This figure graphically depicts the processing of an actual example of a foreground sampling map. In step 1 we see the unprocessed result just after applying the Mahalanobis distance threshold. This example evidently suffers greatly from noise. In step 2, we see a preliminary cleaned version where the spuriously enabled pixels have been disabled. This was achieved using standard morphological techniques (holes, H-connected pixels, and single spurious pixels are removed). The specific algorithms used

were those implemented in function "bwmorph" in MATLAB R2009b Image Processing Toolbox version 6.4. The processing continues and takes use of watershed segmentation (specific algorithm by Meyer, 1994, implemented in MATLAB function "watershed"). The watershed was applied on a preprocessed marker image shown in step 3. This was based on the image distance transform of map in step 2. Step 4 shows the final result after watershed segmentation.

The now cleaned sampling map was hereafter used in step B4. Of the enabled pixels in this map, up to 200 of these were selected – all others were disabled. This sampling map was then used to extract up to 200 foreground pixels for each enabled *svp*-iteration in all $K = 2600$ k-iterations.

5.4. The Second Binary Segmentation

This was the task of distinguishing between short and long seeds in any data-ROI $\mathbf{R}_i$ in any frame $\mathbf{F}$. Pipeline C was used to solve this problem. Technically though, this was not always solved as a binary segmentation (classification) problem. As mentioned in Section 5.1, the classification scheme varied for different choices of mixture index p. For *svp*-iterations with $p = 1, 2, 3$, the segmentation was indeed solved as a binary classification problem. However, for $p = 4, \ldots, 9$, the segmentation was instead solved as a trinary classification problem. There are thus a total of five different classification scenarios. First we have the three binary scenarios defined by label index sets (1) $C_1 = \{0, 1\}$, (2) $C_2 = \{0, 2\}$, and (3) $C_3 = \{0, 4\}$. The final two scenarios are trinary and defined by index sets (1) $C_4 = C_5 = C_6 = \{0, 1, 2\}$ and (2) $C_7 = C_8 = C_9 = \{0, 1, 3\}$.

5.4.1. Pipeline C – Classification

At this point, pipeline A and B have completed and datastore A and datastore B are available on disk holding pre-labelled background and foreground (cannabis, rice, and wheat) pixels. Prior to invoking pipeline C, subsets of both datastore A and datastore B are loaded from disk into memory and prepared for fast lookup.

Step C2 in Figure 5 introduces the concept of a label map. This label map represents the result of the five different classification scenarios described earlier. The task of classifying was to assign a value from the corresponding index set C_p defined in Section 5.1 to each pixel in this label map. The use of pre-labelled background and foreground pixels is indicated graphically in Figure 5 by the arrows leading from datastore A and datastore B to step C2. We used a simple supervised

c	$\mathbf{R}_1$ (%)	$\mathbf{R}_2$ (%)	$\mathbf{R}_3$ (%)	$\mathbf{R}_4$ [%]
0, 1	1.45	0.18	1.89	0.35
0, 2	4.06	1.65	2.42	0.44
0, 3	1.40	1.86	1.69	0.25
0, 1, 2	7.79	2.56	11.66	5.24
0, 1, 3	18.56	16.17	18.68	14.44

Table 2: Misclassification rate in percentages. The five classification scenarios gave rise to five 10-fold cross-validation scenarios. Up to a maximum of 30 000 samples from each class were used. Each row represents data for such a classification scenario (c is the label index) and each of the four columns represent data for each of the four data-ROIs $\mathbf{R}_1$ to $\mathbf{R}_4$. The trinary scenarios can be observed to generally have the highest misclassification rates.

classifier: quadratic discriminant analysis. The analysis was done directly in the normalized three-dimensional RGB space. The number of degrees of freedom remained at three. We used no pairwise products such as quadratic terms or mixed products.

Table 2 lists the 10-fold cross validation estimates of misclassification rate in percentages. The five classification scenarios gave rise to five cross validation scenarios. Up to a maximum of 30 000 samples from each class were used. Each row of Table 2 represents data for such a scenario and each of the four columns represents data for each of the four data-ROIs $\mathbf{R}_1$ to $\mathbf{R}_4$. The lowest misclassification rate observed is 0.18 %. This happens in data-ROI $\mathbf{R}_2$ in the binary case between background ($c = 0$) and foreground/cannabis ($c = 1$). The highest misclassification rate observed is 18.68 %. This happens in data-ROI $\mathbf{R}_3$ in the trinary case between background ($c = 0$), foreground/cannabis ($c = 1$), and foreground/wheat ($c = 3$). Generally, the trinary scenarios can be observed to have the highest misclassification rates.

5.4.2. Pipeline C – Cleaning the Label Map

Due to the statistical noise in the QDA-based classification, the resulting label map was further processed in step C3 using the disjoint analysis procedure. Logical maps were created from this

label map and these were processed individually. Only the pixels labelled with label index $c = 1$, $c = 2$, or $c = 3$ were used. The pixels labelled as background ($c = 0$) were ignored. The seed regions in the now cleaned label map were still influenced by noise in the labelling. This was solved by using a majority vote on counts of labelled pixels in each seed region. If no consensus could be achieved, that particular seed region was be ignored in step C4. This procedure is referred to as "majority vote analysis" in Figure 5.

In Step C4, an approximate centre pixel-coordinate was determined for each labelled seed-region in the final label map. This was achieved by using a combination of the image distance transform (Maurer et al., 2003) and the regional maxima transform (algorithm used was the one implemented in function "imregionalmax" in MATLAB R2009b Image Processing Toolbox 6.4). We refer to this procedure as "distance transform analysis" in Figure 5. These final centre pixel-coordinates were saved in datastore C.

The last step in pipeline C concludes the image analysis. The result was a larger data-structure (datastore C) holding the approximate centre pixel coordinates of all long and short seeds detected in any frame $\mathbf{F}$ for all 360 *svp*-iterations in all $K = 2600$ k-iterations. The remaining processing of the contents of datastore C was done in post-processing.

6. Post-processing

The image analysis concluded with the sampled pixel coordinates of seeds stored on disk in datastore C. The post-processing of this data involved the following two tasks for each available pixel coordinate $\boldsymbol{p}$ in any frame $\mathbf{F}$:

1. Convert $\boldsymbol{p}$ from pixel coordinate space to the physical coordinate space U_{geo}.
2. Estimate angle θ for the now converted $\boldsymbol{p}$.

6.1. Coordinate Space Conversion

Let $U_{\text{img}} = \{[m, n]^\top \in \mathbb{N}_0^2 \setminus \{[0, 0]^\top\} : m \leq N \wedge n \leq N\}$, where $N = 175$ pixels, be the mathematical definition of pixel coordinate space. A detected point $\boldsymbol{p}$ in any frame $\mathbf{F}$ will have to be converted from pixel coordinate space U_{img} to physical coordinate space U_{geo}. For this we used

a linear interpolation function $f_{r,N} : U_{\text{img}} \to U_{\text{geo}}$:

$$f_{r,N}(\boldsymbol{p}) = (\boldsymbol{p} - 0.5)r/N,$$

where $r = 0.2\,\text{m}$. Function $f_{r,N}(\boldsymbol{p})$ maps a coordinate (a pair of integers) from the full $N \times N$ frame to a coordinate in the $r \times r$ subset of $\mathbb{R}^2_+$ of which U_{geo} is a subset.

6.2. Estimating the Angle of Escape

Once a seed has left the inner surface of the cylinder at angle (of escape) θ, it is assumed that its movement will follow a trajectory very similar to a parabola. It is also assumed that the movement of a seed is constrained to a plane perpendicular to the cylinder's axis of rotation. Any movement is thus inherently two-dimensional.

6.2.1. Physical Model

Seeds are modelled as points $\boldsymbol{p} \in U_{\text{geo}}$. Consider the time-dependent location $\boldsymbol{p}(t)$ of any such point, where $t \in [t_{\text{start}}, t_{\text{end}}]$. The movement of this point is modelled only from the moment in time t_0 when the point leaves the circumference of the cylinder at angle $\theta \equiv \theta_\omega(t_0)$. The cylinder has radius r and rotates with angular frequency ω. Here we use a function $\theta_\omega(t) = \omega t$ to denote the fact that the angle θ is dependent on time and the parameter ω. In the following we also use its time derivative $\dot{\theta}_\omega(t) = \omega$.

The location in U_{geo} where point $\boldsymbol{p}(t)$ leaves the surface is the time-dependent initial position $\boldsymbol{p}_0(t) = [x_0(t), y_0(t)]^\top$ of that point. Its components are:

$$x_0(t) = r\cos\theta_\omega(t), \quad y_0(t) = r\sin\theta_\omega(t).$$

Likewise, the components of the time-dependent initial velocity $\dot{\boldsymbol{p}}_0(t) = [\dot{x}_0(t), \dot{y}_0(t)]^\top$ are:

$$\dot{x}_0(t) = -r\dot{\theta}_\omega(t)\sin\theta_\omega(t), \quad \dot{y}_0(t) = r\dot{\theta}_\omega(t)\cos\theta_\omega(t).$$

The components of the time-dependent location $\boldsymbol{p}(t) = [x(t), y(t)]^\top$ for a point leaving the cylinder circumference at time t_0 are:

$$x(t) = x_0(t_0) + \dot{x}_0(t_0)t, \tag{2}$$

$$y(t) = y_0(t_0) + \dot{y}_0(t_0)t - \frac{1}{2}gt^2, \tag{3}$$

where $g = 9.82\,\mathrm{m\,s^{-2}}$ is the constant of gravitational acceleration. Solving for t in (2) and substituting into (3) results in the following expression for $y(t)$:

$$y(t) = y_0(t_0) + \dot{y}_0(t_0)\left[\frac{x(t) - x_0(t_0)}{\dot{x}_0(t_0)}\right] - \frac{1}{2}g\left[\frac{x(t) - x_0(t_0)}{\dot{x}_0(t_0)}\right]^2 \quad . \tag{4}$$

If we substitute the components of the initial location and velocity into (4), a function $\tilde{y}_{\omega,r}(x, \theta)$ can be defined:

$$\tilde{y}_{\omega,r}(\theta, x) = G_\omega \frac{1}{r^2}\csc^2\theta[r\cos\theta - x]^2 + \cot\theta\,[r\cos\theta - x] + r\sin\theta. \tag{5}$$

Here we have used the short form equivalence $\theta_\omega(t_0) \equiv \theta$ and dropped the reference to time t. Use of parameters g and ω now takes place only in factor $G_\omega = -(g/2)\omega^{-2}$.

6.2.2. A Minimization Problem

Consider the i'th point $\boldsymbol{p}_i = [x_i, y_i]^\top$ detected in any frame $\mathbf{F}$. We seek to estimate the value of angle θ_i for any detected point $\boldsymbol{p}_i$, such that $y_i = \tilde{y}_{\omega,r}(\theta_i, x_i)$. For this we define a residual function $\tilde{e}_{\omega,r}(\theta, x, y)$:

$$\tilde{e}_{\omega,r}(\theta, x, y) = \tilde{y}_{\omega,r}(\theta, x) - y,$$

and pose the following minimization problem in $\mathbb{R}$:

$$\theta_i = \underset{\theta}{\operatorname{argmin}} \left|\tilde{e}_{\omega,r}(\theta, x_i, y_i)\right| \quad .$$

This minimization problem can be solved most directly by the use of numerical methods. One simply finds the smallest discrepancies between model and observation. This method was previously used by the authors in Buus et al. (2011). In this work, with the intent of achieving a more mathematical exactness, we instead derived a closed-form solution for θ. In other words, we created a new function $\tilde{\theta}_{\omega,r}(x, y)$ that can give us the exact angle θ_i for any given point $\boldsymbol{p}_i$.

6.2.3. A Closed-form Solution

The trigonometric expressions in $\tilde{e}_{\omega,r}(\theta, x, y)$ can be rewritten using the following tangent half-angle formulae:

$$\sin\theta = \frac{2u}{1+u^2} \quad , \qquad \cos\theta = \frac{1-u^2}{1+u^2} \quad ,$$
$$\csc\theta = \frac{1+u^2}{2u} \quad , \qquad \cot\theta = \frac{1-u^2}{2u} \quad ,$$

where $u = \tan\frac{\theta}{2}$. By using these substitutions in (5) we end up with a quasi-symmetric quartic $\tilde{\theta}_{\omega,r}(u, x, y)$ in u:

$$\begin{aligned}\tilde{\theta}_{\omega,r}(u, x, y) &= G_\omega(r(u^2 - 1) + x(1 + u^2)) \\ &\quad + 2r^2u(r(1 + u^2) + (u^2 - 1)x - 2uy) \\ &= a_0u^4 + a_1u^3 + a_2u^2 + a_1b_0u + a_0b_0^2,\end{aligned}$$

where

$$a_0 = G_\omega(r + x)^2, \qquad a_1 = 2r^2(r + x),$$
$$a_2 = 2G_\omega(x^2 - r^2) - 2r^2y, \qquad b_0 = (r - x)/(r + x).$$

Finding the roots of a quasi-symmetric quartic equation for parameters a_0, a_1, a_2, and b_0, can be done by recursively solving three quadratic equations. In the range $\theta \in [0, \pi/2]$, two of the four roots will be complex and irrelevant, while the two others will be real when $(x + y)^2 < r^2$. These two real roots correspond to the two parabolas that can intersect a detected point $\boldsymbol{p}_i$ and still be tangent at the cylinder circumference in the range $\theta \in [0, \pi/2]$. The relevant one of these two solutions for u, is the one for which $2\arctan u < \arccos(x/r)$, where $x \leq r$. The closed-form expression for this single relevant solution for u is:

$$\tilde{u}_{\omega,r}(x, y) = -\frac{1}{4a_0}\left[a_1 + c_0 - \sqrt{c_1 + (a_1 + c_0)^2}\right]$$

where

$${c_0}^2 = {a_1}^2 - 4a_0(2a_0b_0 - a_2), \quad c_1 = (4a_0)^2b_0.$$

The function $\tilde{\theta}_{\omega,r}(x, y)$ can now be given as:

$$\theta(\omega, \boldsymbol{p}) \equiv \tilde{\theta}_{\omega,r}(x, y) = 2\arctan\,\tilde{u}_{\omega,r}(x, y).$$

6.3. Final Data Generation

Consider a set holding the seed locations detected in any frame **F** in any *svp*-iteration in any *k*-iteration. These sets were, for each *svp*-iteration, combined over all *k*-iterations – resulting in 360 such combined sets. Each of these sets holds all the seed locations detected in frame **F** at all

time indices $k = 1, \ldots, K = 2600$ for any single choice of indent working diameter d, rotational speed ω, and mixture index p.

Such a combined set of points consists of two subsets: (2) one for long seeds and (2) one for short seeds. The size of the smallest of these two sets defines the individual size of both sets. Points from the larger set are randomly selected and removed such that this requirement is met. There are thus always an equal amount of long and short locations available from each svp-iteration. Let $\boldsymbol{\theta}^{\text{long}}_{(s,v,p)}$ and $\boldsymbol{\theta}^{\text{short}}_{(s,v,p)}$ be the vector forms of these two sets:

$$\boldsymbol{\theta}^{\text{long}}_{(s,v,p)} = \left[\theta(\omega_v, \boldsymbol{p}^{\text{long}}_{(s,v,p,1)}), \theta(\omega_v, \boldsymbol{p}^{\text{long}}_{(s,v,p,2)}), \ldots\right]^\top,$$
$$\boldsymbol{\theta}^{\text{short}}_{(s,v,p)} = \left[\theta(\omega_v, \boldsymbol{p}^{\text{short}}_{(s,v,p,1)}), \theta(\omega_v, \boldsymbol{p}^{\text{short}}_{(s,v,p,2)}), \ldots\right]^\top.$$

These vectors hold the estimated values for θ for each detected long and short seed locations $\boldsymbol{p}^{\text{long}}_{(s,v,p,i)}$ and $\boldsymbol{p}^{\text{short}}_{(s,v,p,i)}$. These vectors are the time series introduced in Section 2. There will naturally be 360 of such pairs of vectors – one pair for each svp-iteration. These 720 vectors will be the basis for the final statistical analysis and results presented the next section.

7. Results and Discussion

The overall goal was to create an empirical overview of the indented cylinder's ability to meet the criterion of optimality presented in Section 1. This section will present part of this empirical overview.

The estimation of this overview is based on the assumptions that bundles of trajectories will form in the recorded image sequences (see Section 2.1). Two statistical measures of separation between such of trajectories were presented in Section 2.2. These two measures, (1) the numerical distance between averages and (2) the Hellinger distance, were both applied to calculate the empirical overview. There will thus be two versions of this overview.

These results are given only for the sequences with mixture indices $p = 4, 5, \ldots, 9$. These sequences were created using the binary mixtures. With our overall goal in mind, these sequences are naturally of more interest than the ones created using the unary mixtures – of which no measure of separation can be defined.

7.1. Overview of Separation Ability

We will refer to the two statistical averages for the vectors $\boldsymbol{\theta}^{\text{long}}_{(s,v,p)}$ and $\boldsymbol{\theta}^{\text{short}}_{(s,v,p)}$ as $\mu^{\text{long}}_{(s,v,p)}$ and $\mu^{\text{short}}_{(s,v,p)}$. Similarly, the two standard deviations are referred to as $\sigma^{\text{long}}_{(s,v,p)}$ and $\sigma^{\text{short}}_{(s,v,p)}$. Using this notation we can define the two measures of separation as:

$$a^{\text{num}}_{(s,v,p)} = \mu^{\text{short}}_{(s,v,p)} - \mu^{\text{long}}_{(s,v,p)}, \tag{6}$$

$$a^{\text{hel}}_{(s,v,p)} = H\left(\mu^{\text{long}}_{(s,v,p)}, \sigma^{\text{long}}_{(s,v,p)}, \mu^{\text{short}}_{(s,v,p)}, \sigma^{\text{short}}_{(s,v,p)}\right), \tag{7}$$

where superscript "num" denotes the numerical distance between averages and "hel" denotes the Hellinger distance. The function H is the one defined in (1) in Section 2.2.2. Note that we apply the non-square Hellinger distance here.

We can now define two $S \times V$ matrices $\mathbf{A}^{\text{num}}_p$ and $\mathbf{A}^{\text{hel}}_p$ (defined only for $p = 4, 5, \ldots, 9$):

$$\mathbf{A}^{\text{num}}_p = \begin{bmatrix} a^{\text{num}}_{(1,1,p)} & a^{\text{num}}_{(1,2,p)} & \cdots & a^{\text{num}}_{(1,V,p)} \\ a^{\text{num}}_{(2,1,p)} & a^{\text{num}}_{(2,2,p)} & \cdots & a^{\text{num}}_{(2,V,p)} \\ \vdots & \vdots & \ddots & \vdots \\ a^{\text{num}}_{(S,1,p)} & a^{\text{num}}_{(S,2,p)} & \cdots & a^{\text{num}}_{(S,V,p)} \end{bmatrix}$$

and

$$\mathbf{A}^{\text{hel}}_p = \begin{bmatrix} a^{\text{hel}}_{(1,1,p)} & a^{\text{hel}}_{(1,2,p)} & \cdots & a^{\text{hel}}_{(1,V,p)} \\ a^{\text{hel}}_{(2,1,p)} & a^{\text{hel}}_{(2,2,p)} & \cdots & a^{\text{hel}}_{(2,V,p)} \\ \vdots & \vdots & \ddots & \vdots \\ a^{\text{hel}}_{(S,1,p)} & a^{\text{hel}}_{(S,2,p)} & \cdots & a^{\text{hel}}_{(S,V,p)} \end{bmatrix}.$$

7.1.1. Analysis Using Numerical Distance Between Averages

Figure 7 shows six linearly interpolated contour maps – one for all six sequences using binary mixtures (for $p = 4, 5, \ldots, 9$). These maps were produced using the numerical distance between averages available in matrix $\mathbf{A}^{\text{num}}_p$. The contours and tones of the map are scaled in the range from 1° to 20° for all six maps. These maps give an explicit overview of the inner surface's ability to separate the cannabis/rice mixtures ($p = 4, 5, 6$) and cannabis/wheat mixtures ($p = 7, 8, 9$). The plotted angle values represent the separation of two average parabolic trajectories on the cylinder circumference.

The white area to the left of the zero contour line in all six plots represents values that are all negative. Taking into consideration the mathematical definition of $a^{\text{num}}_{(s,v,p)}$ given in (6), negative values could indicate a situation where the indented cylinder flips the separation behaviour (i.e. long material is generally lifted higher than short material). This particular behaviour is observed, in all six plots, for lower values of rotational speed ω_v (generally below $\omega_5 = 33.96$ r/min) and never seems to occur for $d_4 = 7.0$ mm.

A distinct "band" of higher angles of separation is visible in the first three contour plots from the cannabis/rice mixtures (Figure 7a, 7b, and 7c). In the final three contour plots from the cannabis/rice mixtures (Figure 7d, 7f, and 7f) this band has changed into a region that generally does not include the lowest indent working diameter $d_1 = 5.5$ mm. Generally we can observe that the best separation occurs when the indent working diameter d is between 6.5 mm and 7.0 mm, and the rotational speed ω is between 37 r/min and 43 r/min.

7.1.2. Analysis Using Hellinger Distance

Figure 8 again shows six contour plots. These plots were created using the Hellinger distance measure, and the contours and tones are therefore mapped to a range between 0 and 1. When comparing these plots directly with those presented in Figure 8, the separation ability seems to be similar. The Hellinger distance also takes into consideration the variation of the data – something that the numerical distance of averages does not.

7.2. Analysis of the Best Separations

The best separations were found by statistically analysing the values in both matrices $\mathbf{A}^{\text{num}}_p$ and $\mathbf{A}^{\text{hel}}_p$. This analysis involved finding, for each mixture index p, the single pair of row index s and column index v, for which values of $a^{\text{num}}_{(s,v,p)}$ and $a^{\text{hel}}_{(s,v,p)}$ were both high in magnitude. To find this elite pair of s and v, we used the i'th percentile estimates of the values in matrices $\mathbf{A}^{\text{num}}_p$ and $\mathbf{A}^{\text{hel}}_p$ as the individual maximum cut off value for each of the two distance measures. An iterative algorithm was used to search for the highest i'th percentile for which both matrices $\mathbf{A}^{\text{num}}_p$ and $\mathbf{A}^{\text{hel}}_p$ had at least one value equal to and above – at the same row index s and column index v. This search made it possible to define six pairs of optimal values for s and v. This section presents further results in regard to these six sets of parameter value choices.

			Maximum						Chosen			
p	s	v	d_s [mm]	ω_v [r/min]	ω_v [rad/s]	$a^{\text{num}}_{(s,v,p)}$	s	v	d_s [mm]	ω_v [r/min]	ω_v [rad/s]	$a^{\text{num}}_{(s,v,p)}$
4	3	8	6.5	42.60	4.46	17.7131°	3	8	6.5	42.60	4.46	17.7131°
5	4	6	7.0	36.71	3.84	16.2895°	4	6	7.0	36.71	3.84	16.2895°
6	4	6	7.0	36.71	3.84	15.4651°	3	8	6.5	42.60	4.46	15.4070°
7	3	6	6.5	36.71	3.84	12.2339°	3	6	6.5	36.71	3.84	12.2339°
8	3	7	6.5	39.73	4.16	15.3444°	3	7	6.5	39.73	4.16	15.3444°
9	3	7	6.5	39.73	4.16	15.3914°	3	7	6.5	39.73	4.16	15.3914°

Table 3: Maximum and chosen distance options for s and v. The values are for the numerical distance between averages from matrix $\mathbf{A}^{\text{num}}_p$.

Table 3 and 4 list the maximum distance options (maximum value in $\mathbf{A}^{\text{num}}_p$ and $\mathbf{A}^{\text{hel}}_p$) and the chosen best options for s and v.

7.2.1. Histogram Analysis

Figure 9 shows the normalized histograms generated from vectors $\boldsymbol{\theta}^{\text{long}}_{(s,v,p)}$ and $\boldsymbol{\theta}^{\text{short}}_{(s,v,p)}$. Each plot has a superimposed normal fit for both the long and short distributions. These plots give an overview of the statistical properties of the angle θ. The standard deviations are generally comparably over all six histogram plots.

7.2.2. Trajectory Analysis

The statistical properties of the vectors $\boldsymbol{\theta}^{\text{long}}_{(s,v,p)}$ and $\boldsymbol{\theta}^{\text{short}}_{(s,v,p)}$, can be interpreted geometrically as the statistical properties of the initial locations of the parabolic trajectories of long and short seeds. Figure 10 shows the graphical depictions of such an interpretation. These "trajectory plots" are similar in nature to the example shown earlier in Figure 2. These versions also include up to 300 long and up to 300 short seeds and their (ideal) parabolic trajectories. The standard deviation of the trajectory bundles was set to $\pm(1/2)\sigma^{\text{long}}_{(s,v,p)}$ and $\pm(1/2)\sigma^{\text{short}}_{(s,v,p)}$. The gap between the bundles varies slightly and the trajectory plot for $p = 7$ in Figure 10d is a special sub-optimal case.

			Maximum				Chosen (same as in Table 3)					
p	s	v	d_s [mm]	ω_v [r/min]	ω_v [rad/s]	$a^{\text{hel}}_{(s,v,p)}$	s	v	d_s [mm]	ω_v [r/min]	ω_v [rad/s]	$a^{\text{hel}}_{(s,v,p)}$
4	3	8	6.5	42.60	4.46	0.5136	3	8	6.5	42.60	4.46	0.5136
5	4	6	7.0	36.71	3.84	0.5005	4	6	7.0	36.71	3.84	0.5005
6	1	10	5.5	49.08	5.14	0.5444	3	8	6.5	42.60	4.46	0.4724
7	3	6	6.5	36.71	3.84	0.3605	3	6	6.5	36.71	3.84	0.3605
8	3	6	6.5	36.71	3.84	0.4577	3	7	6.5	39.73	4.16	0.4514
9	4	5	7.0	33.96	3.56	0.4670	3	7	6.5	39.73	4.16	0.4474

Table 4: Maximum and chosen distance options for s and v. The values are for the Hellinger distance measure from matrix $\mathbf{A}^{\text{hel}}_p$.

7.2.3. Temporal Analysis

We have so far presented results for normal fit parameters of six selected pairs of vectors $\boldsymbol{\theta}^{\text{long}}_{(s,v,p)}$ and $\boldsymbol{\theta}^{\text{short}}_{(s,v,p)}$. These vectors were generated by combining the sampled values of θ from all times $k = 1, 2, \ldots, K = 2600$ into two sets of the same size. To do a proper time-series analysis, the seed locations from every 25 k-iterations were combined in to a single set. This resulted in $K/25 = 2600/25 = 104$ pairs of combined sets for each of the 360 svp-iterations. The following pairwise analysis was done on sets with the same size.

Figure 11 shows two scatter plots for each of the six values of p. The upper scatter plot shows the average θ value estimated from the 25 combined sets. The open (white) circular markers are from a normal fit estimated using θ values for short seeds. The closed (black) circular markers were estimated using θ values for long seeds. The lower scatter plot similarly depicts the estimated Hellinger distance. Overall, the plots indicate a stable temporal behaviour (stationarity) for all six mixture situations ($p = 4, 5, \ldots, 9$). The observation of stationarity of the indented cylinder was previously reported by the authors in Buus et al. (2011).

8. Conclusions

In this work we used methods from image analysis to observe and extract information from a laboratory indented cylinder's internal sorting process. A computational processing framework was developed in MATLAB to carry out the image analysis. The image analysis was done in three distinct processing phases (pipelines) by the use of a custom data-processing framework built in MATLAB. We used a combination of distance-based novelty detection and supervised pattern recognition to classify detected seeds as being either long or short. The cross validation errors for all five classification scenarios were all shown to be below 30 % (see Table 2 in Section 5.4.1).

There are multiple conclusions to report from the parts of the empirical overview presented in Section 7:

1. For the three cannabis/rice mixtures ($p = 4, 5, 6$), the optimal ranges for d and ω are 6.5 mm to 7.0 mm and 36.71 r/min to 42.60 r/min, respectively.
2. For the three cannabis/wheat mixtures ($p = 7, 8, 9$), the optimal value for d is 6.5 mm and the optimal range for ω is 36.71 r/min to 39.73 r/min.
3. The histogram plots in Figures 9a to 9f show similar standard deviations of angle θ for both short and long seeds, for $p = 4, 5, \ldots, 9$. This standard deviation for long and short seeds is in the range 10.60° to 11.8° and 10.50° to 11.2°, respectively.
4. The zero contours observed in Figures 7a to 7f indicate that the separation behaviour is flipped for ω values below 33.96 r/min. In such a situation, long material is lifted higher than short material. This observation is tentative and further experiments must be conducted to validate it.
5. The scatter plots in Figures 11a to 11f indicate temporal stability of the indented cylinder.

We have a final practical proposal: The statistical analysis of the initial conditions for the trajectories of long and short seeds, as graphically depicted in the trajectory plots shown in Figures 10a to 10f, could be applicable for properly adjusting the working angle α of the collecting bin. This optimization of the actual sorting outcome would in essence be a direct consequence of an optimization of the separation done by the inner surface of the indented cylinder.

Lastly, we consider this work as an early step toward a paradigm shift where the best parameters for the indented cylinder are not mainly determined by "rule-of-thumb" and other subjective measures, but are instead likely to be fully optimized parameters tied to an actual theory of seed separation in the indented cylinder.

References

Bennedsen, B., Peterson, D., Tabb, A., 2005. Identifying defects in images of rotating apples. Computers and Electronics in Agriculture 48, 92–102.

Bhattacharyya, A., 1943. On a measure of divergence between two statistical populations defined by their probability distributions. Bulletin of the Calcutta Mathematical Society 35, 99–109.

Brosnan, T., Sun, D., 2002. Inspection and grading of agricultural and food products by computer vision systems – a review. Computers and Electronics in Agriculture 36, 193–213.

Bruzzone, L., Roli, F., Serpico, S.B., 1995. An extension of the jeffreys-matusita distance to multiclass cases for feature selection. Geoscience and Remote Sensing, IEEE Transactions on 33, 1318–1321.

Buus, O.T., Carstensen, J.M., Jørgensen, J.R., 201x. Analysis of the indented cylinder part 1: Preliminary image analysis experiments. Computers and Electronics in Agriculture (in this issue).

Buus, O.T., Jørgensen, J.R., Carstensen, J.M., 2011. Analysis of seed sorting process by estimation of seed motion trajectories, in: Heyden, A., Kahl, F. (Eds.), Image Analysis. Springer Berlin / Heidelberg. volume 6688 of *Lecture Notes in Computer Science*, pp. 273–284.

Dana, W., Ivo, W., 2008. Computer image analysis of seed shape and seed color for flax cultivar description. Computers and Electronics in Agriculture 61, 126–135.

Dell'Aquila, A., 2007. Towards new computer imaging techniques applied to seed quality testing and sorting. Seed Science and Technology 35, 519–538.

Dell'Aquila, A., 2009a. Development of novel techniques in conditioning, testing and sorting seed physiological quality. Seed Science and Technology 37, 608–624.

Dell'Aquila, A., 2009b. Digital imaging information technology applied to seed germination testing. a review. Agronomy for Sustainable Development 29, 213–221.

Duda, R.O., Hart, P.E., 1972. Use of the hough transformation to detect lines and curves in pictures. Commun. ACM 15, 11–15.

Gonzalez, R.C., Woods, R.E., 2007. Digital Image Processing. Prentice Hall.

Hough, P.V.C., 1962. Method and means for recognizing complex patterns. U.S. Patent 3,069,654, filed March 25, 1960, and issued December 18, 1962.

Huang, R., Sang, N., Luo, D., Tang, Q., 2011. Image segmentation via coherent clustering in l*a*b* color space. Pattern Recognition Letters 32, 891–902.

Kondo, N., Ahmad, U., Monta, M., Murase, H., 2000. Machine vision based quality evaluation of iyokan orange fruit using neural networks. Computers and Electronics in Agriculture 29, 135–147.

Lam, L., Lee, S.W., Suen, C.Y., 1992. Thinning methodologies-a comprehensive survey. Pattern Analysis and Machine Intelligence, IEEE Transactions on 14, 869–885.

Lee, S.H., Koo, H.I., Cho, N.I., 2010. Image segmentation algorithms based on the machine learning of features. Pattern Recognition Letters 31, 2325–2336.

Li, J., Rao, X., Ying, Y., 2011. Detection of common defects on oranges using hyperspectral reflectance imaging. Computers and Electronics in Agriculture 78, 38–48.

Malvar, H.S., He, L., Cutler, R., 2004. High-quality linear interpolation for demosaicing of bayer-patterned color images, in: Acoustics, Speech, and Signal Processing, 2004. Proceedings. (ICASSP '04). IEEE International Conference on, pp. 485–488.

Markou, M., Singh, S., 2003a. Novelty detection: a review – part 1: statistical approaches. Signal Process. 83, 2481–2497.

Markou, M., Singh, S., 2003b. Novelty detection: a review – part 2: neural network based approaches. Signal Process. 83, 2499–2521.

Matusita, K., 1955. Decision rules, based on the distance, for problems of fit, two samples, and estimation. The Annals of Mathematical Statistics 26, 631–640.

Matusita, K., 1956. Decision rule, based on the distance, for the classification problem. Annals of the Institute of Statistical Mathematics 8, 67–77.

Maurer, C.R., J., Qi, R., Raghavan, V., 2003. A linear time algorithm for computing exact euclidean distance transforms of binary images in arbitrary dimensions. Pattern Analysis and Machine Intelligence, IEEE Transactions on 25, 265–270.

Meyer, F., 1994. Topographic distance and watershed lines. Signal Processing 38, 113–125.

Pearson, T., 2009. Hardware-based image processing for high-speed inspection of grains. Computers and Electronics in Agriculture 69, 12–18.

Pearson, T., Brabec, D., Haley, S., 2008. Color image based sorter for separating red and white wheat. Sensing and Instrumentation for Food Quality and Safety 2, 280–288.

Pizer, S.M., Amburn, E.P., Austin, J.D., Cromartie, R., Geselowitz, A., Greer, T., ter Haar Romeny, B., Zimmerman, J.B., Zuiderveld, K., 1987. Adaptive histogram equalization and its variations. Computer Vision, Graphics, and Image Processing 39, 355–368.

Ruiz-Altisent, M., Ruiz-Garcia, L., Moreda, G., Lu, R., Hernandez-Sanchez, N., Correa, E., Diezma, B., Nicolaï, B., García-Ramos, J., 2010. Sensors for product characterization and quality of specialty crops – a review. Computers

and Electronics in Agriculture 74, 176–194.

Sobieranski, A.C., Abdala, D.D., Comunello, E., von Wangenheim, A., 2009. Learning a color distance metric for region-based image segmentation. Pattern Recognition Letters 30, 1496–1506.

Szczypiński, P.M., Zapotoczny, P., 2012. Computer vision algorithm for barley kernel identification, orientation estimation and surface structure assessment. Computers and Electronics in Agriculture 87, 32–38.

Xiao-bo, Z., Jie-wen, Z., Yanxiao, L., Holmes, M., 2010. In-line detection of apple defects using three color cameras system. Computers and Electronics in Agriculture 70, 129–134.

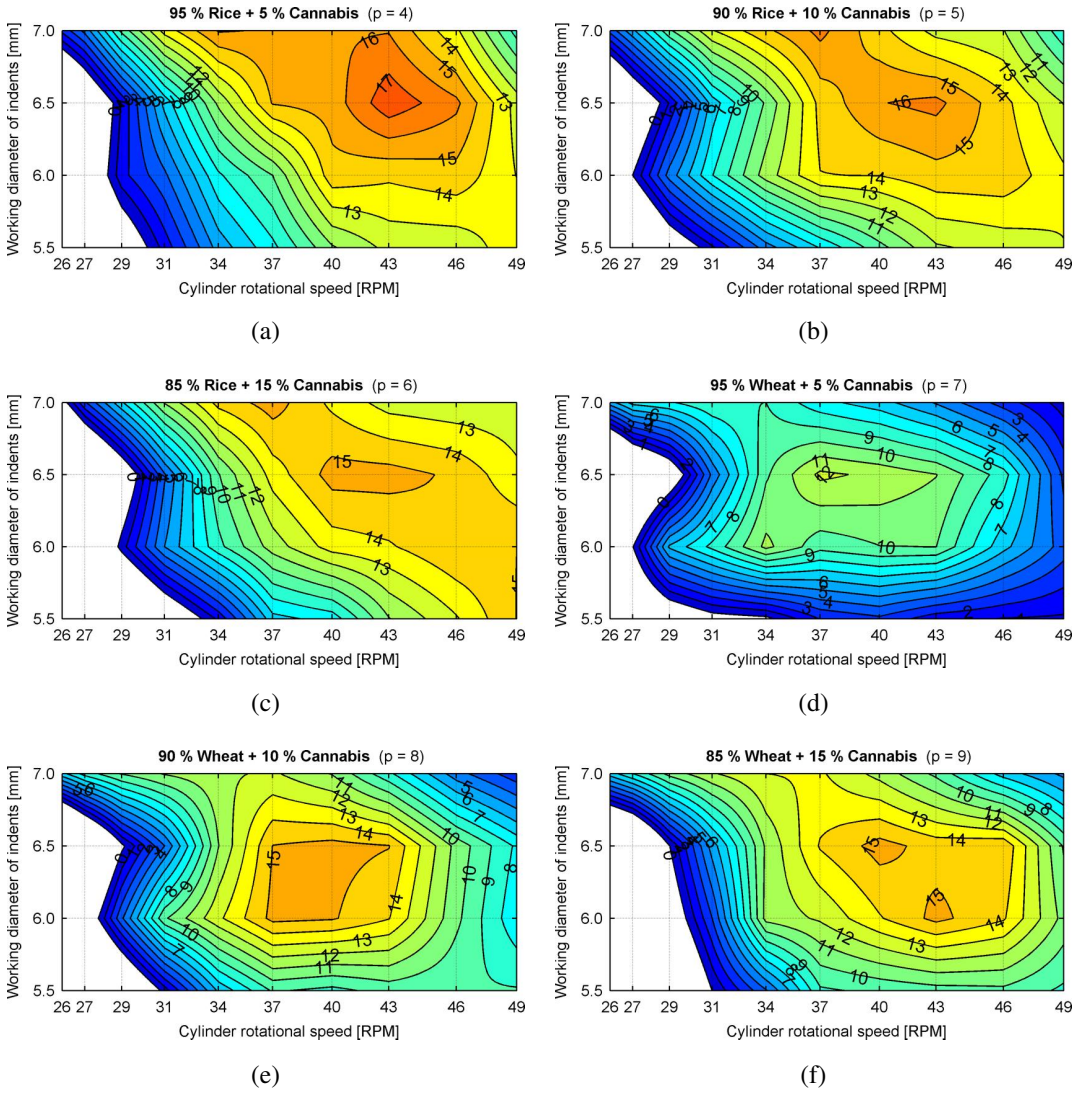

Figure 7: Contour plots of numerical distances between averages. The figure shows six linearly interpolated contour maps – one for all six sequences using binary mixtures (for $p = 4, 5, \ldots, 9$). These maps were produced using the numerical distance between averages available in matrix $\mathbf{A}_p^{\text{num}}$. The contours and tones of the map are scaled in the range from 1° to 20° for all six maps. These maps give an explicit overview of the inner surface's ability to separate the cannabis/rice mixtures ($p = 4, 5, 6$) and cannabis/wheat mixtures ($p = 7, 8, 9$). The plotted angle values represent the separation of two average parabolic trajectories on the cylinder circumference.

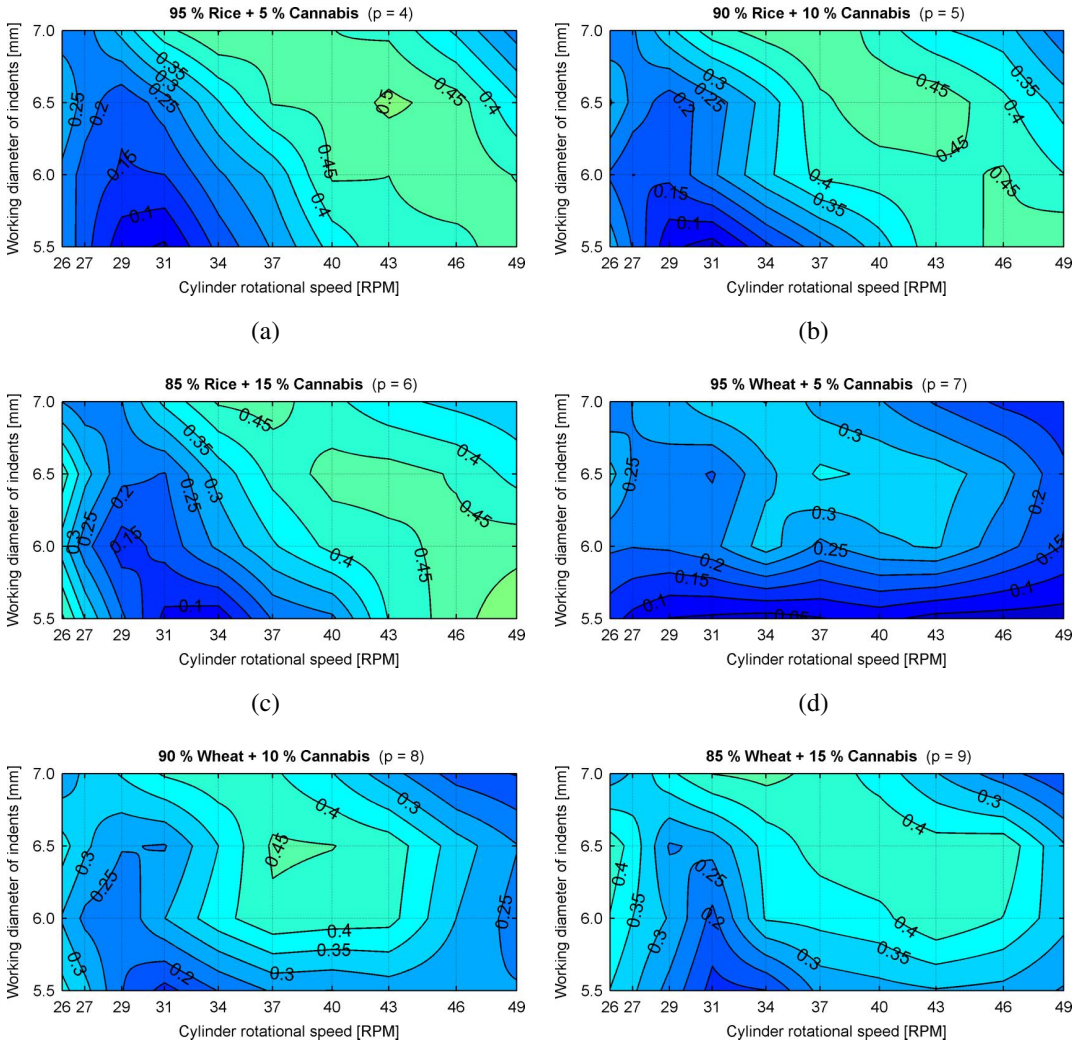

Figure 8: Contour plots of Hellinger distances. The figure shows six linearly interpolated contour maps – one for all six sequences using binary mixtures (for $p = 4, 5, \ldots, 9$). These maps were produced using the Hellinger distance estimates available in matrix $\mathbf{A}_p^{\text{hel}}$. The contours and tones of the map are scaled in the range from 0.0 to 1.0 for all six maps.

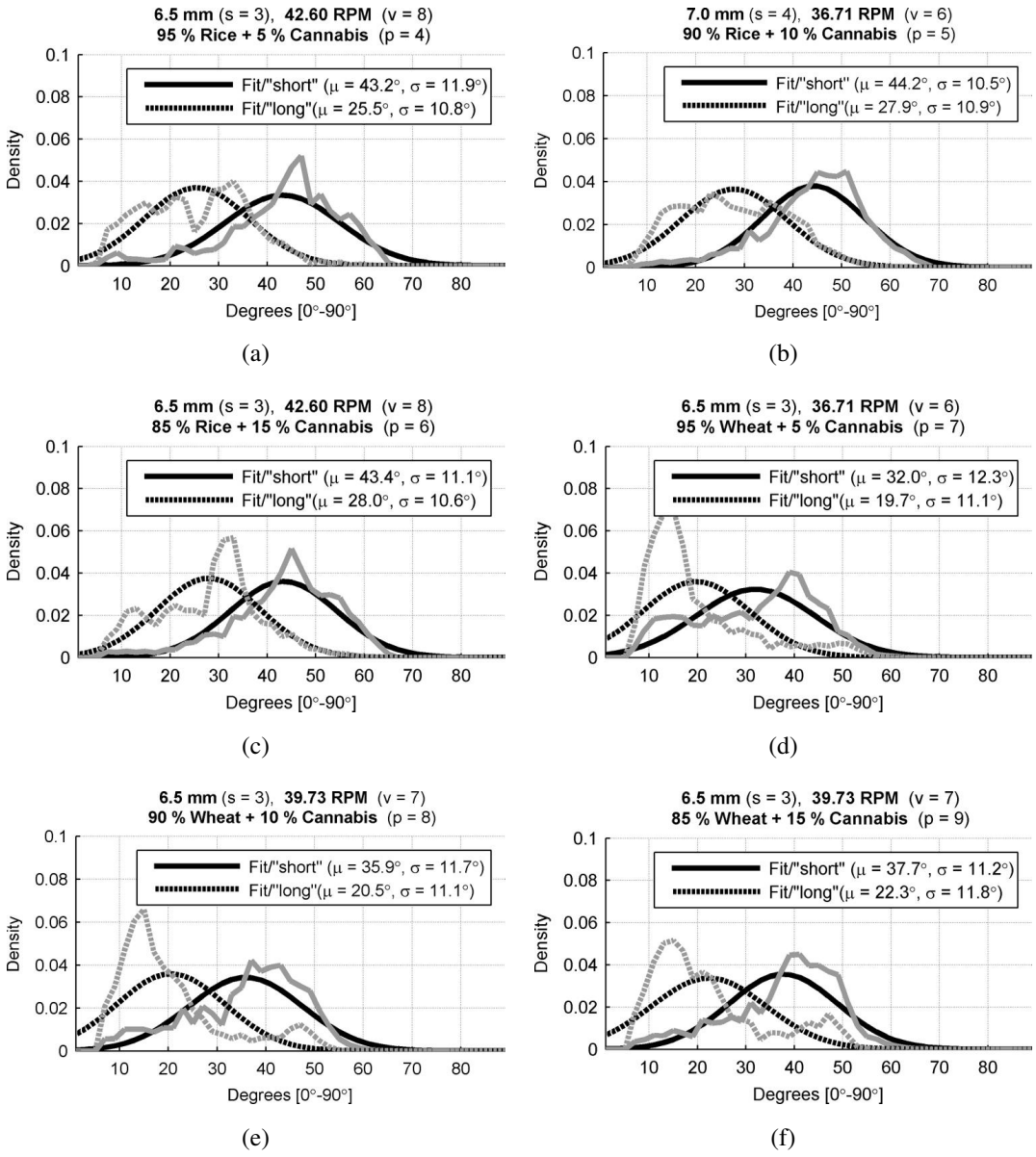

Figure 9: Normalized histogram plots with a superimposed normal fit. These histograms were generated from vectors $\boldsymbol{\theta}^{\text{long}}_{(s,v,p)}$ (dotted curves) and $\boldsymbol{\theta}^{\text{short}}_{(s,v,p)}$ (solid curves).

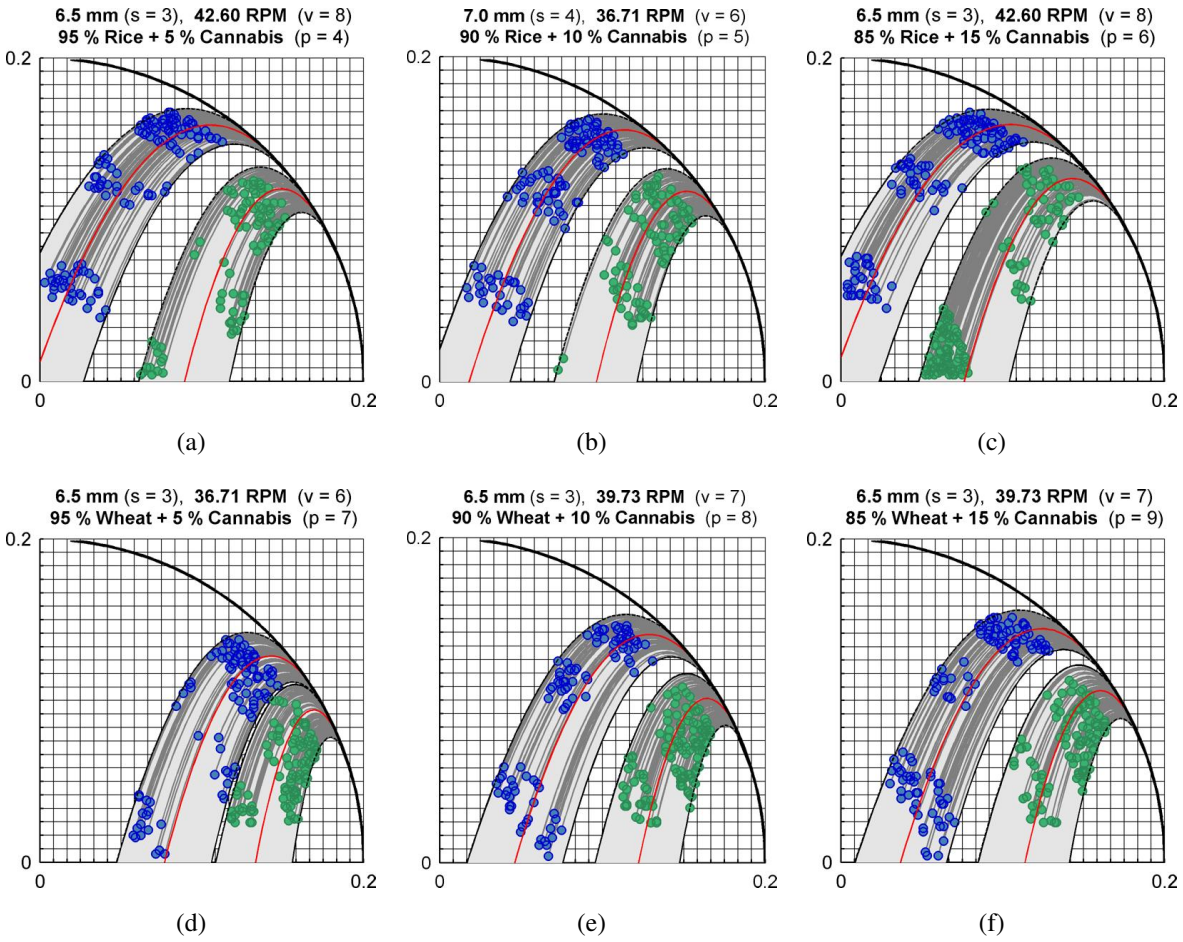

Figure 10: Trajectory plots for long and short seeds. These plots are graphical depictions of the statistical properties of the initial locations of the parabolic trajectories of long and short seeds. The plots were generated using the normal fit parameters estimated from the θ values available in vectors $\boldsymbol{\theta}^{\text{long}}_{(s,v,p)}$ and $\boldsymbol{\theta}^{\text{short}}_{(s,v,p)}$. The plots include up to 300 long and 300 short seeds and their (ideal) parabolic trajectories are also included. The lower set of parabolas represents trajectories for long seeds and the upper set does the same but for short seeds. The standard deviation of each set of parabolas was set to $\pm(1/2)\sigma^{\text{long}}_{(s,v,p)}$ and $\pm(1/2)\sigma^{\text{short}}_{(s,v,p)}$.

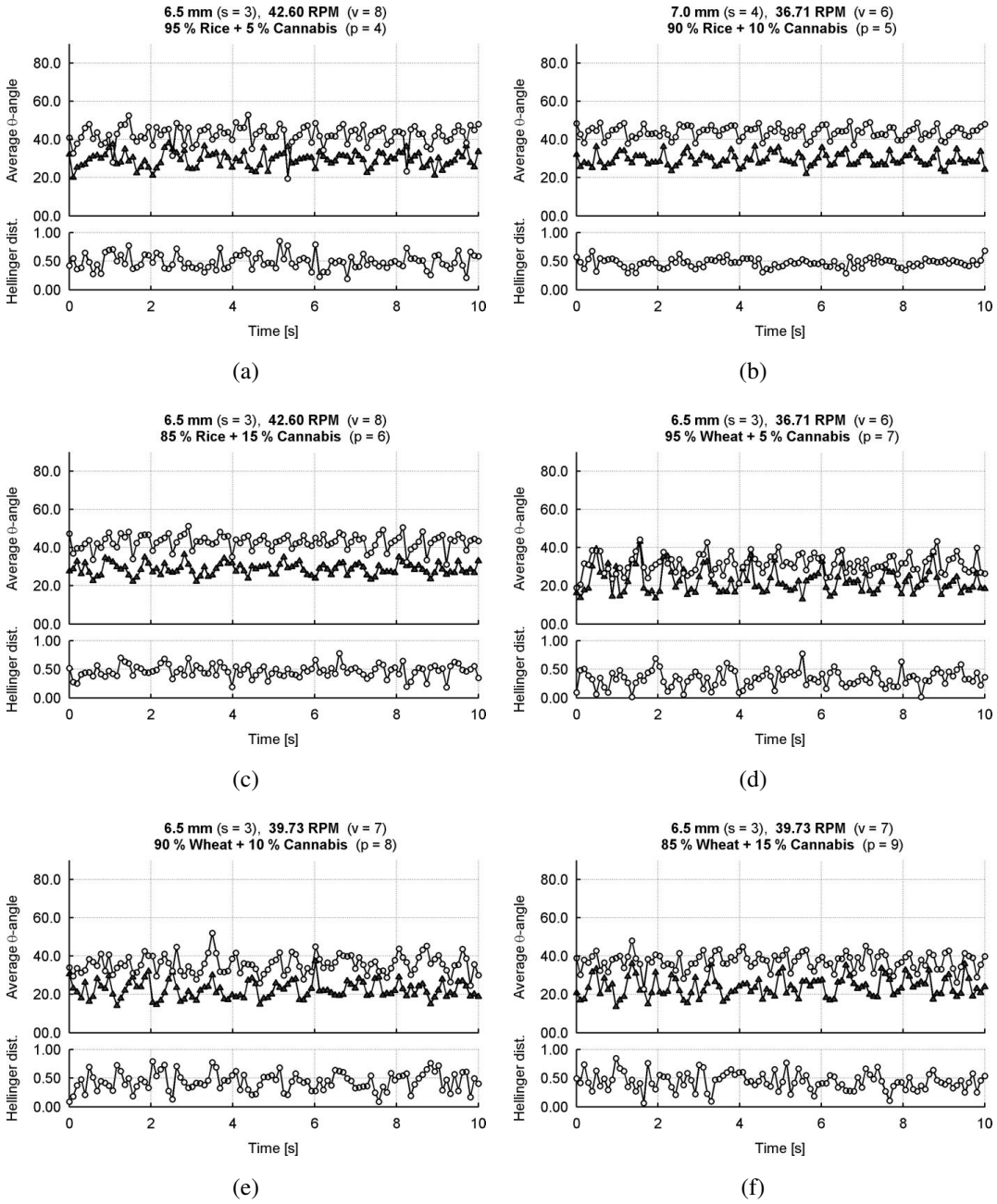

Figure 11: Temporal behaviour of the indented cylinder. Each sample was created using estimates from 25 time steps k – resulting in 104 samples over 10 seconds. The upper scatter plot for each value of p shows the estimated average θ value over time. The open (white) circular markers are from a normal fit estimated using θ values for short seeds. The closed (black) circular markers were estimated using θ values for long seeds. The lower scatter plot depicts the estimated Hellinger distance.

Appendix D

Poster I – Towards Tracking of Seeds in an Indented Cylinder

Buus O.T., Carstensen J.M., Jørgensen, J.R., 2010. **Towards Tracking of Seeds in an Indented Cylinder**. Industrial Visionday 2010 in May 2010 at Technical University of Denmark, Lyngby, Denmark.

This poster was the result of some preliminary tracking experiments using the Kalman-filter algorithm. It was displayed at Visionday 2010 *at Technical University of Denmark in May 2010.*

DEPARTMENT OF GENETICS AND BIOTECHNOLOGY
FACULTY OF AGRICULTURAL SCIENCES
AARHUS UNIVERSITY

DTU Informatics
Department of Informatics and Mathematical Modelling

Towards Tracking of Seeds in an Indented Cylinder

O. Buus[a], J. M. Carstensen[b] & J. R. Jørgensen[a]

[a]Aarhus University, Faculty of Agricultural Sciences, Department of Genetics and Biotechnology, Forsøgsvej 1, DK-4200 Slagelse, Denmark (*Ole.Buus@agrsci.dk*). [b]Technical University of Denmark, Department of Mathematics and Mathematical Modelling, Denmark.

The rotating indented cylinder is used for processing various kinds of seeds. The indented cylinder was invented in the 1840s and is still very much used in seed processing. It separates on the basis of seed length into atleast two outputs: long and short seeds. The seeds are feed from the one end of the rotating cylinder and small pockets in the inner surfuce will catch the seeds. The long seeds will not fit entirely in these pockets and will thus fall out at a lower angle than shorter seeds. This principle makes sorting possible. The optimization of the indented cylinder is the ultimate goal.

There is a growing in interest in the application of vision from the seed processing industry. In a collaboration with Westrup A/S we investigate the possibilities in doing offline tracking in highspeed video recordings of rice seeds being processed in an indented cylinder, using relatively simple image processing and the Kalman Filter for for state prediction. The video frames were recorded at ~263 frames/second. The immidiate goal was to extract the trajectories of single rice seeds while moving in the cylinder. If successful, online process-adjustments of the indented cylinder could become possible in the foreseeable future.

The indented Cylinder and Seed Trajectories

When the seeds are being processed in the cylinder they will eventually be thrown of the cylinder surface. The trajectory they produce in the image plane is assumed a parabola. The hypethesis is that if these tracjectories can be extracted; possibly a classifier can be trained from the trajectories for long and short seeds and feedback to the indented cylinder could then be used as machine adjustments.

We use the following 4-element state-vector (no drag is introduced in the current model):

$$\mathbf{x}_k = \begin{bmatrix} v_k^x \\ v_k^y \\ p_k^x \\ p_k^y \end{bmatrix} = \begin{bmatrix} v_{k-1}^x \\ v_{k-1}^y - gT \\ p_{k-1}^x + v_{k-1}^x T \\ p_k^y + v_{k-1}^y T - \frac{1}{2} g T^2 \end{bmatrix}$$

The Kalman Filter

The Kalman filter is used to predict the next state of the process. In our case we model the process as being the current 2D velocity and position. This filter is useful since it is able to minimize the variance of estimation error (in most cases).

The following shows some of the fundamental equations of the filter and our choices for the model matrices $\mathbf{A}, \mathbf{B}, \mathbf{H}$, and the process control input vector $\mathbf{u}$.

$$\mathbf{x}_k = \mathbf{A}\mathbf{x}_{k-1} + \mathbf{B}\mathbf{u}_{k-1} + w_{k-1}$$
$$\mathbf{z}_k = \mathbf{H}\mathbf{x}_k + \mathbf{w}_k$$
$$\mathbf{u}_k = \begin{bmatrix} 0 \\ -g \end{bmatrix} \quad \mathbf{A} = \begin{bmatrix} T & 0 & 0 & 0 \\ 0 & T & 0 & 0 \\ T & 0 & 1 & 0 \\ 0 & T & 0 & 1 \end{bmatrix} \quad \mathbf{B} = \begin{bmatrix} 0 & 0 \\ 0 & T \\ 0 & 0 \\ 0 & \left(\frac{T^2}{2}\right) \end{bmatrix} \quad \mathbf{H} = \begin{bmatrix} 0 & 0 & 1 & 0 \\ 0 & 0 & 0 & 1 \end{bmatrix}$$

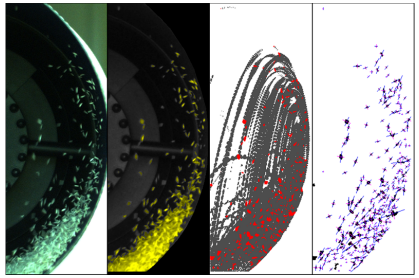

Figure 1: Several version of the same highspeed frame. This shows how the seeds move in parabolas. Video is available at http://www.youtube.com/watch?v=dsjqcVVdTPA.

Figure 2: The Kalman filter is based on a loop with two different stages. The measurement update stage is used to read a position from the images.

Discussion

The goal of offline tracking of single seeds in the indented cylinder is ambitious at best. The results achieved in this work can be approved in many ways. More elaborate segmentation techniques could be used – Markov Random Fields is one example. The tracking could also become more robust by using other state estimators such as Extended Kalman, H-Infinity or Particle Filter. Work will continue in these areas.

Conclusion

The images currently suffer too greatly from cases of multiple occlusions and nonlinear changes in object orientation. This makes segmentation difficult and the attempt at single seed tracking is currently not working. The tracking takes spurios measurements and ultimately fails to catch the intended seed. Work continues.

Image Processing

The image processing was done locally on a small part of the image in each iteration of the kalman filter. These examples show how a global processing would look like:

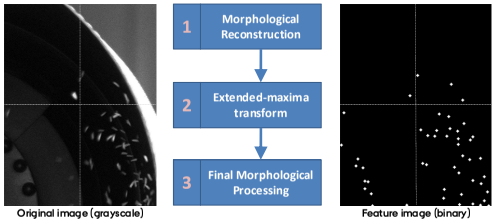

Tracking Results

The tracking can still be improved but these results should be considered important steps in the right direction. The images suffer from multiple occlusions and difference in seed orientation.

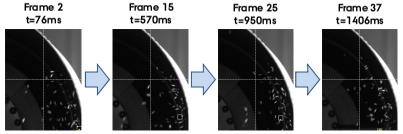

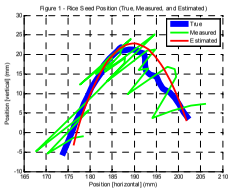

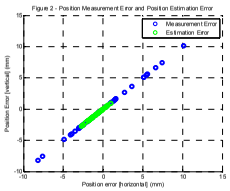

Presented at DTU Visiondays (Industrial - 26/5 2010)

PhD project sponsered by Westrup A/S

Appendix E

Poster II – Analysis of Seed Sorting Process by Estimation of Seed Motion Trajectories

Buus O.T., Carstensen J.M., Jørgensen, J.R., 2011. **Analysis of Seed Sorting Process by Estimation of Seed Motion Trajectories**. Scandinavian Conference in Image Analysis 2011 in May 2011, Ystad, Sweden.

This poster graphically depicts certain key aspects of the research published in Paper I available in Appendix A.

AARHUS UNIVERSITY

Technical University of Denmark

Analysis of Seed Sorting Process by Estimation of Seed Motion Trajectories

Ole Thomsen Buus[1], Johannes Ravn Jørgensen[1], and Jens Michael Carstensen[2]

[1]Aarhus University, Faculty of Agricultural Sciences, Department of Genetics and Biotechnology, 4200 Slagelse, Denmark.
[2]Informatics and Mathematical Modelling, Technical University of Denmark, Building 321, DK-2800 Lyngby, Denmark.

ABSTRACT & INTRO

Seed sorting is a mechanical process in which the goal is to achieve a high level of purity and quality in the final product. Prediction and control of such processes are generally considered very difficult.

One possible solution is a systems identification approach in which the seeds and their movement are directly observed and data about important process parameters extracted.

Image analysis was used to extract such data from the internal sorting process in one particular seed sorting device - the so-called "indented cylinder".

Twenty high speed image sequences were recorded of the indented cylinder in action, sorting a batch of barley with both whole and broken kernels.

The motion trajectories and angle of escape for each seed in each frame were estimated. Motion trajectories and frequency distributions for the angle of escape are shown for different velocities and pocket sizes.

Materials and Methods

1 The Indented Cylinder

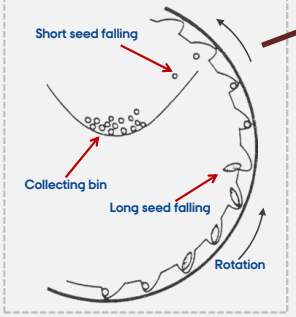

2 Experimental Setup

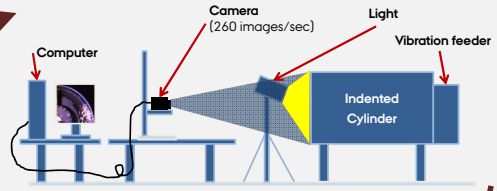

3 Image Processing

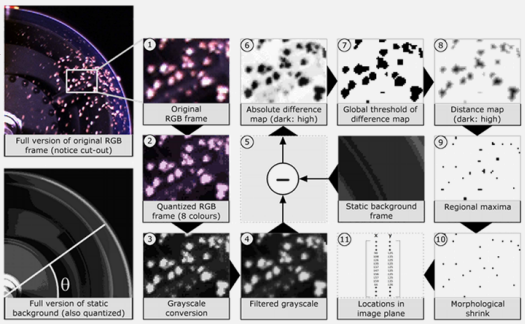

4 Trajectory Estimation

$$y = f(R, \omega, x, \theta)$$

R = radius of cylinder
ω = rotational speed
θ = angle of escape

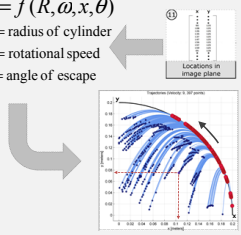

Results

1 Trajectory Plots

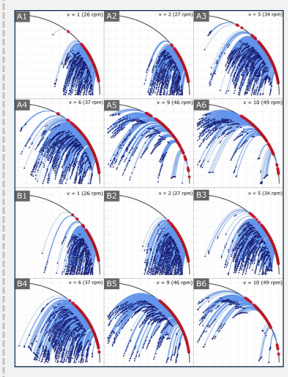

2 "Angle-of-escape" distributions

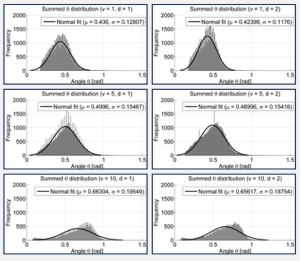

3 Process Stability

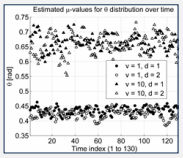

4 Algorithm Stability

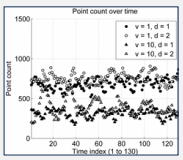

5 A linearity?

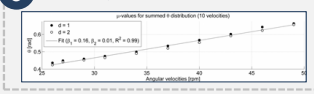

CONCLUSIONS

In this work we have experimentally verified a certain behaviour of the sorting process in the indented cylinder. **First** and foremost we show that the process has some stability (but mostly for the lower velocity steps).

Secondly, we show a linear relation between rotational speed and angle of escape .

A **third** results is a more tentative one: We have shown that image analysis can be used for flow analysis of particles moving in an indented cylinder. This is a novel step toward the goal of predicting and controlling the sorting process in these machines.

Poster paper is available in conference proceedings on pages 273-284.
Presented at the **Scandinavian Conference in Image Analysis 2011** - 23-27 May 2011